ADDIS ABABA UNIVERSITY

Department of Chemistry

Developing Polymer/Dye based Radiochromic Dosimeters for Medical and Environmental applications

Hagos Tesfay

(Doctoral Thesis)

ADDIS ABABA, ETHIOPIA

June 2015

Chemistry Department College of Natural Sciences Addis Ababa University

Developing Polymer /Dye Based Radiochromic Dosimeters for Medical and Environmental Applications.

By Hagos Tesfay

Approved by:

1. Professor Teketel Yohannes
   Advisor
2. Dr. Negussie Megersa
   Advisor
3. Professor Olgun Güven
   External Examiner
4. Professor B.S Chandravanshi
   Examiner
5. Dr. Feleke Zewge
   Examiner
6. Dr. Ahmed Mustefa
   Chairman

June 2015

Abstract

Developing Polymer/Dye based Radio-chromic Dosimeters for Medical and Environmental applications

Hagos Tesfay

Addis Ababa University, 2015

Dye/polymer based dosimeters are developed by various researchers for medical, industrial and environmental applications. Most of these radiochromic dosimeters are focused on applications related to detection of high dose ionizing radiation. Development of dosimeters from different materials such as polymers, dyes, semiconductors, metal oxides and other materials is an active research area. The development of a radiochromic dosimeter from cheap materials such as polymers and dyes for low dose radiation dosimetry is also getting much attention. At present different research groups are working on developing radiochromic dosimeters using dyes and polymers.

Some polymethine cyanine dyes were studied for their dosimetric characteristics. The results of the studies show that these dyes could be promising materials for developing radiation dosimeters for the measurement of low dose radiation in medicine and environment. A traditional turmeric dye called curcumin was also studied in film form for high dose dosimetry. However, heptamethine dyes and curcumin have not been profoundly investigated for low dose dosimetry.

On the other hand, conjugated polymers and other conventional polymers are being investigated for developing polymer based radiochromic dosimeters. Some promising results were reported especially for low dose radiotherapy and high dose industrial applications.

In this research work, dosimetric studies were carried out on the heptamethine cyanine dyes, curcumin dye and P3HT solutions and polyvinyl alcohol (PVA) films using UV-Vis spectrophotometry, spectrofluorometry, mass spectrometry (MS), optical densitometry and Fourier transform infra-red spectroscopy (FT-IR) methods. The two heptemethine cyanine dyes and curcumin showed promising dosimetric characteristics for low dose applications. P3HT in chloroform with the addition of DDT also showed promising results opening for a possibility of developing a low dose dosimeter using P3HT solutions in other non-toxic solvents in the presence of less hazardous chemicals such as chloral hydrate and trichloroacetic acid as radiosensitizers instead of DDT. The heptamethine/PVA/HCl film nanocomposite doped with TiO_2 nanoparticles showed enhanced dosimetric response confirming the catalytic role TiO_2 nanoparticles play in improving the dosimetric characteristics of these dyes in solid state for low dose applications.

A mechanism for the radiation-induced decomposition of the heptamethine dye solutions in chloroform was proposed based on the MS, FTIR and UV-Vis spectroscopic data. The proposed mechanism involves a two step reaction. In the first step, radiolysis of chloroform occurs, which results in radicals and stable molecules. In the second step, decomposition of the heptamethine dye occurs *via* interaction of the dyes with these radicals ($Cl^{\cdot}$ and $^{\cdot}CHCl_2$) and stable molecule (HCl) to produce smaller chromophoric groups. In the proposed mechanism, the various

chromophoric groups formed are described based on UV-Vis, MS and FTIR data showing extensive loss of conjugation due to breakdown of the π-bond of the polymethine bridge on interaction with radiolysis products of chloroform.

The heptamethine dosimetric dye solutions also show visual color changes with intensity of color being proportional to absorbed doses which is very useful for precise monitoring of doses delivered to patients in radiotherapy applications. The shelf life of the pre-irradiated dye solutions also show good stability up to 20 days.

The dosimetric dye solutions (heptamethine dyes and curcumin) prepared from non-toxic solvents such as ethanol and acetone in the presence of radical generating species trichloroacetic acid and chloral hydrate showed promising results which will have great potential for real low dose applications in medicine and environment.

Key words: heptamethine dyes, curcumin, X-ray radiation, gamma radiation, gray, radiation dose, dosimetry, polyvinyl alcohol, radiochromic, environmental, medical.

Dedication

This work is dedicated to the memory of my father Tesfay Medhin, my mother Kebedech Gebrewahid, my grand mother Silas Kidanu, my brother Tsegay Tesfay (aka Qokah) and all martyers who sacrificed their life for the well being of Ethiopians.

Acknowledgements

I am especially thankful to my supervisors, Prof. Teketel Yohannes and Dr. Negussie Megerssa for their advice and support throughout my PhD. I would like to thank Prof. Carlos F.O. Graeff, Department of Physics, FC-UNESP, Brazil for giving me the opportunity to do experimental work in his research lab and for giving me advice and support throughout my stay in Brazil. I would like also to thank Dr. Erica Bronze-Uhle for her fruitful guidance and assistance, Dr. Augusto Batagin-Neto for his unreserved support and guidance during my stay in Brazil. Special thanks go to Anna Véron and Prof. Thomas Geiger from Swiss Federal Laboratories for Materials Science and Technology (Empa), Switzerland for providing me with the heptamethine dyes to do my research work.

Special thanks also go to Mrs. Simone for the X-ray irradiation and Mrs. Cassiana for the Co-60 gamma irradiation of the samples. Great thanks to Dr. Thomas Chernet, Head of the National Tse Tse Fly Eradication Institute for allowing me to use the Co-60 Gamma Cell 220 Excel. I would like to extend my sincere thanks to Dr. Solomon Mekonen, Dr. Abeba Demmisse and Mr. Emanuel Abera of the National Tse Tse Fly Eradication Institute for facilitating the irradiation of my samples.

Great thanks also go to Mirko Congui, Silvia Fernandes, Gustavo Albano, Bruna Bregadiolli, Eliane Matusara, and Oswaldo Neto for their kind assistance and support during my stay in Brazil.

I want to thank Dr. Gedion Getahun from Germany for his encouragement and all his unreserved support during my studies.

I would like to thank Dr. Ahmed Mustefa, Head of the Chemistry Department for his advice and support. I would like to thank Prof. Negussie Retta, Dean of College of Natural and Computational Sciences for his advice and support. I would like also to thank Dr. Merid Tessema, Department of Chemistry Addis Ababa University for his kind advice and support.

I would like to thank Graduate program Addis Ababa University for sponsoring me to do my PhD studies. I would like also to thank São Paulo State University (UNESP) for giving me scholarship for my stay in Brazil.

I would like to thank my colleagues: Ato Yohannes Jorge, Dr. Solomon Demena, Ato Ejigu Kebede, Mulubrhan Belay, Fedlu Kedir, Dr. Siraye Esubalew, Kiros Guesh, Hagos Tikue, Yishak Tsegazeab, Henok Kiros and Rahel Tilahun for their ongoing help, technical support and work.

The assistance and wisdom of many people went into this work. I would gratefully like to acknowledge the contributions, in whatever form they were, of the following: Ato Sahlemichael Deme, W/ro Mehret G/Meskel, W/ro Saba Mesfin, W/ro Woinshet Gebeyehu, and W/ro Elsa Berhe.

Finally, I would like to thank my family: my wife W/ro Alem Tadesse, my daughter Betelhem Hagos, my sons Mussie Hagos and Natanim Hagos, and my brothers Aregawi Tesfay and Meressa Tesfay for their constant encouragement and for always being there for me.

Table of Contents

List of Figures

List of Tables

List of Abbreviations

ΔA	change in absorbance
ε	extinction coefficient
λ	wavelength
ρ	density
^{60}Co	Cobalt-60
A	absorbance
BCP	bromo cresol purple
BGO	bismuth germinate
CH	chloral hydrate
cGy	centiGray
Cy7-I	heptamethine iodide
Cy7-PF_6	heptamethine hexafluorophosphate
D	dose
E	energy
EB	electron beam
EMPA	Swiss Federal Laboratories for Materials Science and Technology
eV	electron-volt
FWHM	full width half maximum
G	radiochemical yield

GSO	gadolinium orthosilicate
Gy	gray
HPGe	high purity germanium
HV	high voltage
I	intensity
IAEA	International Atomic Energy Agency
ICRP	International Commission on Radiological Protection
ICRU	International Commission of Radiation Units
IMRT	intensity modulated radiation therapy
KE	kinetic energy
K eV	kilo electron-volt
l	length
LET	linear energy transfer
LINAC	linear accelerator
LMD	leucogel malachite dosimeter
LMG	leuco malachite green
LOD	limit of detection
LUAP	lutetium aluminum perovskite
MD-55	radiochromic film intended for Medium Dose
MEH-PPV	poly [2-methoxy-5(-2-ethylhexyloxy-)-1,4 -phenylenevinylene
MeV	mega electron-volt
MR	methyl red

MS-ESI	electron spray ionization mass spectrometer
MV	megavolt
NBT	nitro blue tetrazolium
NCRP	National Commission for Radiation Protection
OFET	organic field effect transistor
OSL	optically stimulated luminescence
P3HT	poly (3-hexylthiophene)
PMT	photomultiplier tube
PVA	polyvinyl alcohol
PVC	polyvinyl chloride
SSD	source-to-surface distance
t	time
TLD	thermoluminescent dosimeter
UNESP	São Paulo State University
USP	University of São Paulo
UV	ultraviolet
X	radiation exposure
YAP	yttrium aluminum perovskite
Z	atomic number

1. Introduction

1.1. Radiation dosimetry and its applications in health and environment

A radiation dosimeter is a device, instrument or system that measures or evaluates, either directly or indirectly, the quantities exposure, absorbed dose or equivalent dose, or their time derivatives (rates), or related quantities of ionizing radiation. A dosimeter along with its reader is referred to as a dosimetry system [1].

Ionizing radiation technology is being used in various areas of applications including medicine, industrial processing, environment, pest control, energy and many others.

Currently, there are three main applications for industrial radiation processing: the sterilization of medical devices, the treatment of foodstuffs, and the modification of polymers [2]. These radiation processing are performed at high radiation doses.

The other two important areas which use ionizing radiation technology are medicine and environment. While the utilization of irradiation facility for treatment of flue gases, wastewater and other environmental wastes require high radiation doses, low and high doses of radiation are measured during environmental radiation monitoring. On the other hand, low dose of radiation is employed and measured in medicine.

For example, in medicine determination of gamma ray is often most important measurement in radiotherapy [3] and medical diagnosis [4]. In environment, it is important to monitor environmental natural background radiation to detect changes in environmental radiation dose such as accidental leakage of radioactivity from radiation facility [5 - 6] and personal dosimetry [7].

Effective and safe use of radiation requires strict monitoring of radiation doses in each area of applications. Therefore, radiation dosimetry finds great applications especially in medicine and environment as these two areas of radiation technologies are related to human health and safety.

Many types of radiation dosimeters have been developed and commercialized for the measurement of high doses of radiation at affordable prices. The dosimeters developed for measuring low doses of radiation are expensive [2] and, therefore, not affordable for routine dosimetry in medicine and environment.

Radiation dosimeters that are cheap, respond to low doses of radiation, high sensitivity, easy to use, give real time response are highly needed for medical and environmental applications.

To meet these demands, considerable research into new dosimeters is underway, including efforts to enhance the dosimeter performance through both the material properties and manufacturing technologies [2].

1.2. Motivation of the research work

In medicine such as nuclear medicine, radiotherapy and radiology where radiation sources are used, there is a need for strict monitoring of personal radiation dose of people working in these departments and also patients who come to these departments for either diagnosis or treatment. Therefore, it is very crucial to precisely and regularly measure the amount of radiation exposure for the personnel working in these departments and also the patients.

For example, in clinical radiotherapy, dosimetry is particularly important to the patient. Being able to accurately monitor the dose to high-risk organs (e.g., the eyes) when using implanted therapeutic radioactive seeds (brachyterapy) requires detectors with the best achievable spatial resolution. In general, the health sciences are dominated (in number) by x-ray detectors and improvements are constantly sought [8].

Natural radioactive elements from mining activities enter to the river streams and contaminate the environment. Radioactive gases such as iodine-131 (^{131}I) could be released from nuclear accidents and pose a threat to the public.

Such radioactive elements need strict follow up to protect the public from radiation hazard. Radioactive toxicity can be caused by human activities. For example, radioactive wastes from medical centers, nuclear facilities and others could enter into ground water, air or soil and cause radiation toxicity in humans and other living things. Ionizing radiation is used in the treatment of flue gases from burning fossil fuels, hygienization of swage sledges, and detoxification of industrial wastewater [9]. In all these cases, monitoring of the radiation doses should be regularly implemented to keep the public safe.

Therefore, there is a need for cheap, ragged and sensitive dosimeters for monitoring of doses of ionizing radiation to minimize radiation toxicity from radioactive wastes and from radiation facilities for treatment of environmental pollutants.

Therefore, the developing of polymer-based and dye-based dosimeters will result in sensors that are cost effective, highly sensitive, and applicable in medicine and environment.

This work will also result in new knowledge in polymer and dye as well as composite dosimeters and their interaction with ionizing radiation and will be very useful in developing new composite materials as radiation dosimeters.

Finally this research work will open a new area of investigation in the development of polymer and dye based composite dosimeters.

1.3. Significance of the research undertaking

The enormous advances in the understanding of human anatomy, physiology and pathology in recent decades have led to ever-improving methods of disease prevention, diagnosis and treatment. Many of these achievements have been enabled, at least in part, by advances in ionizing radiation detectors [10]. One of the areas of medicine that utilizes ionizing radiation is emission radiography where a radiopharmaceutical is administered that will follow a particular biological pathway. Measuring the resulting emission reveals the functioning of a particular organ. Single photon emission computed tomography (SPECT) and positron emission tomography (PET) remain commonly prescribed diagnostic procedures especially for brain and cardiac studies. With an aging population and society's great desire for improved diagnoses and treatments, medicine will most assuredly drive the development of radiation detectors of all kinds for many years to come [8].

The use of ionizing radiation in the treatment of environmental pollutants such as flue gases (SO_x, NO_x), detoxification of wastewaters and treatment of waste sludges helps in improving environmental safety. The greatest challenge of radiation processing is the relatively high capital cost of such irradiation facilities [9]. The other challenge could be safety of the personnel working in such facilities. In such cases low doses of radiation could be utilized.

Therefore, the safety of such radiation facilities could be assured by using dosimeters for low dose radiation detection that find applications in such irradiation facilities.

Therefore, this research undertaking will have significance in the area of medicine and environment in developing new types of dosimeters that are based on polymers and dyes with the merits of low cost, high sensitivity, ability to give direct reading *via* color changes.

1.4. Objectives

1.4.1. General Objective

To develop a new polymer, dye and composite based dosimeters for low dose ionizing radiation detection that can be used in medicine and environment.

1.4.2. Specific Objectives

i. To identify and select candidate polymers/dyes for the development of low dose radiation dosimeters.

ii. To study the dosimetric characteristics of polymer/dye solutions for environmental and medical applications

iii. To study polymer- dye- nanoparticle composites in gel form for low dose radiation dosimetery.

iv. To investigate the mechanism of dosimetric characteristics of the polymer/dye dosimeter solution by applying various analytical techniques such as FT-IR, MS, and UV-Vis.

v. To evaluate the sensitivity, stability, detection limit and other merits of these dosimeters and compare with the currently available radiation dosimeters.

vi. To develop a dosimeter gel film that serves as a dosimeter for detection of ionizing radiation (gamma and X-ray radiation) using the polymer-dye- nano-particle composite.

2. Fundamentals of Radiation Detection and Dosimetry

2.1. Review of radiation techniques

It is found that a few naturally occurring substances consist of atoms which are unstable – that is, they undergo spontaneous transformation into more stable product atoms. Such substances are said to be radioactive, and the transformation process is known as radioactive decay. Radioactive decay is usually accompanied by the emission of radiation in the form of charged particles and gamma (γ) rays [11]. These radioactive decay processes are categorized in to four general types as fast electrons, heavy charged particles (charged particulate radiation), electromagnetic radiation and neutrons (uncharged radiation) [12].

Fast electrons include beta particles (positive or negative) emitted in nuclear decay, as well as energetic electrons produced by any other process. Heavy charged particles denote a category that encompasses all energetic ions with mass of one atomic mass unit or greater, such as alpha particles, protons, fission products, or the products of many nuclear reactions. Electromagnetic radiation includes X-rays emitted in the rearrangement of electron shells of atoms and gamma rays that originate from transitions within the nucleus itself. Neutrons originate from various nuclear processes and are sub-categorized as slow and fast neutrons [12].

These radiation sources have various applications in different areas such as food processing [13 - 15], pest control [16 - 17], polymer processing [18-20], medicine [21 - 25], environment [19, 26], energy [27 - 28] and others [29]. However, their use requires accurate and precise

monitoring of doses [30 - 32] in order to minimize potential hazards that could cause damages to humans [33 - 34].

2.1.1. Ionizing Radiation

Radiation that has enough energy to move atoms in a molecule around or cause them to vibrate, but not enough to change them chemically, is referred to as non-ionizing radiation. Examples of this kind of radiation are sound waves, visible light, and microwaves. Radiation that falls within the ionizing radiation range has enough energy to actually break the chemical bonds. Ionizing radiation falls into two categories: direct ionizing (charged particles such as electrons and protons) and indirect ionizing (such as photons and neutrons) [2]. The directly and indirectly ionizing radiation types are briefly discussed below.

2.1.1.1. Beta particles

Beta particles are electrons emitted during nuclear decay process [12], which is schematically written as:

$$ {}^{A}_{Z}X \rightarrow {}^{A}_{Z+1}Y + \beta^{-} + \bar{\nu} \qquad (1) $$

Where *X* and *Y* are the initial and final nuclear species and $\bar{\nu}$ is the antineutrino. Beta particles have the same mass as an electron but may be either negatively or positively charged. With their small size and charge, they penetrate matter more easily than alpha particles but are more easily deflected [35]. These particles are classified as directly ionizing radiation.

2.1.1.2. Alpha particles

Heavy nuclei are energetically unstable against the spontaneous emission of alpha particle (or ^{4}He nucleus). The decay process is schematically written as [12]:

$$ {}^{A}_{Z}X \rightarrow {}^{A-4}_{Z-2}Y + {}^{4}_{2}\alpha \qquad (2) $$

where X and Y are the initial and final nuclear species.

Alpha-emitting atoms tend to have high atomic numbers. Alpha rays from radio-nuclides with energies of a few MeV travel only a few inches in air and are easily shielded by skin, clothing, or a piece of paper. External alpha irradiation of the human body is therefore of little concern. However, ingested radio-nuclides can lead to direct alpha exposure of critical cells in organs, such as the lung and bone. Alpha rays are dangerous because they deposit their energy in a small volume, thus causing great damage to a few cells [2]. Alpha particles are also classified as directly ionizing radiation.

2.1.1.3. Gamma and X-rays

A gamma photon is a packet of electromagnetic energy having no mass and no electrical charge. Henri Becquerel is credited with discovering of gamma radiation in 1896. Gamma photons are the most energetic photons in the electromagnetic spectrum and can range from a few keV up to around 10 MeV [2]. While gamma rays and X-rays are photon energies, they differ in their origins. Gamma radiation emission occurs when the nucleus of a radioactive atom has too much energy and often follows the emission of a beta particle. Atoms emit X-rays when electrons fall from a higher energy shell to a lower energy shell [2].

2.1.1.4. Neutrons

A neutron has the same mass as a proton but has no charge and is difficult to stop. The capture of a neutron results in the emission of a gamma ray. Neutrons are classified according to their energy: thermal (< 1 eV); intermediate; and fast (> 100 keV). Water is regarded as an effective shield for neutrons [2, 12].

2.1.2. Interaction of ionizing radiation with matter

The phenomena associated with the radiation interaction in matter are commonly understood to include a wide variety of physical effects. Moreover, the nature of interactions in matter depends on the incoming type of radiation and energy [36]. In this section stopping power, particle range, linear energy transfer, the Brag curve and effects of ionizing radiation on matter for the design of dosimeters will be discussed.

2.1.2.1. Stopping power

The rate of loss of energy E with distance traversed is known as the stopping power of the material and is given by [37]:

$$-\frac{dE}{dx} = \frac{2e^4 z^2 N_A Z}{mv^2 A} B \qquad (3)$$

Where N_A is Avogadro's number, (6×10^{23} atoms per mole); A is the atomic mass; z and v are the charge number (1 for an electron) and velocity of the incident particle, respectively; and x is the path length or distance measured along the track of an electron; m is the electron rest mass and e

is the electrostatic charge. *B* is known as the stopping power of the material and varies slowly with particle energy as follows [12]:

$$B = Z\left[\ln\frac{2mv^2}{I} - \ln\left(1-\frac{v^2}{c^2}\right) - \frac{v^2}{c^2}\right] \quad (4)$$

The parameter I represents the average excitation and ionization potential of the absorber and is normally treated as an experimentally determined parameter for each element. The minimum stopping power for electrons occurs at energies in the range of 1 – 2 MeV. Note that stopping power is often quoted in units of energy lost per unit mass thickness, measured along the particle path in MeV cm^2 g^{-1}. In addition to the energy loss by collision, there is a further contribution to stopping power due to radiation loss (bremstrahlung generation). At energies below 1 MeV, this is extremely small when compared with collision loss as a mechanism for stopping electrons. It is a rising function of energy, but it does not dominate over collision loss until the energies exceed well over 10 MeV [35].

The expression for B in Equation 4 varies slowly with particle energy. Thus, the general behavior of dE/dx can be inferred from the behavior of the multiplicative factor. For a given particle, dE/dx therefore varies as $1/v^2$, or inversely with particle energy. The charged particle spends a greater time in the vicinity of any given electron when its velocity is low, the impulse felt by the electron, and hence the energy transfer, is the largest. When comparing different charged particles of the same velocity, the only factor that may change outside the logarithmic term in Equation 3 is z^2, which occurs in the numerator of the expression. Therefore, particles with the greatest charge will have the largest specific energy loss. Alpha particles, for example,

will lose energy at a rate that is greater than protons of the same velocity but less than that of more highly charged ions [2].

2.1.2.2. Mass attenuation coefficient

For a given thickness, the probability of interaction is dependent on the number of atoms per volume. This dependency can be overcome by normalizing the linear attenuation coefficient for the density of the material. The linear attenuation coefficient, normalized to unit density, is called the mass attenuation coefficient [12]:

$$\text{Mass attenuation coefficient } (\mu/\rho)\ [\text{cm}^2/\text{g}] = \frac{Linear\ \ Attenuatio\ n\ Coefficien\ t\ (\mu)\left[cm^{-1}\right]}{Density\ of\ \ Material\ (\rho)\left[g/cm^3\right]} \quad (5)$$

The mass attenuation coefficient is independent of density. Therefore, for a given photon energy:

$(\mu/\rho)_{\text{water}} = (\mu/\rho)_{\text{ice}} = (\mu/\rho)_{\text{water vapor}}$

2.1.1.3. Particle range

A charged particle moving through a certain material loses its kinetic energy through interactions with the electrons and nuclei of the material. Eventually, the particle will stop, pick up the necessary number of electrons from the surrounding matter, and become neutral. For example [37],

$p^+ + e^- \rightarrow$ hydrogen atom

$\alpha^{2+} + 2\ e^- \rightarrow$ He atom

The thickness of materials that just stops a particle of kinetic energy KE, mass M, and charge *z* is called the range, R, of the particle in that material. Range is distance, and its basic dimension is meter (m). In addition to meters, another common unit used for range is kg/m^2 (or g/cm^2). The relationship between the two is [38] given by Equation (6).

$$R\ (kg/m^2) = [R(m)]x\ [\rho(Kg/m^3)] \quad (6)$$

where ρ is the density of the material in which the particle travels. The range measured in kg/m^2 is independent of the state of matter. That is, a particle will have the same range in kg/m^2 whether it moves in ice, water, or stream [38]. The range is an average quantity. Particles of the same type with the same kinetic energy moving in the same medium will not stop after traveling exactly the same thickness R. Their path length will not be the same either. What actually happens is that the end points of the path lengths will be distributed around an average thickness called the range [38].

To illustrate the particles range, the range of alpha particle is discussed below. A collimated source of mono-energetic alpha particles is counted after passing through an absorber of variable thickness and is shown in Figure1 [12].

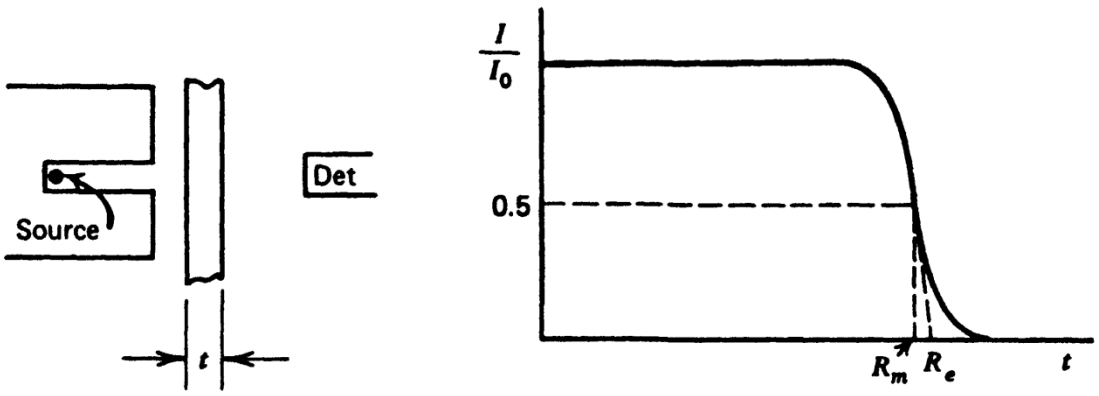

Figure 1 An alpha particle transmission experiment. I is the detected number of alpha particles through an absorber thickness t, whereas Io, is the number detected without the absorber. The mean range Rm and extrapolated Re are indicated [12].

The range of the alpha particles in the absorber material depicted in Fig.1 can be determined in several ways from the curve. The mean range is defined as the absorber thickness that reduces the alpha particle count to exactly one-half of its value in the absence of the absorber. This definition is most commonly used in tables of numerical range values. Another version that appears in the literature is the extrapolated range, which is obtained by extrapolating the linear portion of the end of the transmission curve to zero [12]. The difference between Rm and Re is 5 percent or less. Unless otherwise specified, when range is used, it is the mean range Rm. [38].

Semi-empirical formulas have been developed that give the range as a function of particle kinetic energy. For alpha particles, the range in air at normal temperature and pressure is given by [38]

$$R\ (mm) = \exp[1.61\sqrt{T(Mev)} \qquad 1 < T \leq 4\ MeV$$

$$\text{R (mm)} = (0.05T + 2.85)T^{3/2}(MeV) \qquad 4 \le \text{T} \le 15 \text{ MeV} \tag{7}$$

If the range is known for one material, it can be determined for any other by applying the Bragg-Kleeman rule [38]:

$$\frac{R_1}{R_2} = \frac{\rho_2}{\rho_1}\sqrt{\frac{A_1}{A_2}} \tag{8}$$

Where ρ_i and A_i are the density and atomic weight, respectively, of material i. For a compound or mixture, an effective molecular weight is used, obtained from Equation (9),

$$\sqrt{A_{ef}} = \left(\sum_{i=1}^{L}\frac{w_i}{\sqrt{A_i}}\right)^{-1} \tag{9}$$

Where L = number of elements in the compound or mixture, w_i = weight fraction of i^{th} element, A_i = atomic weight of i^{th} element, and for a compound of molecular mass M and number of atoms N, the weight fraction is given by:

$$w_i = \frac{N_i A_i}{M} \tag{10}$$

The range of electron is discussed here in more detail because electrons are much more used frequently in radiation measurements because secondary electrons or (δ-rays) are produced during ionization processes in radiation detection processes. For electrons, the transmission curve does not have a flat part as shown in Figure 2. It decreases gradually to a level which is the background. The range is equal to the thickness of the material, which is defined by the point where the linear extrapolation of the transmission curve meets the background [38].

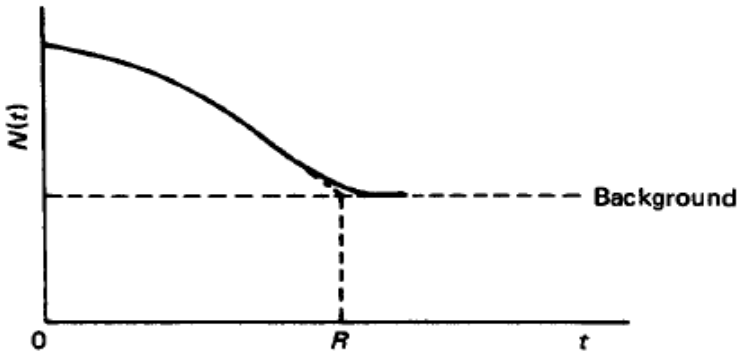

Figure 2 The number of electrons transmitted through thickness t [38].

The semi-empirical equation giving the range of electrons for the energy range 0.3 keV to 30 MeV has been developed by Tabata, Ito, and Okabe [38], based on the experimental results available since 1972. This equation (Equation 11) named as TIO equation has the following form:

$$R(kg/m^2) = a_1\left(\frac{\ln\left[1+a_2(\gamma-1)\right]}{a_2} - \frac{a_3(\gamma-1)}{1+a_4(\gamma-1)^{a_5}}\right) \tag{11}$$

Where A = atomic weight, M = rest mass of particle, $\gamma = \frac{\left(KE+Mc^2\right)}{Mc^2}$; $a_1 = \frac{2.335A}{Z^{1.209}}$;

$a_3 = 0.9891 - \left(3.01x10^{-4}Z\right)$; $a_4 = 1.468 - \left(1.180x10^{-2}Z\right)$; $a_5 = \frac{1.232}{Z^{0.109}}$

For equivalent energy, the specific energy loss of electrons is much lower than that of heavy charged particles, so their path length in typical absorbers is hundreds of times greater. As a very crude estimate, electron ranges tend to be about 2 mm per MeV in low density materials, or about 1 mm in materials of moderate density [12].

Knowing the particle range is extremely important when designing radiation detectors. Any detector that has to measure the full incident energy of a charged particle must have an active thickness, which is greater than the range of that particle in the detector material [2].

2.1.1.4. Linear Energy Transfer

The local energy deposition along the particle track of a radiation is known as linear energy transfer (LET) [2]. The linear energy transfer is nearly identical to the specific energy loss or stopping power (-dE/dx) defined earlier. The only differences are when the specific energy loss includes the bremstrahlung as part of the energy loss of the particle, but linear energy transfer LET (L) counts only the energy that is deposited along the track and therefore excludes the bremsstrahlung [2]. It is expressed by the expression in Equation (12) [12]:

$$L = \frac{dE_L}{dl} \tag{12}$$

Where dE_L is the average energy imparted locally to the medium and dl is the distance traversed in the medium along the local particle track.

The energy transfer to atom and atomic nuclei can result in biochemical reactions with the molecules as well as in biological changes to cells or cell components. In addition to direct energy transfer by interaction, energy can be transferred indirectly to a molecule by radicals or their reaction products, such as H_2O_2 (obtained from radiolysis of water). Depending on the irradiation conditions, damage to the organism can result from the energy transfer and may extend to single organs, organ systems, or the whole body [2]. Detailed treatment of LET is available at the ICRU Report 16 which includes major sections on the interaction of radiation

with matter, definition and concepts of LET, calculation of distributions of absorbed dose in LET, applications of LET calculations, LET in radiation protection, application of LET in radiation biology and chemical dosimetry [40].

2.1.1.5. The Brag curve

As a heavy charged particle moves through matter, it loses energy and consequently stopping power changes. Since stopping power measures the effectiveness of a particle to cause ionization, therefore, as the particle moves through matter its ionization capability also changes. To understand this dependence, let us plot the simplified Beth-Bloch formula shown in equation 13 for α-particles with respect to their residual energy [41].

$$\left[-\frac{dE}{dx}\right]_{Bethe-Bloch} = \frac{K}{\beta^2}\left[\ln\left(\frac{w_{\max}}{10^{-4}}\right) - \beta^2\right] MeVcm^{-1} \qquad (13)$$

By residual energy we mean the instantaneous energy of the particle retained by it as it travels through the material. Where K = 0.30548ρZq2/A is a constant for a given material. Since we are only concerned with the shape of the curve and not its numerical value, therefore we have used I = 10^{-4} MeV in the above expression. This value is typical of low Z materials. A plot of the above equation is shown in Figure 3 (the Brag curve). As one would expect, the stopping power increases with the residual energy of the particle. Hence as the particle looses energy it causes more and more ionization in its path until it reaches the highest point known as Bragg peak. After that point the particles have lost almost all of their energy and get quickly neutralized by attracting electrons from their surroundings [41].

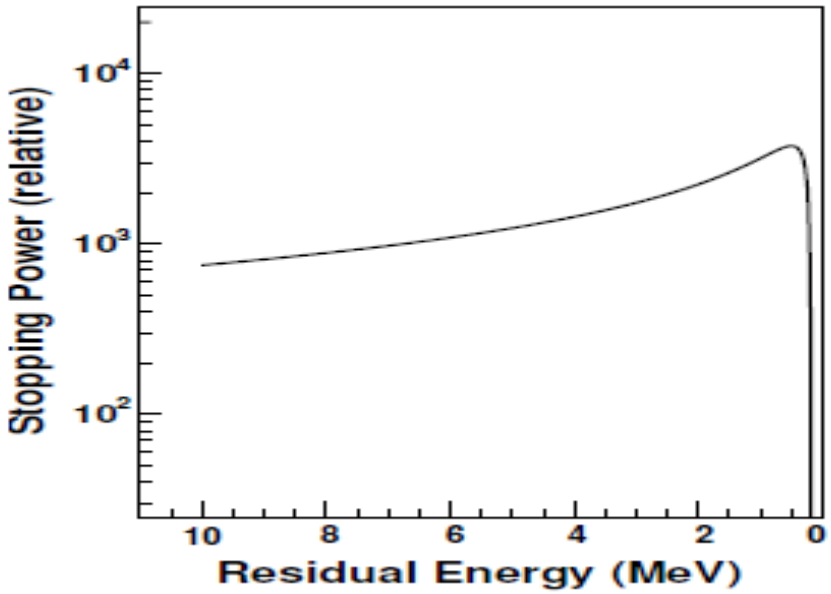

Figure 3 Plot of equation 13 for α-particles having initial energy of 10 MeV passing through a material having an ionization potential of 100 eV. This variation of stopping power with respect to residual energy of the particles is generally known as Bragg curve [41].

2.1.2. Radiation units and types of biological effects of radiation

2.1.3.1. Radiation units

The first widely used radiation unit, the roentgen, was based on the ionizing effect on air of X- and γ- radiation. This unit had several limitations and so two further units, the rad and the rem, were introduced. Later, these two units were replaced in the SI system (Systeme International Units) by the gray (Gy) and the sievert (Sv), respectively. The gray and the sievert have been approved by the International Commission on Radiation Units and Measurements (ICRU) and

used by the International Commission on Radiological Protection (ICRP). However, the older units, the rad and the rem, are still used in some countries [11].

A detailed description of all the units that are used in various areas related to radiation and their relations can be found in NCRP Report 82 [42]. Table 1 summarizes the units that are used most frequently in measuring ionizing radiation and radiation dose.

Table 1 Units used in measuring ionizing radiation [12]

Quantity	Definition	Units
Absorbed dose	The amount of energy deposited per unit mass.	SI unit: gray (Gy); 1Gy= 1J/kg Historic unit: rad; 1 rad= 100 erg/g; 100 rad = 1 Gy
Equivalent dose	The dose equivalent H is the product of the absorbed dose D and the quality factor Q, which characterizes the specific radiation.	SI unit: sievert (Sv) Historic unit: rem (roentgen equivalent man) 1 Sv = 100 rem rem = rad x Q
Radioactivity	Curie (Ci) is the traditional unit of radioactivity of 1 g of pure ^{226}Ra. Becquerel (Bq) is the SI unit of radioactivity equal to 1 disintegration per second.	1 Ci = 37 billion Bq 1nC i= 37 Bq 1Bq = 27 pCi
Gamma ray	The SI unit of exposure is coulomb per kilogram	1R= 2.58 x 10^4 C/kg

exposure	(C/kg) The historical unit of gamma exposure has been the roentgen (R) defined as the exposure which results in the generation of 1 electrostatic unit of charge per 0.001293 g (1 cm^3) of air.	1 R= 86.9 erg g^{-1} (air) 1 R of 1 MeV photons = 1.95 x 10^9 cm^{-2}

2.1.2.3. **Types of biological effects of radiation**

Human exposure to ionizing radiation is a natural part of life on earth. These exposures occur every day from radiation associated with naturally occurring radionuclides in soil, air, and food, and also from cosmic rays. In addition, many people are exposed to dental and medical diagnostic procedures and therapy involving: X-rays, gamma rays, charged particles, radionuclides, or other ionizing radiation sources. Others may be exposed in their workplaces such as in laboratories, hospitals, underground mines, or nuclear power plants. Excessive exposures may lead to the development of cancer by promotion of ongoing carcinogenic biological processes or by independent cancer induction [43]. Current knowledge about the biological effects of radiation was obtained from different sources such extensive research on animals, from epidemiological studies of human populations exposed to high radiation like early workers with X-rays and radium, patients treated with radiation, uranium mine workers, Japanese population that survived the atomic bombings of Hiroshima and Nagasaki as well as Chernobyl survivors [2].

The ionizing radiation, which has sufficient energy to interact with matter, especially in the human body is capable of producing ions, that is, it can eject an electron from an atom of the DNA (deoxyribonucleic acid) [44]. As a result, the bonding properties of the DNA atom change, causing a physical change of the DNA. Figure 4 shows the damaged molecule of DNA that regulates vital cell process.

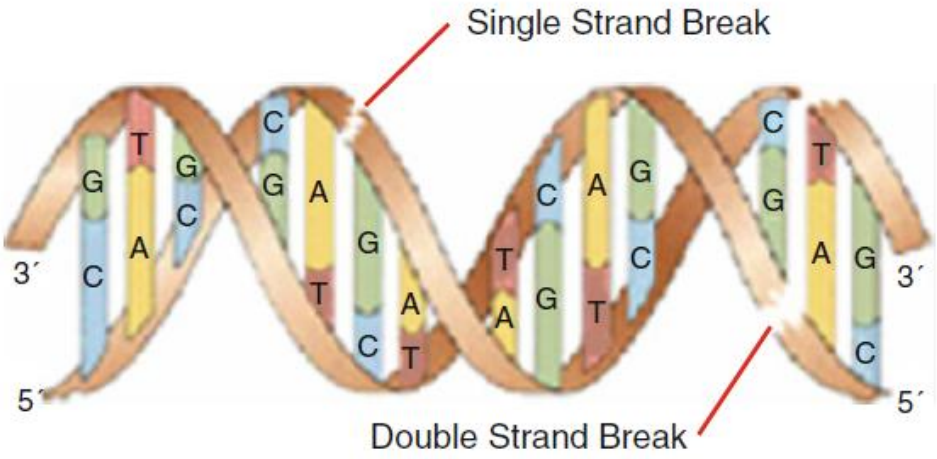

Figure 4 The damaged molecules of DNA that regulates vital cell process [44].

Two types of biological effects of radiation are known. These are stochastic and deterministic effects [11, 35-36]. In living creatures, 70% of the damage to DNA can be caused by water radiolysis [44].

Before we discuss these effects, let's briefly look into the processes that occur during interaction of radiation with cells that cause these biological effects. The interaction of radiation with cells is usually considered to occur in the following four stages [11]:

1. The initial physical stage, lasting only an extremely small fraction (10^{-16}) of a second in which energy is deposited in the cell and causes ionization. In water, the process may be written as:

$$H_2O \xrightarrow{Radiation} H_2O^+ + e^-$$

Where H_2O^+ is the positive ion and e^- is the negative ion.

2. The physicochemical stage, lasting about 10^{-6} s, in which the ions interact with other water molecules, resulting in a number of new products. For example, the positive ion dissociates:

$$H_2O^+ \rightarrow H^+ + OH$$

The negative ion, that is the electron, attaches to a neutral water molecule, which then dissociates:

$$H_2O + e^- \rightarrow H_2O^-$$

$$H_2O^- \rightarrow H + OH^-$$

Thus, the products of the reactions are H^+, OH^-, H and OH. The first two ions, which are present to quite a large extent in ordinary water, take no part in subsequent reactions. The other two products, H and OH, are called free radicals, that is, they have an unpaired electron and are chemically highly reactive. Another reaction product is hydrogen peroxide, H_2O_2, which is a strong oxidizing agent formed by the reaction:

$$OH + OH \rightarrow H_2O_2$$

3. The chemical stage, lasting a few seconds, in which the reaction products interact with the important organic molecules of the cell. The free radicals and oxidizing agents may attack the complex molecules which form the chromosomes. They may, for example, attach themselves to a molecule or cause links in long-chain molecules to be broken.

4. The biological stage, in which the time scale varies from tens of minutes to tens of years depending on the particular symptoms. The chemical changes discussed above can affect an individual cell in a number of ways. For example, they may result in:

    (a) the early death of the cell or the prevention or delay of cell division; or

    (b) a permanent modification which is passed on to daughter cells.

Stochastic Effects are effects in which the probability of occurrence of the effect increases with dose. The effects include cancer induction and heritable effects in future generations. Deterministic effects which are nowadays termed as harmful tissue reactions are biological effects in which, above a certain threshold dose, the severity of the effects increase with increasing dose. The comparative whole body dose and its health effects are presented in Table 2 [45].

Table 2 Some comparative whole-body radiation doses and their effects [45].

Dose	Exposure and effects
2.4 mSv/yr	Typical background radiation experienced by everyone
1.5- 2.5 mSv/yr	Average dose to Australian uranium miners and US nuclear industry workers
Upto 5 mSv/yr	Typical incremental dose for aircrew in middle latitudes
9 mSv/yr	Exposure by airline crew flying the New York – Tokyo polar route
10 mSv	Effective dose from abdomen and pelvis CT scan
20 mSv/yr	Current limit (average) for nuclear industry employees and uranium miners
50 mSv/yr	Natural background levels in several places in Iran, India and Europe
50 mSv	Short-term allowable dose for emergency workers (IAEA)
100 mSv	Lowest annual level at which increase in cancer risk is evident (UNSCEAR). Above this, the probability of cancer occurrence (rather than the severity) is assumed to increase with dose. No harm has been demonstrated below this dose. Allowable short-term dose for emergency workers taking vital remedial actions (IAEA).
130 mSv/yr	Long-term safe level for public after radiological incident, measured 1 m above contaminated ground, calculated from published hourly rate x 0.6. Risk too low to justify any action below this (IAEA).
170 mSv/wk	7-day provisionally safe level for public after radiological incident, measured 1 m above contaminated ground (IAEA).
250 mSv	Allowable short-term dose for workers controlling the 2011 Fukushima accident.

250 mSv/yr	Natural background level at Ramsar in Iran, with no identified health effects. (Some exposures reach 700 mSv/yr.)
350 mSv/lifetime	Criterion for relocating people after Chernobyl accident.
500 mSv	Allowable short-term dose for emergency workers
680 mSv/yr	Tolerance dose level allowable to 1955 (assuming gamma, X-ray and beta radiation).
700 mSv/yr	Suggested threshold for maintaining evacuation after nuclear accident. (IAEA has 880 mSv/yr over one month as provisionally safe.
800 mSv/yr	Highest level of natural background radiation recorded, on a Brazilian beach.
1000 mSv Short-term	Assumed to be likely to cause a fatal cancer many years later in about 5 of every 100 persons exposed to it (*i.e.* if the normal incidence of fatal cancer were 25%, this dose would increase it to 30%).
1000 mSv Short-term	Threshold for causing (temporary) radiation sickness (Acute Radiation Syndrome) such as nausea and decreased white blood cell count, but not death. Above this, severity of illness increases with dose.
5000 mSv Short-term	Would kill about half those receiving it within a month. (However, this is only twice a typical daily therapeutic dose applied to a very small area of the body over 4 to 6 weeks or so.)
10,000 mSv Short-term	Fatal within a few weeks.

2.1.3. Basic principles of radiation protection and safety

The basic task of radiation protection consists of avoiding undue exposure of man and the environment to ionizing radiation [46]. International organizations such as the ICRP, IAEA, and ICRU developed recommendations on basic radiation safety for protection of humans and the environment against undue exposure of ionizing radiation. Many countries adapt such recommendations into their national laws to protect their citizens and environment from harmful effects of ionizing radiation.

The basic principles of radiation protection and safety are summarized below [47]:

- practice that entails or that could entail exposure to radiation should only be adopted if it yields sufficient benefit to the exposed individuals or to society to outweigh the radiation deteriment it causes or could cause (i.e. the practice must be justified);
-individual doses due to the combination of exposures from all relevant practices should not exceed specified dose limits;
- radiation sources and installations should be provided with the best available protection and safety measures under the prevailing circumstances, so that the magnitudes and likelihood of exposures and the numbers of individuals exposed be As Low As Reasonably Achievable (ALARA), economic and social factors being taken into account, and the doses they deliver and the risk they entail be constrained (i.e. protection and safety should be optimized);
- radiation exposure due to sources of radiation that are not part of a practice should be reduced by intervention when this is justified, and the intervention measures should

be optimized; the legal person authorized to engage in a practice involving a source of radiation should bear the primary responsibility for protection and safety;

- safety culture should be inculcated that governs the attitudes and behavior in relation to protection and safety of all individuals and organizations dealing with sources of radiation; in-depth defensive measures should be incorporated into the design and operating procedures for radiation sources to compensate for potential failures in protection or safety measures; and
- protection and safety should be ensured by sound management and good engineering, quality assurance, training and qualification of personnel, comprehensive safety assessments and attention to lessons learned from experience and research.

2.1.5. General uses of ionizing radiation

Radioisotopes and ionizing radiation have contributed tremendously to fulfill the need of mankind such as food, health and medicine, energy production, environmental protection, etc. In agriculture, ionizing radiation and radioisotopes are used in the nutritional studies of trace elements, mechanism of photosynthesis, plant protection including action of insecticides, metabolisms in plants, uptake of fertilizers, ions mobility in soils and plants and food preservation [48].

In medicine ionizing radiation is used in sterilization of medical equipment, new drug testing, medical imaging and therapy [49]. For example, over 80% of all new drugs are tested with radioactive tagging before approval. Approximately 10% of medical procedures use radiation to

treat a variety of diseases, including many types of cancers, heart disease, gastrointestinal, endocrine, neurological and other abnormalities within the body [48, 50].

In industry, radiation processing is an expanding technology with numerous applications in, for example, health care products sterilization, sewage and hospital waste treatment, polymer modification, and food processing. The effectiveness of such irradiation process depends on the proper application of dose and its measurement [2].

2.2. General principles of radiation detection and dosimetry

2.2.1. Effects of ionizing radiation on matter and dosimeter design

Radiation dosimeters are employed which use a wide range of different physical and chemical interactions to convert dose to a directly measurable quantity, such as electronic charge collected from air ionization or color change arising from changes in atomic electronic states. The range and complexity of the different physical and chemical effects that are routinely used for radiation detection make this subject both a delight and a challenge [51].

Therefore, whenever we want to detect or measure radiation we have to make it interact with some material and then study the resulting change in the system configuration. According to our present understanding, it is not possible to detect radiation or measure its properties without letting it interact with a measuring device. In fact, this can be stated as a universal rule for any kind of measurement. Even our five senses are no exception. For example, our eyes sense photons that strike cells on its retina after being reflected from the objects [40]. Without such interactions we would not be able to see anything [41]. For the detection of radiation, reliance

must be placed on detection devices which are based on the physical or chemical effects of radiation. These effects include: ionization in gases; ionization and excitation in certain solids; changes in chemical systems; and activation by neutrons [11]. Therefore, deep understanding of physical properties of the materials under the influence of radiation is vital for the effective design of devices for radiation-sensing applications [2].

The general principle underlying most methods of detection of nuclear radiation is that whatever the form of the radiation, it gives up part or all of its energy to the detecting medium either by ionizing it directly or by causing the emission of a particle, which in turn produces ionization in the medium [26]. Some of the processes involved in the detection of nuclear radiation are briefly discussed using semiconductors and inorganic solids as detector materials to illustrate the general principles of nuclear radiation detection. The various types of radiation detectors and their basic working principles will be covered in detail in later sections of this chapter.

When an energetic nuclear particle penetrates a semiconductor, it knocks many atoms out of their normal lattice position by its impact [42]. Most of these knocked-out atoms find their way back to normal lattice positions, but there are always a few lattice sites left vacant and perhaps a few atoms left in interstitial positions. If either of these lattice imperfections is capable of trapping either holes or electrons, it will have a marked effect on the electrical conductivity of the material. In germanium of moderate resistivity, it is observed that irradiation with high-energy particles always seems to produce electrically active p-type centers. This means that p-type material will lower its resistivity [42].

The predominant effect of radiation on inorganic solids is to displace atoms or ions, producing defects in the lattice structure. These defects are responsible for coloration of the samples and for changes in their physical properties, particularly electrical conduction. A lattice vacancy will be produced when an atom or ion is displaced and interstitial defect will be formed (if the atom or ion is trapped between the lattice planes). These defects may be produced by direct displacement or as a result of ionization. An electron can be readily trapped in an anion vacancy; this is known as F-center. It causes coloration and can be detected by electron spin resonance (ESR). The ESR spectra can provide information on the interaction of the trapped electron with the neighboring ions, and frequently several types of F-centers can be distinguished. These color centers and other radiation-induced defects in materials may be removed by annealing or ultraviolet light. Considerable annealing takes place with only a small temperature rise after irradiation at low temperatures, such as near a few Kelvins (K). At certain temperatures corresponding to defect or trap energies, strong luminescence is frequently observed [2]. Such luminescence phenomenon as a result of thermal annealing is the principle behind thermo- luminescence dosimetry.

2.2.1. Radiation exposure and absorbed dose

Radiation exposure (X) with its unit roentgen (abbreviated by R or r) was the first quantity to be defined. 1 R equals exposure due to X-rays or gamma-rays of such intensity that the electrons produced by this radiation in 1 cm^3 of dry air, at standard temperature and pressure, generate along their tracks electron-ion pairs carrying a total charge of 1 esu of either sign. The SI unit of exposure is defined as 1 C/kg air, without any new name proposed for it. Numerically,

$$1\ R = 2.58\ X\ 10^4\ C/kg\ air$$

The roentgen suffers from two limitations:

1. It was defined in terms of electromagnetic radiation only.
2. It was defined in terms of air only [39].

Since the ways photons interact with target materials are very different from other particles, such as neutrons or α-particles, therefore exposure has not been found to be very useful in characterizing damage due to other types of radiation [40]. For this reason, another unit was defined which was named absorbed dose [39].

Absorbed dose is a measure of energy deposition in any medium by any type of ionizing radiation. The original unit of absorbed dose was the rad, which was defined as an energy deposition of 0.01 joule per kilogram (J/kg). The unit of absorbed dose in SI units is the gray (Gy) and is defined as an energy deposition of 1 J/kg. When quoting an absorbed dose, it is important to specify the absorbing medium [11].

2.2.2. Radiochemical yield

Radiochemical yield of species x (G(x)) is defined as a number of molecules, ions, atoms or free radicals of product or dissolved reaction components for 100 eV of energy. Values of *G(x)* are influenced not only by the relative occurrence of ionizations and excitations among the primary products of interaction but also by the spatial proximity of the excitations and ionizations along the charged particle tracks, crudely described by the concept of linear energy transfer, LET, and by inter-track interferences [9]. One specific type of radiochemical yield is the G- value of dye molecule which is used as a part of a radiochemical dosimeter. It is defined as follows. The

radiation-chemical yield (G-value) is also defined as the number of moles of dye degraded by the absorption of 1 J of energy (unit: mol/J). The G-value can be calculated using Equation (14).

$$G(-dye) = \Delta A / D.\varepsilon.\rho.b(mol / J) \quad (14)$$

Where ΔA is absorbance change, D stands for radiation dose in Gy, ε stands for absorbitivity coefficient, ρ stands for density and b film thickness.

2.2.3. General properties of radiation detectors

The function of the detector is to produce a signal for every particle entering into it. Every detector works by using some interaction of particles with matter [36]. Some general properties that apply to all types of radiation detectors, basic definitions of detector properties, such as efficiency and energy resolution, together with some general modes of operation and methods of recording data that are helpful in categorizing detector applications can be found in references [12, 38, 44, 53 – 57].

2.2.4. Methods for characterizing radiation detectors

The interaction of ionizing radiation with matter can produce chemical, mechanical and physical modifications, since the resulting energy is higher than the atomic bonds. The changes occurring in the irradiated material can be correlated with the radiation dose; these changes characterize a radiation detector or dosimeter [58].

As was briefly explained in section 2.2.1 previously, the design of radiation detectors is based on the interaction of radiation with the detecting medium that gives up part of its energy resulting mainly in ionization of the detecting medium [2]. Besides ionization, the detector responds to the

ionizing radiation in various ways such as excitation, changes in chemical systems or activation by neutrons [11]. Therefore, radiation detectors can be characterized based on their responses to the ionizing radiation. Some of the methods used for characterizing radiation detectors are briefly discussed below.

2.2.5.1. Optical methods

Optical absorption analysis has widely proven to be an important and efficient tool in exploring and interpreting the various phenomena of electronic structures and processes in the materials subjected to radiation [59- 61]. Spectrophotometric and spectrofluorometric methods are commonly employed to evaluate dosimetric characteristics of various types of radiation detectors. Of these methods, UV-Vis spectrophotometric methods are routinely used for characterizing radiation detectors. The following examples show the application of UV-Vis absorption methods in characterizing radiation detectors.

UV-Vis spectrophotometric methods are used to characterize and evaluate dye solutions [62-63], radio-chromic gels [64-65], films [66] and polymers [67] for their possible use as ionizing radiation detectors. From the UV-Vis spectrophotometric measurements, response curves of absorbance change of irradiated samples (ΔA), percent of absorbance changes ($\%\Delta A$), logarithm of absorbance changes ($\log(\Delta A)$) are plotted against absorbed doses and evaluated for their dosimetric characteristics such as linearity, dose range, sensitivity and other parameters.

For example, the change in absorbance band of PPV derivatives has been employed as an indirect parameter to detect ionizing radiation (< 1 kGy) for radiotherapy [68]. Kahn et al

characterized aqueous solution of brilliant green spectrophotometrically for its applications in low dose food irradiation dosimetry. Absorption spectra of unirradiated and irradiated solutions were determined which showed two absorption bands with peaks at 427 and 626nm and a decrease in absorption as the radiation dose is increased. Radiation-induced bleaching of the dye was measured at wavelengths of maximum absorbance (427 and 626 nm) as well as at 550 and 570 nm. At all these wavelengths, the decrease in absorbance of the dosimeter was linear with respect to the absorbed dose from 20 to 120 Gy [69].

2.2.5.2. Electrical Methods

Radiation detectors such as gas ionization chambers [44] and semiconductors [37] are based on measurement of electrical parameters such as voltage or current as a function of radiation dose. The use of semiconductor materials as radiation detectors can result in a much larger number of carriers for a given incident radiation event than is possible with any other common detector type. Consequently, the best energy resolution from radiation spectrometers in routine use is achieved using semiconductor detectors. The fundamental information carriers are electron-hole pairs created along the path taken by the charged particle (primary radiation or secondary particle) through the detector. The electron-hole pair is somewhat analogous to the ion pair created in gas-filled detectors [12]. For example, the semiconductor detectors benefit from a small energy gap between their valence and conduction bands. Therefore, a small energy deposition can move electrons from the valence band to the conduction band, leaving holes behind. When an electric field is applied, the two charge carriers (electron and hole) drift and produce a signal [37].

Different materials [70-73] were investigated to evaluate their potential applications in radiation detection by studying their electrical responses such as current, conductivity, resistivity, and etc as a function of radiation dose. The following examples show applications of electrical methods for characterizing radiation detectors.

Applications of organic semiconducting material device sensors for determining ionizing radiation and detection based on changes in various electrical parameters were reported [74], wherein the change in conductivity of an organic material was measured as a function of ionizing radiation using an organic semiconductor-based resistor and an organic field-effect transistor (OFET). Ercan et al [75] investigated the effect of gamma radiation on the ac and dc conductivity of polypyrrole. The result of their studies shows a maximum ac and dc conductivities at 1.8 KGy dose. Sonkawade et al [76] investigated the effect of gamma and neutron irradiation on polyaniline. They studied the current voltage (I-V) characteristics using four-probe setup.

2.2.5. Classification of radiation detectors

Different types of detectors are known that are characterized by the nature of interaction of radiation with matter. The gas filled, scintillator, and semiconductor are the most commonly employed detectors for the detection of ionizing radiation. A brief discussion of each detector is presented below.

2.2.6.1. Gas-filled detectors

Gas filled detectors operate by utilizing the ionization produced by radiation as it passes through a gas. Such a counter consists of two electrodes to which a certain electrical potential is applied. The space between the electrodes is filled with a gas. Ionizing radiation, passing through the space between the electrodes dissipates part or all of its energy by generating electron-ion pairs. They are charge carriers that move under the influence of the electric field. This induces a current on the electrodes, which may be measured or through appropriate electronics, the charge produced by the radiation may be transformed into a pulse, in which case particles are counted individually [38].

The first type of counter (Figure 5a) is called current or integrating chamber; the second type (Figure 5b) is called pulse chamber. To get an idea of what charges and currents one might expect to measure, consider following representative example.

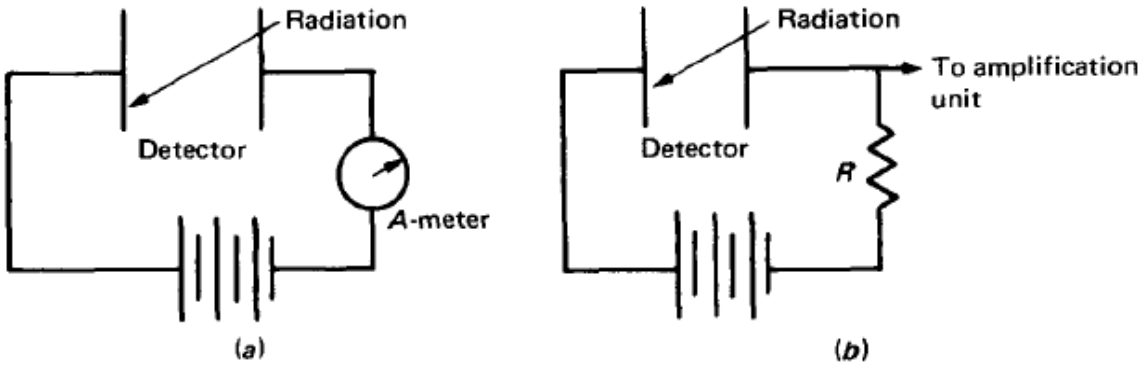

Figure 5 A typical gas-filled detector (a) the direct current produced in the circuit is measured; *(b)* individual pulses are detected [38].

For most gases, the average energy required to produce an electron-ion pair is about 30 eV. This number takes into account all collisions, including those that lead to excitation. If a 3-MeV alpha and beta particle deposits all its energy in the counter, it will produce, on the average, $\frac{3x10^6}{30} = 10^5$ electron-ion pairs.

A typical gas counter has a capacitance of about *50* pF, and the charge will be collected in a time of the order of 1 ps. If all the charge created by the 3-MeV particle is collected, the voltage and current expected are of the order of

$$V = \frac{Q}{C} = \frac{10^5 x1.6x10^{-19} C/el}{50x10^{-12} F} = 0.5x10^{-3} V = 0.5mV$$

$$I = \frac{Q}{t} = \frac{10^5 x1.6x10^{-19}}{10^{-6}} A \approx 1.6x10^{-8} A$$

In an ionized gas without an electric field, electrons and positive ions will move at random with an average kinetic energy equal to $\frac{3}{2}kT$, where k = Boltzmann's constant and T = temperature of the gas (Kelvin). When an electric field is present, both electrons and positive ions acquire a net velocity component along the lines of the electric field. There are types of gas counters in which the electric field is so strong that the electrons of the primary ionization acquire enough kinetic energy between collisions to produce new electron-ion pairs. These new charges constitute the secondary ionization. Primary and secondary ionization are generated within such a short period of time that they contribute to one and the same pulse [38]. To be able to generate high electric field, high voltage is applied in gas-field detectors. If the HV applied to the counter is steadily increased, the charge collected per unit time changes as shown in Figure 6.

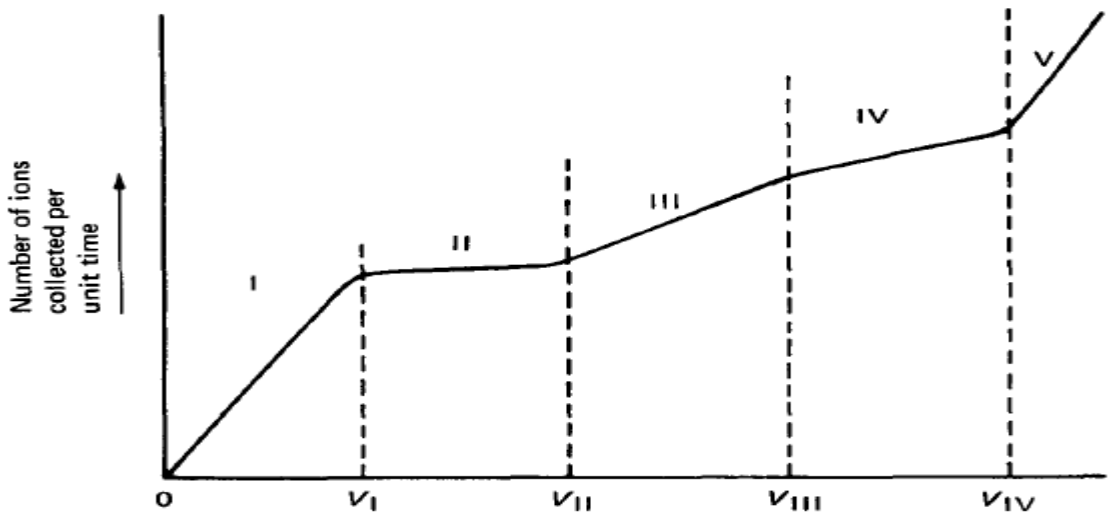

Figure 6 The relationship between voltage applied to the counter and charge collected [38].

The five regions indicated in the figure are explained in [38].

Region I When the voltage is very low, the electric field in the counter is not strong. Electrons and ions move with relatively slow speeds, and their recombination rate is considerable. As V increases, the field becomes stronger, the carriers move faster, and their recombination rate decreases up to the point where it becomes zero. Then, all the charge created by the ionizing radiation is being collected ($V = V_I$). Region I is called the recombination region.

Region II In region II, the charge collected stays constant despite a change in the voltage because the recombination rate is zero and no new charge is produced. This is called the ionization region. Ionization chambers operate in this region. The voltage applied is less than 1000 V.

Region III In this region, the collected charge starts increasing because the electrons produce secondary ionization that results in charge multiplication. The electric field is so strong, in a certain fraction of the counter volume, that electrons from the primary ionization acquire enough energy between collisions to produce additional ionization. The gas multiplication factor π, the ratio of the total ionization produced divided by the primary ionization-is, for a given voltage, independent of the primary ionization. Thus the output of the counter is proportional to the primary ionization. The pulse height at the output is proportional to the energy dissipated inside the counter; therefore particle identification and energy measurement are possible. Proportional counters work in this region. The voltage applied to proportional counters is in the range between 800 and 2000 V.

Region IV In this region, the electric field inside the counter is so strong that a single electron-ion pair generated in the chamber is enough to initiate an avalanche of electron-ion pairs. This avalanche will produce a strong signal with shape and height independent of the primary ionization and the type of particle, a signal that depends only on the electronics of the counter. Region IV is called the ***Geiger-Muller*** **(GM)** region. GM counters work in this region. The voltage applied to the GM counters is in the range from 500 to 2000 V.

Region V If the applied voltage is raised beyond the value V_{IV}, a single ionizing event initiates a continuous discharge in the gas, and the device is not a particle detector anymore. No gas counter should operate with voltage $V > V_{IV}$.

2.2.6.2. Scintillation detectors

A Scintillator is a material that exhibits luminescence upon irradiation by charged particles, neutrons, gamma rays, and X-rays. In a scintillator, the excitons transfer their energy to luminescent centers (fluors) that are intentionally introduced. The fluors release the energy radiatively, via a fluorescence or phosphorescence decay pathway. The resulting photons, typically in the visible wavelength range, escape the scintillator and are collected by a coupled photo-multiplier tube (PMT) or a photodetector to obtain information about the incident particles. A schematic diagram of a typical scintillation detector is shown in Figure 7.

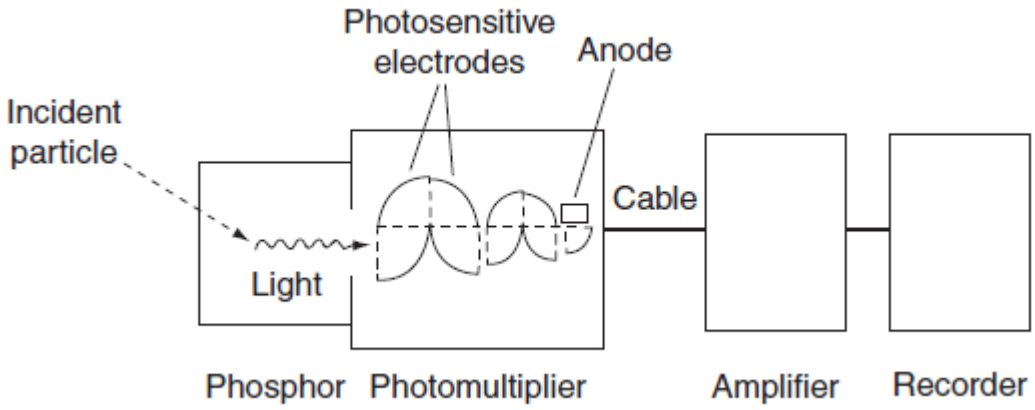

Figure 7 Scintillation detection system [77].

There have been a wide variety of materials studied and used for scintillation since the employment of ZnS for a-particle detection early last century. In 1948, PMTs were incorporated into detection systems that exploited the capability of scintillator materials [78]. The performance of a scintillator depends on several factors, including stopping power (absorption efficiency of the incident radiation), photoelectric generation, proportionality, internal quantum

efficiency, transparency, decay time, light yield, emission wavelength, stability and physical form [79- 80]. These parameters are taken into account in three stages during the process of photon generation upon irradiation [81].

First, an incident ionizing particle collides and deposits its energy in the material. Here high stopping power is required to absorb incident energy as much as possible. The selection of materials for high stopping power depends on the radiation to be detected. For gamma rays, high material density and large-size are essential. When a gamma ray photon collides with matter, the photoelectric effect ratio is proportional to the 4^{th} to 5^{th} powers of the atomic number (Z), and as such high-Z is required for high energy resolution.

In the second step, the deposited energy is transferred to luminescent centers to generate visible photons. There are three parameters to be considered: internal quantum efficiency, decay time of the luminescent centers, and proportionality. High quantum efficiency ensures that more photons are generated. It is closely related to the electronic configuration of the species, and is influenced by its surrounding as well. Decay time depends on the luminescent center as well, which largely determines the response time and counting rate of a scintillator. Proportionality, or converting linearity, is the uniformity of light output under different irradiation energies, which affects the eventual energy resolution.

In the last step, the generated photons transport through the material and escape from the surface. The scintillation material has to be transparent to the emitted photons, and scattering is not favored. Light yield is thus obtained by measuring the number of photons produced per MeV of

radiation energy during the whole process. In general, high light yield is indicative of high sensitivity and also of high energy resolution.

Scintillators often have modest energy resolution compared to semiconductor detector materials. In semiconductors, information carriers are electrons and holes that originate from excitons, which are generated upon irradiation within an electrical field. This concerns energy resolution of semiconductors in two ways; first, the energy required to create an electron and hole- pair is roughly three times the band gap of the detector material, which is in the range of several eV. As a comparison, the energy consumed to create a scintillation photon (the information carrier in scintillators) comes to several tens of eV. Assuming the same carrier collection efficiency for a given irradiation, the maximum theoretical light yield of semiconductors should be 10 times greater than that for scintillators. Second, the intrinsic variance of a semiconductor signal upon irradiation is far smaller than for scintillator signals [81].

Sodium iodide doped with thallium, NaI(Tl) has been the significant scintillator since its discovery in 1948 [82]. The photoelectric peak can be readily observed in the NaI(Tl) spectrum, which is considered to be a landmark in gamma ray spectroscopy [83]. The emission spectrum of NaI(Tl) peaks at 415 nm, and under the irradiation of ^{137}Cs (662 keV gamma ray) the light yield is 38 000 photons/MeV, and the energy resolution is less than 6%. NaI (Tl) is attractive due to a combination of low material cost, acceptable energy resolution, and ease of fabrication, but it is hygroscopic, and is usually sealed with stainless steel, which could limit the sensitivity of detecting low energy particles.

A number of new inorganic scintillators have been developed and optimized, including bismuth germanate (BGO), gadolinium orthosilicate (GSO), caesium iodide (CsI), yttrium aluminum perovskite (YAP), and lutetium aluminum perovskite (LuAP) though none of these has reshaped the landscape of the field of gamma ray detection dominated by NaI(Tl).

However, recently developed $LaBr_3$(Ce) scintillators may eventually replace NaI (Tl) for spectroscopic identification. This lanthanide compound is 1.5 times denser than NaI (Tl), with a light yield of 63 000 photons/MeV, almost twice as much as that of NaI (Tl). The reported energy resolution achieves 2.9% for 662 keV gamma- radiations [83]. $LaBr_3$ (Ce) has a decay time of 26 ns, which is sufficient to match the electric circuit frequency for relative high flow detection. The blue-shifted emission peak at 380 nm matches well the sensitivity peak of most PMTs. A few other cerium-activated lanthanide halides also show promising results [84- 85]. LuI_3 (Ce) has a reported light yield of 95 000 photons/MeV. Other iodides, selenides, and tellurides have also been proposed, and their smaller band gaps may help to obtain even higher light yields. The main challenge with the lanthanides is the difficulty in growing large-size crystals. The crystals also have drawbacks such as anisotropy in thermal and mechanical properties and hygroscopicity.

Scintillation processes in polymers differ from inorganic semiconductors in many ways. One important difference is the fact that the scintillation processes in these materials takes place in two steps called primary and secondary processes. In the primary step ionizing radiation is absorbed to produce excited states, and these excited states decay to the ground state via various

pathways in the secondary step. To follow the course of energy transfer, it is preferred to regard the primary step as the energy deposition process, and the secondary step as the energy release process.

When an irradiated particle traverses through a plastic scintillator, it undergoes the following process: first, energy deposition takes place to generate excitation of π-electrons in conjugated system in less than 0.1 picoseconds. After fast internal energy degradation in less than 10 picoseconds, excitations are mainly transferred to luminescent centers, which overwhelm all competing processes in the polymer matrix. This follows the Forster energy transfer mechanism with a probability of about 0.7 [85]. In the next several nanoseconds (or possibly longer) excitations in luminescent centers relax by emitting photons with a quantum efficiency of around 0.7. The detailed discussion of the process can be obtained in [86].

2.2.5.3. Semiconductor detectors

In a semiconductor detector, an electric field is applied to disassociate the electron-hole pairs and sweep the electrons and holes to the positive and negative electrodes, respectively. The resulting photocurrent is recorded to analyze the energy of the incident high-energy radiation particles [87]. Figure 8 shows a schematic diagram of typical semiconductor p-n type radiation detector.

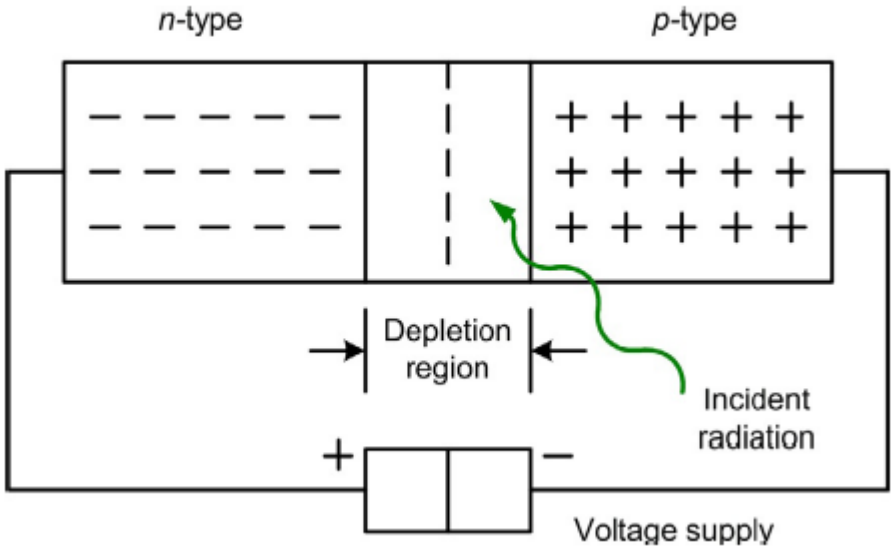

Figure 8 Solid state semiconductor p-n junction detector [77].

In 1945, Van Heerden observed the conductivity change of silver chloride crystals upon irradiation at low temperatures, and this observation triggered the exploration of new materials with an electrical response to radiation. In 1949, an elemental semiconductor (germanium) based detector was demonstrated to produce each electron- hole pair with less than 3 eV [88]. In 1956, a germanium based detector with an active area of 6 mm^2 was fabricated to obtain an energy resolution of 12% for α-particles [89]. Alongside the rapid progress of the semiconductor industry, semiconductor crystal growth technology was greatly advanced in the 1970's. Germanium single crystals with high purity (one part in 10^{12}) and large volumes became available. Detectors based on these high purity germanium (HPGe) single crystals were reported to produce an outstanding energy resolution below 0.25% at cryogenic temperatures for 662 keV gamma ray radiation, which remains the best spectroscopic resolution so far [90]. The low bandgap of germanium (0.70 eV) is beneficial for the generation of large numbers of charge

carriers per MeV radiation; on the other hand, the low band gap also leads to severe thermal fluctuation at room temperature. Therefore, the HPGe based detectors require auxiliary cooling with liquid-nitrogen. In addition, these elemental semiconductors (i.e. germanium and silicon) have low atomic number, relatively low density, and low radiation hardness necessary for certain applications.

Compound semiconductors provide several advantages over their elemental counterparts. They have band gaps ranging from 1.3–2.6 eV, average atomic numbers from 30–80 and a wide range of physical properties tunable for application needs [91]. This group includes both binary materials derived from elements in group II–VI and group III–V, as well as ternary and higher order compounds. Among the varieties, cadmium zinc telluride (CZT) and mercury iodide (HgI_2) have been used in commercial radiation detectors. Detectors based on CZT 1 cm^3 in size have a reported energy resolution less than 1% at room temperature for 662 keV gamma radiations [92]. There are still barriers for wide deployment of these semiconductor detectors, particularly the difficulty in growing large-size, high-quality crystals. Micro-crystallinity, high defect densities, impurities, and stoichiometric imbalances are all detrimental to detector resolution. These limitations prompt the desire to develop new alternative materials [93].

2.3. Dosimeters

A dosimeter is a device that provides a reading, R, which is a function of the dose absorbed in its sensitive volume. The dose in the dosimeter is related to the dose deposited in the surrounding

medium. Dosimetry is the determination of radiation dose or a related radiological quantity that results from the interaction of ionizing radiation with matter.

2.3.1. Working principles

The extensive use of radiation in many fields has prompted the development of the field of radiation dosimetry. Originally the emphasis was on determining the integrated dose received by a person working in a radiation intensive environment with the intention to limit the exposure for personal safety. However, the discovery that radiation may also affect materials to the point that they become unusable, has stretched the applicability of this field to industrial and research purposes [41]. The working principles of radiation dosimeters vary depending on the type of radiation and application. Therefore, there is a multitude of established dosimetric methods and some of them are listed in Table 3 [94].

Table 3 Examples of dosimetry systems [94].

Dosimeter Type	Type of Readout	Examples	Absorbed Dose Range (Gy)
Calorimeters	Temperature measurements	Graphite, water, polystyrene	10^1- 10^4
Radiochromic films	Spectrophotometers	Dyed and clear plastic films	10^0- 10^6
Inorganic crystals	EPR spectra	LiF, SiO_2	10^3- 10^7
Organic crystals	EPR spectra	Alanine, sucrose, cellulose	10^0- 10^5
Chemical solutions	Spectrophotometers	Cerric-cerrous, organic acids	10^2- 10^5
Semiconductors	Electrical measurements	Si-diodes	10^0- 10^4

2.3.1. Important characteristics of dosimeters

Radiation dosimeters are defined by some important characteristic properties. Some of these important characteristics are discussed below.

2.3.2.1. Detection limit

The detection limit (also called limit of detection (LOD) or limiting detectable concentration) is usually defined as the smallest concentration or mass which can be detected with a specified level of confidence [95]. The LOD is taken as the lowest concentration of an analyte in a sample

that can be detected, but not necessarily quantified, under the stated conditions of the test [96] and can be mathematically stated as:

$$DL = \frac{FxSD}{b} \quad (15)$$

where F = factor of 3.3, SD: Standard deviation of the blank, standard deviation of the ordinate intercept, or residual standard deviation of the linear regression and *b* is slope of the regression line.

In radiation detection, the quantity to be measured could be optical density (absorbance) or current or voltage or other optical or electrical parameter.

2.3.2.2. Pre-irradiation shelf life

Pre-irradiation shelf life of dosimeters is a useful parameter for evaluating the feasibility of a dosimeter. For a dosimeter to be feasible, it has to have long pre-irradiation shelf life. It can be determined by applying spectrophotometry, spectrofluorometry and other methods. Useful parameters such as absorbance change (ΔA) and absorbance change per film thickness (ΔA/t) as a function of time of storage are often used to evaluate the pre-irradiation shelf life of a dosimeter.

For example, Akhtar et al [97] evaluated the pre-irradiation shelf life of Methylene blue-polyvinyl alcohol radiochromic film spectrophotometrically. In their studies they used ratio of absorbance change per film thickness as a function of time of storage. They found that the film was stable in a dark for 30 days while the film stored in light was found to show slight decrease

in stability. Similarly, Khan et al [66] investigated dosimeteric characteristics of aqueous solutions of brilliant green. To observe any changes in the absorption due to storage time, they studied the absorption spectra at different time intervals after the preparation of solution. No spectral changes in the solution were observed for a storage period of about 60 days in dark and up to 40 days under white fluorescent light inside the laboratory. However, the solution was unstable in direct sunlight and significant changes in absorption spectra were observed even after 30 min exposure to direct sunlight. The results of their studies suggest that the stock solution of brilliant green at its natural pH (4.1) can be used up to 40 days and for daily experiments fresh solution preparation is not necessary.

2.3.1.3. Post –irradiation stability

Post –irradiation stability of a dosimeter is another useful parameter employed to characterize dosimeters. Its merits lie especially in keeping records of dose measurements. Evaluation of post-irradiation stability is also based on absorbance change or absorbance change per unit thickness as a function of storage time as explained previously in section 2.3.2.2.

Kattan et al [98] investigated the effect of storage conditions on the post-irradiation stability of polyvinyl chloride dyed with malachite green. Two batches of three replicates were irradiated with 100 kGy and kept at room temperature at two conditions, one in darkness and the other in day light. Measurements at 628 nm were carried out periodically during the period of storage. Figure 9 shows the change of absorbance during storage. From their studies, it was noticed that the irradiated films had a good stability in darkness, and the change of absorbance during the

storage had stability within 2% of absorbance change. Whereas, the change of absorbance after irradiation during the storage in day light was very clear during 2 weeks of storage.

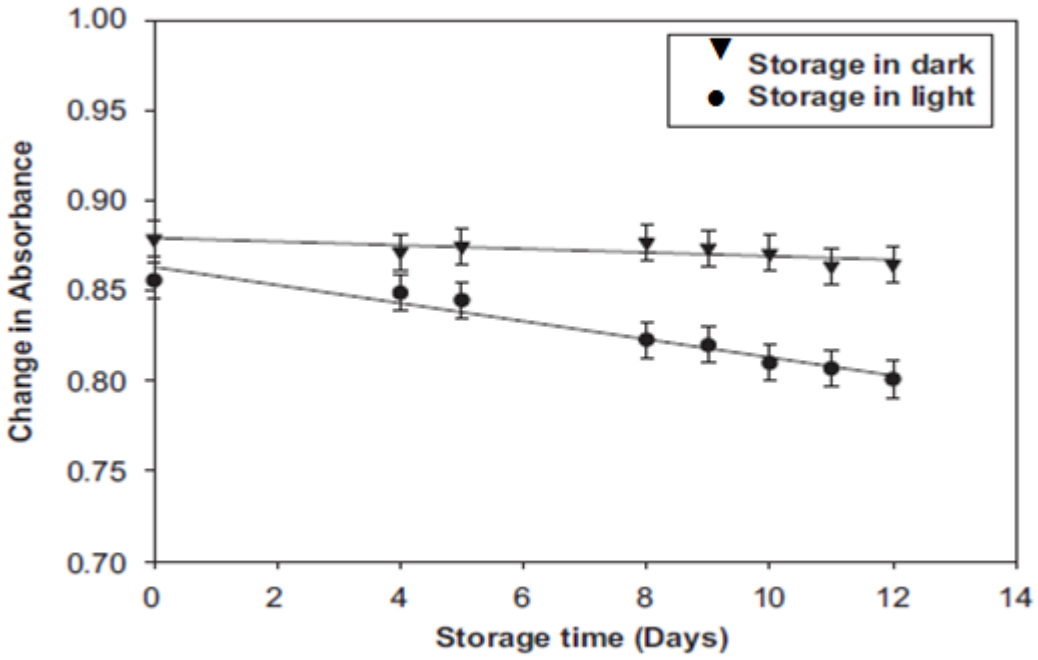

Figure 9 Post-irradiation stability of PVC dyed films in dark and indirect daylight at ambient temperature absorbed dose [98].

Other investigators [99 - 102] used spectrophotmetric responses to evaluate post irradiation stabilities of dosimeters.

2.3.1.4. Dose rate independence

For a dosimeter to be useful, the measured dosimetric quantity should be independent of the dose rate. Ideally, the response of a dosimetry system M/Q at two different dose rates $((dQ/dt)_1$ and $(dQ/dt)_2$ should remain constant. M stands for the measured dosimetric quantity and Q stands for the radiation dose. In reality, the dose rate may influence the dosimeter readings and appropriate corrections are necessary, for example recombination corrections for ionization chambers in pulsed beams [11]. Kattan et al [103] investigated the dose rate effects on the polyvinyl chloride (PVC) dyed with bromocresol purple (BCP) for high dose radiation dosimetry applications. The results of their studies show that films of PVC dyed with bromocresol purple were not affected by dose rate. Al Zahrany et al [104] studied methyl red (MR) dyed polyvinyl butyral (PVB) films for dosimetric applications spectrophotometrically. They evaluated the dose rate effects on the MR-PVB film dosimeters at two dose rates (11.98 kGy/hr and 1 kGy/s). The results of their studies show that no significant effect resulted due to dose rate on the response of the dosimeter films. Other similar study was done by Basfar et al [105] on nitro- blue tetrazolium- polyvinyl butyral (NBT-PVB) film dosimeter. They evaluated the effect of dose rate on the response of NBT-PVB film dosimeter by using a dose rate of 11.98 kGy/hr from a ^{60}Co source and an electron beam accelerated dose rate of 15 kGy/s. They found that the dose rate has no significant effect on the dose response of the dosimeter.

2.3.1.5. Energy Independence

The response of a dosimetry system M/Q is generally a function of radiation beam quality (energy). Since the dosimetry systems are calibrated at a specified radiation beam quality (or qualities) and used over a much wider energy range, the variation of the response of a dosimetry system with radiation quality (called energy dependence) requires correction. Ideally, the energy response should be flat (i.e. the system calibration should be independent of energy over a certain range of radiation qualities). In reality, the energy correction has to be included in the determination of the quantity Q for most measurement situations [102]. Vandecasteele et al [106] studied the radio-physical properties of radiochromic leucodye gel dosimeters. They investigated the energy dependence of two leucodye gel dosimeters LMD1 (prepared from a gelling agent gelatin), a leucodye-leuco malachite green (LMG), a radiation sensitizer (trichloroacetic acid (CCl_3COOH)) and a surfactant (Triton X-100) all dissolved in de-ionized water) and LMD2 (its composition: gelatin, $CHCl_3$, SDS, CCl_3COOH, LMG and deionized water), using 6 MV and 18 MV clinical linear accelerators at 30 Gy and 10 Gy doses. Their studies show no energy dependence for LMD1- or LMD2-type dosimeters for photon energies of 6 and 18 MV.

2.3.1.6. Dose response linearity and sensitivity

Dose response linearity

Ideally, the dosimeter reading M should be linearly proportional to the dosimetric quantity Q. However, beyond a certain dose range a non-linearity sets in. The linearity range and the non-linearity behaviour depend on the type of dosimeter and its physical characteristics [97]. The

linear portion of the dosimeter is taken as the working range. Two typical examples of response characteristics of dosimetry systems are shown in Figure 10. Curve A first exhibits linearity with dose, then a supralinear behaviour, and finally saturation. Curve B first exhibits linearity and then saturation at high doses [103].

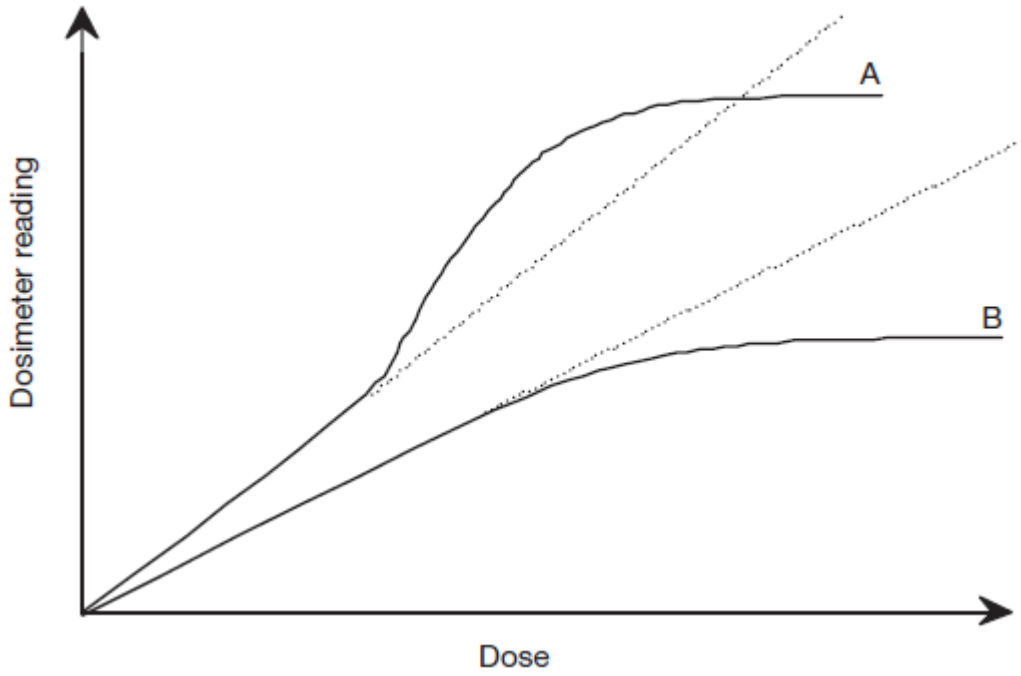

Figure 10 Response characteristics of two dosimetry systems, Curve A first exhibits linearity with dose, then supralinear behavior and finally saturation. Curve B first exhibits linearity and then saturation at high doses [103].

Dose response sensitivity

In section 2.2.4.4, it was stated that sensitivity is defined as the ratio of incremental change in the output of the detector to its incremental change of the measurand in input [52]. Routinely,

sensitivity of radiation dosimeters is evaluated from slopes of a calibration curve versus radiation dose as used in [55]. Some researchers used slopes of dose response curve to evaluate sensitivities of radiochromic films. For example, Abdel-Fattah et al investigated the dosimetric characteristics of radiochromic polyvinylbutyral film containing 2,4-hexadiyn-1,6-bis(n-butylurethane) (HDDBU) to form a dosimeter for industrial irradiation facilities. They evaluated the sensitivity of the radiochromic film based on values of slope obtained from absorbance change *versus* radiation dose curve. The sensitivity of the films to radiation doses, expressed as the slope of the dose response curve, increases linearly with the HDDBU concentration. They showed that the film with 15 phr of HDDBU is approximately 2.4 times more sensitive than the film with 5 phr of HDDBU [102]. The dose response sensitivity of dosimeters differs from one application to another. For example, for diagnostic applications, systems which can measure absorbed doses on the order of 10 mGy are required, while for therapy applications, sensitivity at the 1 Gy level is sufficient. For radiation protection applications sensitivities at the 0.1 mGy level are desirable [10].

2.3.1.7. Dose response reproducibility and repeatability

Dose response reproducibility

The reproducibility of the measurements of radiation dose under similar conditions can be estimated from the data obtained in repeated measurements. In radiation dosimetry, precision is specified by the dose response reproducibility. High precision or reproducibility is associated

with a small standard deviation of the distribution of the measurement results [103]. The percent relative standard deviation (% σ) is calculated using methods in the literature [108] as:

$$\% \sigma = \frac{SD}{\overline{X}} x100\% \quad (16)$$

The dose response reproducibility of dosimeters is evaluated by calculating the relative standard deviation of replicate dosimeters under different radiation doses. The following example illustrates how reproducibility of dosimeters is determined.

Rabaeh et al [108] evaluated the reproducibility of three sets of 5 mM nitro blue tetrazolium – polyvinyl alcohol (NBT-PVA) film dosimeters prepared separately and irradiated to different doses as presented in Table 4. The results of their studies demonstrated that the absorbance has good precision values with standard deviation values ($\sigma \leq 4\%$), indicating that the film preparation has a good degree of reproducibility for radiation processing industry.

Table 4 Absorbance of NBT-PVA films with precision values [108].

	Absorbance (a.u) for different doses		
Film no.	5 kGy	15 kGy	40 kGy
1	0.498	2.320	7.800
2	0.530	2.420	7.410
3	0.524	2.510	7.640
Average	0.517	2.417	7.617
S.D	0.017	0.095	0.196
Precision (%)	+3.3	+3.93	+2.6

Dose response repeatability

Repeatability is measurement results under repeatability conditions where independent measurement results are obtained with the same method on the identical test items in the same laboratory by the same operator using the same equipment within short intervals of time [109]. The relative standard deviation (% σ) is calculated using Equation (16). The results of measurements are considered to be of good precision if the relative standard deviation is less than 5 %.

2.3.1.8. Useful Dose range

Useful dose range of dosimeters are obtained from dose response plots such as absorbance (A), absorbance change (ΔA), ratio of absorbance change to absorbance of control sample ($\Delta A/A_0$),

log (A), log(ΔA), log ($\Delta A/A_0$), -log(A), -log(ΔA), -log ($\Delta A/A_0$) *versus* radiation dose (D). The linear portion of the dose response plots is considered as the useful dose range. In Figure 10 above, the linear portions of both dosimeters A and B are taken as the useful dose range.

For example, Kahn et al [69] studied aqueous brilliant green solution for high dose dosimetry applications. They plotted absorbance against absorbed dose and showed linearity with the absorbed dose up to 120 Gy at all the wavelengths and then some deviation from linearity was observed. However, when negative logarithm of the absorbance (-log A) was plotted *versus* absorbed dose, a linear response was observed up to 200 Gy as shown in Figure 11 for all four wavelengths. Therefore, their studies show that the dosimetric solution can be used in the dose range of 20 – 200 Gy. This low-dose range covered by the brilliant green solution was found to be useful for dosimetric applications in the inhibition of sprouting in vegetables, such as onion, potatoes and garlic.

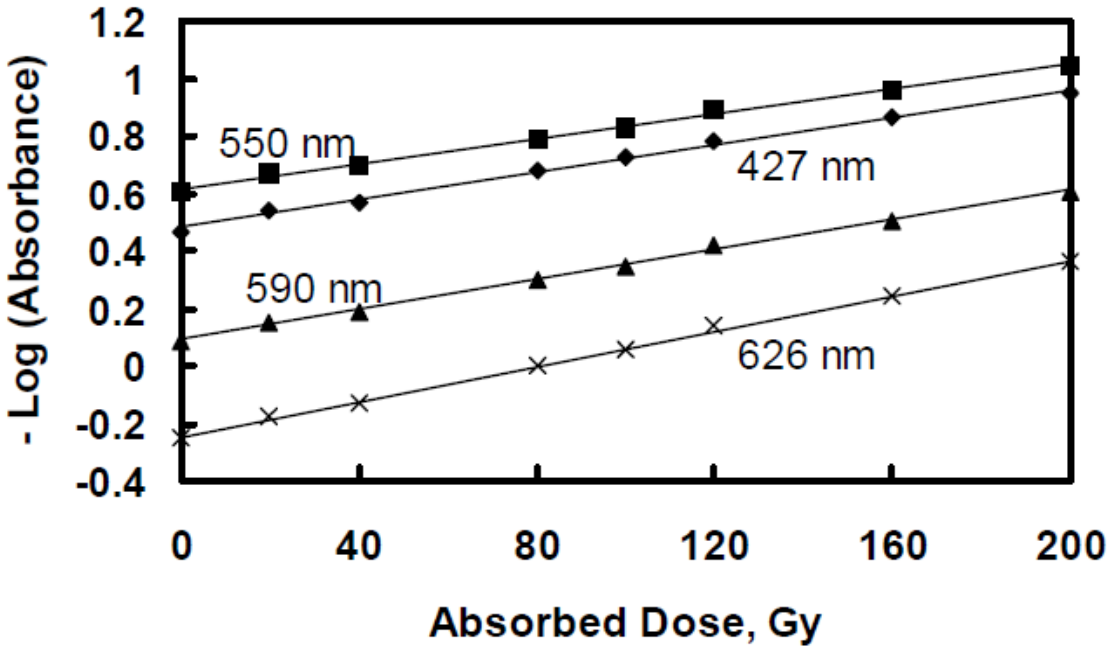

Figure 11 Radiation response function (in terms of negative logarithm of absorbance) versus absorbed dose in water for 25 mmol L^{-1} aqueous solution of brilliant green measured at 427, 550, 590 and 626 nm [69].

2.3.1.9. Ruggedness, robustness and cost effectiveness

Ruggedness of dosimeters

A rugged dosimeter is relatively independent to changes in experimental conditions such as temperature, acidity, reaction time etc [110]. Ideally a dosimeter should be rugged. Since practically it is not possible to get a dosimeter which is not affected by external changes such as moisture, light, temperature and other factors, usually methods are devised to control these parameters so as to use the dosimeter.

In some applications it is desirable to use the dosimeter in liquid water and in others one might want to deform the dosimeter by wrapping it around some object. For radiochromic film dosimeters, the ability to cut the film to a desired size without undue damage or loss of sensitivity near the cut edges is also highly desirable [111].

Robustness of dosimeters

A robust dosimeter is relatively free of chemical interferences [110]. Ideally a radiation dosimeter should be robust. In practice, it is not easy to get a dosimeter which is not affected by chemical interferences. Therefore, identifying and controlling chemical interferences is a commonly employed technique in the development of radiation dosimeters.

Cost effectiveness

Low cost radiation dosimeters are highly needed in various applications such as industry, health, particle physics research, and others. Dosimeters that require a reader or a laboratory facility for data processing are not highly needed because of cost ineffectiveness.

2.3.2. Calorimeter dosimeters

Calorimeter dosimetry is perhaps the most direct physical measurement of absorbed dose, and works on the assumption that all energy imparted by ionizing radiation ultimately leads to temperature rise and expressed by the Equation 17 [10]:

$$D_m = c_m \Delta T_m \tag{17}$$

where c_m is the specific heat capacity of the absorbing medium and ΔT_m is the temperature rise resulting from the absorbed dose D_m. A clear advantage of calorimeter dosimetry over other measurement techniques is the fact that calorimeter calibration can be carried out based entirely on quantities that do not require a reference ionizing radiation field (e.g. electrical power and temperature). However, measurement of the extremely small temperature rises required (typically μK) is challenging, requiring highly stable measurement conditions. Calorimeter dosimetry is therefore not practical for routine measurement in medicine, but is widely used in standards laboratories, where the direct physical connection between absorbed dose and temperature rise make it an obvious choice for a primary standard. Primary absorbed dose standards for dosimetry of high-energy photon beams are reviewed in [112 - 114].

2.3.3. Chemical dosimeters

Chemical dosimeters are systems in which measurable chemical changes are produced by ionizing radiation. Many molecules dissociate by radiation, but only a few can be used as dosimeters, mainly due to calibration problems. The reactions taking place in chemical dosimetry have two steps, a very fast ($10^{-11} - 10^{-10}$ s) ionization by interaction of energetic charged particles and a chemical reaction according to the chemical kinetics. Radiation produces acids in the system, the amount of which can be determined from visible color changes or, more accurately, by titration or pH readings [2]. The most commonly used chemical dosimeter called the Fricke dosimeter is briefly discussed below.

The Fricke dosimeter, also known as ferrous sulphate dosimeter, is an optical density sensor. It is a secondary standard chemical dosimeter based on the change in oxidation state from ferrous ions to ferric ions [115]. The Fricke dosimeter consists of an aerated dilute solution of ferrous sulfate in 0.8 *N* sulfuric acid: 0.001 *M* $FeSO_4$ or $Fe(NH_4)_2(SO_4)_2$ + 0.8 N H_2SO_4 air saturated [116]. This solution is glass-sealed, and the absorbance of light is read by a spectrophotometer. The maximum absorbed radiation dose is reached when all ferrous ions are converted into ferric ions.

2.3.4. Optically stimulated luminescence dosimeters (OSLDs)

A newer luminescence signal readout method called optically stimulated luminescence dosimeter (OSLD) is based on optical rather than thermal stimulation to release charge carriers from trapping centers. The use of light from a laser source rather than heat to stimulate the release of the trapped charges allows for significant versatility and flexibility compared to thermal stimulation. Some examples are [12]:

1. The use of multiple stimulation time profiles such as constant stimulation intensity, pulsed or ramped stimulation schemes;
2. Different wavelengths of excitation to selectively empty certain trapping centers (TCs) while leaving others populated with charges;
3. Rereading of the dosimeter following partial emptying of the TCs with low-power stimulation;
4. Remote reading of the dosimeter using optical fibers to guide stimulation light to, and luminescence from, the dosimeter;

5. Position-sensitive measurements.

Their principle of operation is very similar to TLDs, except that trapped charge is released by controlled illumination instead of heating [117].

2.3.5. Thermoluminescence dosimeters (TLDs)

Thermoluminescent dosimetry uses materials that trap the charge-formed ionization electron/hole pairs in metastable states within the crystal. A very common material used is lithium fluoride doped with Mg and Ti (LiF: Mg, Ti), which is supplied in a range of shapes and sizes, including 1 mm diameter rods and 3.2 mm × 3.2 mm 'chips' with a range of thicknesses. Alternative materials have also been used, including CaF_2: Mn and LiF: Mg, Cu, P, the latter being preferred by some laboratories for environmental and personal dosimetry due to its improved linearity and reproducibility compared with LiF: Mg, Ti [118 - 119].

Many crystalline materials exhibit thermoluminescence. Light is emitted when the material is heated after the exposure to radiation. Electron and hole traps are filled during radiation exposure (solid-state ionization effect); heating frees electrons and holes from these traps. Light is emitted when the electrons and holes recombine. The emitted light is a characteristic of the material and a function of temperature. The plot of light output *versus* temperature is known as the glow curve for that particular material. A schematic *glow curve* of phosphor material is shown in Figure 12 [2].

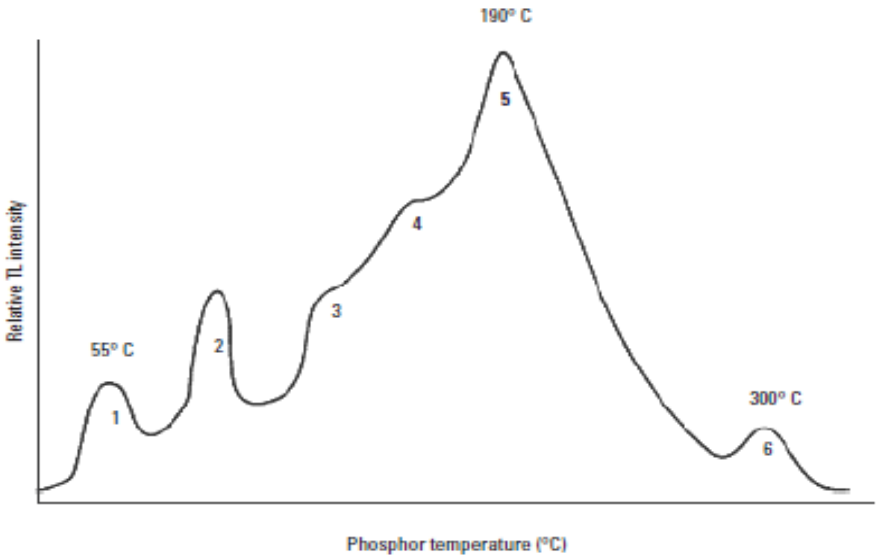

Figure 12 A schematic glow curve of a phosphor material [26]

2.3.6. Radiochromic dosimeters

Radiochromic effects involve the direct coloration of a material by the absorption of energetic radiation without requiring latent chemical, optical, or thermal development or amplification [2]. The historical background, types and medical and environmental applications of radiochromic dosimeters are briefly discussed below.

2.3.7.1. Historical background

Radio-chromic dosimeters (material that turns color due to a radiation-induced chemical changes) have a long history in the field of ionizing radiation dosimetry [10]. An early unit of radiation exposure was the “erythema dose”, defined as the amount of ionizing radiation required to produce visible reddening of the skin of the hand or arm. This unit soon gave way to other, more reproducible (not to mention less harmful) quantification methods, however, the use of a

detector which gave a visible, colorful indication of dose remained popular. A very early radiochromic process, first demonstrated in 1826 by Niepce [120] involved an unsaturated hydrocarbon polymeric mixture based on bitumen that cross links upon irradiation, leaving a light-scattering pattern. Many radiation cross-linking organic systems have subsequently been used for radiographic imaging [121 - 123].

In the early part of the 20th century, barium platinocyanide pastille discs were used along with color wheels to quantify absorbed dose in terms of fractions and multiples of the erythema dose [124]. With commencement of time, radiochromic dosimeters that do not require processing were developed especially for high dose applications [125]. However, in recent times new radiochromic film dosimeters that are more sensitive for low doses have emerged and are finding wider acceptance in medical dosimetry [126]. Further greater sensitivity for imaging and personnel occupational dosimetry is a requirement [127]. Therefore, the search for more sensitive, rugged, and cost effective radiochromic dosimeters is still going on. Recent reports [111, 127-129] show that developing radiochromic dosimeters from a variety of materials such as dyes and polymers for medical, industrial, high energy physics and other related applications is an area of active research.

2.3.7.2. Types of Radiochromic dosimeters

Polymer-based radiochromic dosimeters

Irradiation of polymers causes structural and chemical variations, which in turn lead to the variations in physical properties. Radiation-induced changes in optical properties of a number of

polymers have been investigated for dosimetry applications, including cellulose triacetate [130], diacetylene Langmuir-Blodgett films [131], polyaniline nanofilms [132], and tetrafluoroethylene-per-fluoromethoxyethylene (PFA) and tetrafluoroethylene-hexa-fluoropropylene (FEP) thin films [133]. A comprehensive review of optical properties of 17 different polymers under irradiation can be found in reference [134]. Some polymer-based radiochromic dosimeters are based on conversion of their monomers to colored polymers upon exposure by ionizing radiation. For example, conjugated diacetylene monomers are radiation-sensitive materials. When irradiated in the crystalline state, they undergo a topochemical polymerization (1, 4-addition reaction) to form intensely colored fully conjugated polydiacetylenes [135 - 139]. The color of polydiacetylenes stems from the extensive delocalization of π-electrons along π-conjugated polymer chains. The color intensifies progressively with increasing absorbed dose [140 - 141]. Figure 13 (a–c) shows a diagram of topochemical polymerization of π-conjugated polydiacetylene under ionizing radiation in the crystalline state [139 - 140]. However, there is also cross linking in the non-crystalline state, as shown in Fig. 13 (d and e) [140]. However, there is also cross linking in the non-crystalline state, as shown in Fig. 13 (d and e) [140].

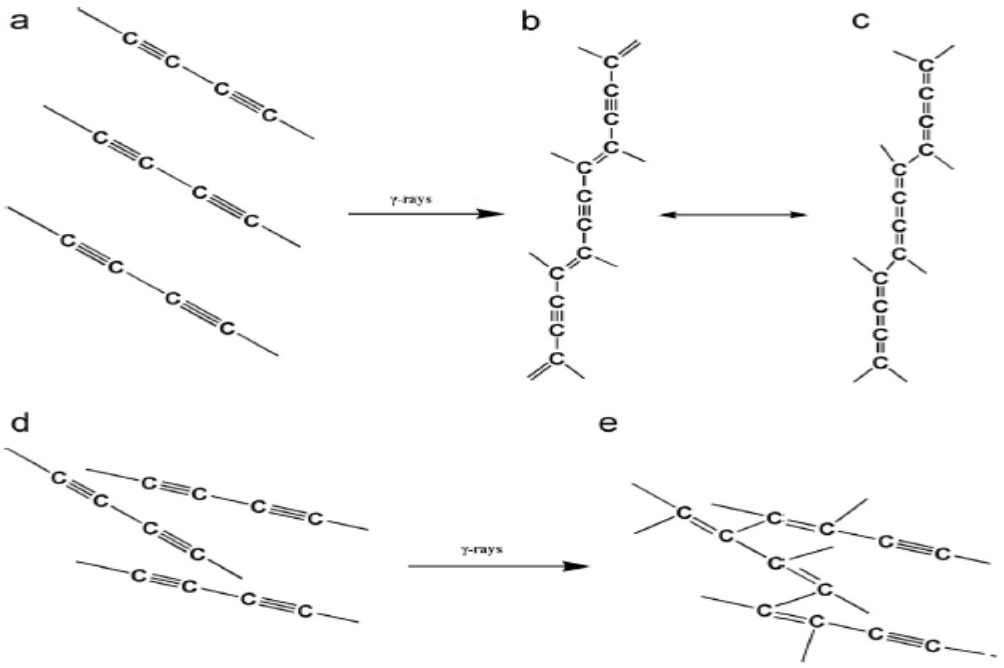

Figure 13 Possible reactions of conjugated diacetylene molecules under ionizing radiation; Diacetylene units in a stack in a crystal (a) react *via* topochemical solid-state polymerization to form polydiacetylene chains (b) and (c). By contrast, conjugated diacetylene units in a non-crystalline environment (d) cross link via random reactions of C≡C triple bonds to form polymer (e) [140].

Ali et al [128] investigated the possibility of developing a radiochromic dosimeter based on gamma radiation- induced polymerization of aniline hydrochloride monomer solution. Their studies show that aniline hydrochloride monomer undergoes polymerization to polyaniline salt (emeraldine salt) and the characterization reveal that it is an electrochromic material after direct γ-radiation exposure to high dose up to 50 kGy. The electrochromic material was deduced by direct step wise appearance of light green color to dark green color following the radiation doses.

The radiochromic and polymerization was confirmed by using UV-visible spectroscopy, which gave rise to absorbance band at 790 nm that showed exponential increase in intensity of absorption band following increase in radiation dose. Similarly, Laranjeira et al [132] developed a polyaniline based radiochromic film for the detection of gamma radiation in the dose range of 1 - 10 kGy. Some investigators reported polymer–based radiochromic dosimeters which have potential applications in medicine [20, 138, 133 - 134].

Dye-based radiochromic dosimeters

Dye-based radiochromic dosimeters work on the principle of radiation induced chemical changes that results in color changes. Such color changes could be effected directly through the interaction of ionizing radiation with the dye molecule or indirectly through formation of radicals or some reactive groups that in turn interact with the dye molecule resulting in color changes.

For example, reduction/oxidation reactions in tetrazolium salts and the change in their colors by forming formazans can take place using ionizing radiation [115, 145].

Farahani and McLaughlin [146] developed a radiochromic dosimeter solution using fuchsin cyanide in a mixture of dimethyl sulfoxide and triethyl phosphate containing small amounts of additives such as acetic acid, p-nitrobenzoic acid and polyvinyl butyral. Their rodiochromic dosimeter solution was found to have a dose range of 10^2 - 10^4 kGy with the attributes of being able to prepare from off- the- shelf reagents without needing for purification. Their studies on the effect of additives were also found to show improvements in the shelf life, radiochemical yield

and dose range of the dosimeter. Research works for developing dye-based radiochromic dosimeters for different types of applications can be found in [147 - 148].

2.3.6.3. Medical and environmental applications

Treatment of cancer by radiotherapy has increased and developed greatly, therefore quality control of dosimetric techniques in medical applications are needed for providing accurate evaluation of doses absorbed in tumor volume and adjacent tissues [71]. One important application of radiation dosimetry is in the field of brachytherapy. Advances in the delivery of brachytherapy fields and external therapeutic beams continue to place considerable demands on the performance of dosimetric systems, for both point-dose and dose distribution evaluations. Challenges include obtaining a well-behaved characterized response across the large dynamic range of dose (the so-called high field gradient) presented at for instance tissue interfaces, close up to brachytherapy sources, in intensity modulated radiotherapy (IMRT). The spatial resolution and dynamic range required of a dosimeter to accurately evaluate the radiotherapy dose distribution of such complex three-dimensional geometries, especially at the micro spatial resolution scale, is indeed becoming increasingly challenging [149]. Radiochromic dosimeters are getting popularity in the medical field because of their high resolution compared to ionization chambers and thermoluminescence dosimeters (TLDs). Compared to radiographic film, radiochromic film offers greater X-ray sensitivity, reduced processing and handling demands, and an ability to be used in water without waterproof encapsulation [150]. A review of radiochromic dosimeters useful for medical application can be found in reference [141].

Treatment of flue gases, waste water and other environmental pollutants can be done by using electron beam (EB) or cobalt-60 irradiation facilities. In such facilities, radiation dosimeters are needed that can accurately monitor radiation doses applied during the treatment processes and of workers in these facilites. Other application of radiation dosimetry in environment is in monitoring of background radiation that could arise due to accidental leakage of radioactive materials or release of radioactive material by terrorist groups [151].

The disposal of radioactive wastes has the probable consequence of increasing the radiation exposure of native wild organisms, both now and in the future. The magnitude of this hazard depends upon the radionuclides in the wastes (their quantities, half-lives and the radiations emitted) and their behaviour in the biosphere (their physical and chemical form) [152]. Monitoring of such radioactive wastes requires dosimeters that are cheap, sensitive, and can be fabricated for remote sensing applications. Research in the area of radiochromic dosimetry is going on in order to develop dosimeters that could find applications especially in medicine and environment.

2.3.7. Semiconductor polymer/small molecules dosimeters

Conjugated or semiconducting polymers offer device solutions that challenge those of conventional silicon-based semiconductor technologies. For example, in the past decade, exploitation of the properties of polymers has led to the development of organic sensors for radiation detection and dosimetry [70, 80] and imaging [153]. These detectors complement solid-state dosimeters based on traditional inorganic materials, [154] and emerging technologies, [155] but also present their own unique advantages over their inorganic counterparts [156]. Many

investigators studied conjugated polymers as well as composite polymers to develop radiation dosimeters [74, 157- 160]. By virtue of their ability to undergo radiation-induced structural or chemical changes, some small molecules are also being explored for their potential applications in low dose radiation dosimetry. The following example illustrates the small molecule dosimeter investigated for its potential applications in low dose dosimetry.

Very recently, J. –Min Han et al [161] developed a new fluorescence sensor molecule, 4, 4'-di (1H phenanthro [9, 10-di] imidazol-2-yl) biphenyl (DPI-BP), which can be dissolved into halogenated solvents (e.g., $CHCl_3$, CH_2Cl_2) to enable instant detection of gamma radiation down to the 0.01 Gy level. The sensing mechanism is primarily based on radiation induced fluorescence quenching of DPI-BP. Pristine DPI-BP is strongly fluorescent in halogenated solvents. When exposed to gamma radiation, the halogenated solvents decompose into various radicals, including hydrogen and chlorine, which then combine to produce hydrochloric acid (HCl). This strong acid interacts with the imidazole group of DPI-BP to convert it into DPI-BP/HCl adduct. DPI-BP/HCl adduct possesses more planar configuration than DPI-BP, enhancing the π-π staking and thus molecular aggregation. The strong molecular fluorescence of DPI-BP gets quenched upon aggregation, due to the π-π staking interaction (forming forbidden low-energy excitonic transition). Figure 14 shows the sensing mechanism.

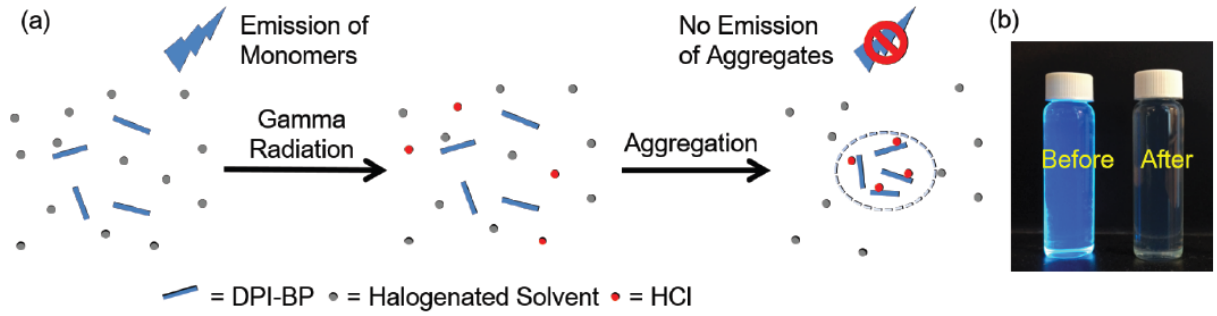

Figure 14 (a) Schematic drawing of the fluorescence sensing mechanism of DPI-BP. Protonation interaction with radiation generated HCl causes molecular aggregation of DPI-BP, which in turn results in fluorescence quenching due to π-π stacking. (b) Fluorescence photograph of a DPI-BP solution in $CHCl_3$ taken before (left) and after (right) 3.0 Gy of gamma radiation, indicating complete fluorescence quenching.

2.4. Reactions for radiation induced decomposition of chloroform, trichloroacetic acid and chloral hydrate

2.4.1. Radiation induced decomposition of chloroform

The radiolysis of chloroform was studied by many researchers for over fourty years [162]. Hummel et al [163] have put emphasis on the decomposition of ionized molecules and on the dissociative capture of the electrons freed from the parent ions, in order to explain the formation of free radicals which are the active chemical species giving rise to the products of chloroform radiolysis.

$CHCl_3 + \gamma\text{-ray} \rightarrow CHCl_3^+ + e^-$

$CHCl_3^+ \rightarrow CCl_3^{\cdot} + H^+$

$CHCl_3 + e^- \rightarrow CHCl_3.^-$

$\underline{CHCl_3.^- \rightarrow CHCl_2. + Cl^-}$

$2CHCl_3 + \gamma\text{-ray} \rightarrow CCl_3^{\cdot} + CHCl_2^{\cdot} + HCl$

Abramson [164] showed the formation of Cl. radicals from the reaction of Cl^- and ionized molecules as follows:

$CHCl_3 + e^- \rightarrow CHCl_2^{\cdot} + Cl^-$

$Cl^- + CHCl_3^+ \rightarrow CHCl_3^* + Cl^{\cdot}$

The excited molecules, $CHCl_3$*, can either return to the ground state or decompose in three ways depending on their energy level:

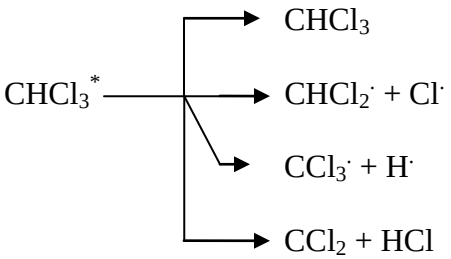

These mechanisms were suggested to explain the reactions leading to stable products of the radiolysis of chloroform in an oxygen-free atmosphere. The major products of the radiolysis of chloroform in oxygen-free atmosphere together with their respective G-values (molecules/100 eV) are: HCl (5.30), CH_2Cl_2 (2.20), CCl_4 (0.70), $C_2H_2Cl_4$ (0.67), C_2HCl_5 (1.48), and C_2Cl_6 (2.40) [163].

2.4.2. Radiation induced decomposition of trichloroacetic acid and chloral hydrate solutions in non-halogenated solvents

Myron and Freeman [165] showed that the γ- radiolysis of ethanol produces H radical, acetaldehyde and 2, 3- butanediol as major products with their corresponding G-values, 4.2, 1.9, and 2.2, respectively. Kučera [166] showed that irradiation of degassed liquid acetone with a ^{60}Co γ - ray produces foramaldehyde, acetaldehyde, acetylacetone and many other products. The proposed mechanism shows the involvement of H and CH_3 radicals. Kosubutski [167] studied the γ- radiation initiated dehydrochlorination of trichloroacetic acid in aqueous solution under different concentrations of alkali solutions. The result of this study shows formation of Cl^- and $C_2O_4^{-2}$ ions. The reaction of $H^{\cdot}$ radical with Cl_3COOH resulted in the formation of $^{\cdot}Cl_2COOH$ radical and HCl.

Andrews and Shore [168] studied the radiolysis of chloral hydrate in aqueous solution. In their studies the appearance of hydrochloric acid was followed by measureinent of the electrical conductivity of the solution.

3. Experimental

3.1. Chemicals and reagents

Heptamethinde Iodide and heptamethine hexafluorophosphate supplied by EMPA were utilized as received for the preparation of the X-ray and gamma dosimeter solutions for experimental works from 3.2 to 3.4 and 3.7. The chemical structures of these dyes are shown in Figure 15. Cy7- I (2-[2-[2-chloro-3-[(3-ethyl-1,3-dihydro-1,1-dimethyl-2H-benz[e]indol- 2-ylidene)ethylidene]-1-cyclohexen-1-yl]ethenyl]-3-ethyl-1,1- dimethyl-1H-benz[e]indolium iodide) & Cy7- PF_6 (2-[2-[2-chloro-3-[(3-ethyl-1,3-dihydro-1,1-dimethyl-2H-benz[e]indol- 2-ylidene)ethylidene]-1-cyclohexen-1-yl]ethenyl]-3-ethyl-1,1- dimethyl-1H-benz[e]indolium hexafluorophosphate were used as received for the preparation of dosimetric solutions.

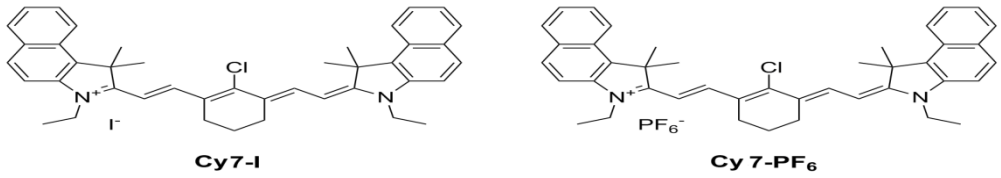

Figure 15 Chemical structures of heptamethine dyes Cy7-I and Cy7-PF_6 used in this study.

Curcumin purchased from Sigma Aldrich was utilized for the preparation of the dosimeter solutions. The chemical structure of curcumin dye is shown in Figure 16.

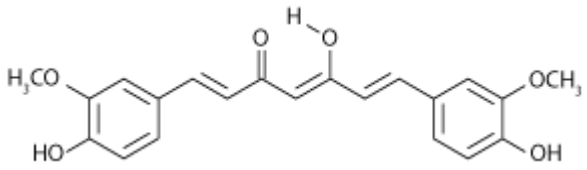

Figure 16 Chemical structure of Turmeric dye (curcumin) 1,7-bis(4-hydroxy-3-methoxyphenyl)-1, 6-heptadiene-3, 5-dione.

Poly 3-hexylthiophene (P3HT) purchased from Sigma Aldrich was utilized for the preparation of the dosimeter solutions. Polymethylmetacrylate (PMMA) and DDT were purchased from Sigma Aldrich and were used as received.

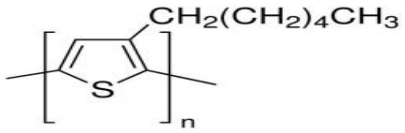

Figure 17 Chemical structure of poly 3-hexylthiophene.

Ethanol (ACROSS –New Jersy, USA), chloroform ($CHCl_3$) stabilized with ethanol (max. 0.8%) Grade 99.8%) (ACROSS –New Jersy, USA), acetone (Research Lab Fine Chemicals Industries, India), trichloroacetic acid (Sigma-Aldrich), TiO_2 nanoparticles (Sigma-Aldrich), chloral hydrate (Sigma-Aldrich), dichloromethane (ACROSS –New Jersy, USA), toluene (ACROSS –New Jersy, USA), polyvinyl alcohol (Sigma-Aldrich), hydrochloric acid (Sigma-Aldrich), ferrous ammonium sulfate (Sigma-Aldrich), sodium chloride (Sigma-Aldrich), sulfuric acid (Sigma aldrich) were used as received.

3.2. Preparation of dosimetric solutions

A study was conducted to evaluate the absorption spectral characteristics of the two heptamethine dye solutions. These dye solutions show peak saturation above 0.01 mg/mL concentration. Similar properties were observed in polymeric dyes of similar structure [169]. Therefore, a slightly lower concentration i.e. 0.009 mg/mL and below were taken in this study.

The solutions having concentration of 0.006 - 0.009 mg/mL in different solvents (chloroform, toluene and dichloromethane) were prepared by dissolving calculated amounts of the dyes in 100 mL of the solvents. The dosimetric solutions were prepared in duplicates for both the un-irradiated and irradiated samples. The solutions having concentration of 0.006 mg/mL in ethanol with trichloroacetic acid (0.003% w/w) and 0.003% w/w chloral hydrate were prepared by dissolving calculated amounts of the dye and trichloroacetic acid/chloral hydrate in 100 mL of the solvent. A solution having concentration of 0.006 mg/mL in acetone with chloral hydrate (0.003% w/w) was also prepared.

The solutions having concentration of 0.006 mg/mL in chloroform were prepared by dissolving calculated amounts of the curcumin dye in 100 mL of the solvent. Solutions of curcumin in ethanol with 0.003% w/w chloral hydrate were prepared by dissolving calculated amounts of the dye in 100 mL of solvent.

The solutions having concentration of 0.0375 mg/mL in chloroform were prepared by dissolving calculated amounts of the P3HT in 100 mL of the solvent. To study effects of additives polymethyl metacrylate (PMMA) and DDT on dosimetric characteristics of P3HT solutions in

chloroform, composite solution of P3HT (0.01 mg/mL), PMMA (0.01 mg/mL) and DDT (0.02 mg/mL) were prepared.

3.3. Preparation of dosimetric films

3.3.1. Preparation of Cy7-I-PVA-HCl film

Three grams of polyvinyl alcohol (PVA) powder purchased from Sigma-Aldrich was dissolved in 50 mL of 0.1 M HCl by heating upto 60 ^{0}C for 2 hrs. The solution was then allowed to cool to room temperature with continous stirring.

1 mg/mL of Cy7-I in ethanol was prepared. 1 mL of this solution was mixed with 3 mL of 0.1 M HCl- PVA gel solution. The gel solution obtained was dropcasted on a clean petridish placed on a level plane table. The petridish was covered by aluminum foil to protect the film from light exposure. The gel solution was kept in an oven for 3 hrs at 50 ^{0}C. The films were peeled off from the petridish and cut into 1.0 cm x 1.5 cm dimensions.

3.3.1. Preparation of Cy7-I-PVA-HCl-TiO_2 nanocomposite film

A 0.1 M HCl-PVA-Cy7-I gel solution was prepared as in 3.3.1. 2 mL of this gel solution was mixed with 0.085 mg of TiO_2 nanoparticle (at 50% w/w) to make Cy7-I-PVA-HCl-TiO_2 nanocomposite gel solution. Three drops of Zonyl®FS-300 fluoro surfactant (Fluka) was added and ultrasonicated for 30 minutes (to make uniform distribution of the nanoparticles in the gel solution) and poured into a clean petridish placed on a level plane table. The petridish was covered by aluminum foil to protect the film from light exposure. The gel solution was kept in an

oven for 3 hrs at 50 ^{0}C. The films were peeled off from the petridish and cut into 1.0 cm x 1.5 cm dimensions.

3.4. Irradiation of samples

3.4.1. 6 MV Medical Linear Accelerator (6 MV MLINAC)

Irradiation of dosimetric solutions was carried out using 6 MV Medical Linear Accelerator at Centro de Radioterapia da Região de Bauru, Bauru, São Paulo, Brazil (Figure 18a). The irradiation was conducted at a dose rate 300 and 600 cGy/minute with a field size of 10 cm x 10 cm, source to surface distance (SSD) of 100 cm, 1.5 cm acrylic build-up and additional acrylic layers at the bottom for secondary electron equilibrium (Figure 18b). About 4 mL of the dosimetric solution was irradiated in each glass vial fitted with a solvent resistant plastic cap.

3.4.2. Co-60 radiotherapy unit

Co-60 source of Department of Psychology at University of São Paulo (USP) in Ribeirão Preto, São Paulo, Brazil was used for the irradiation of heptamethine dye solutions in chloroform for doses 0 to 1 Gy. The irradiation dimensions are the same as in 3.4.1.

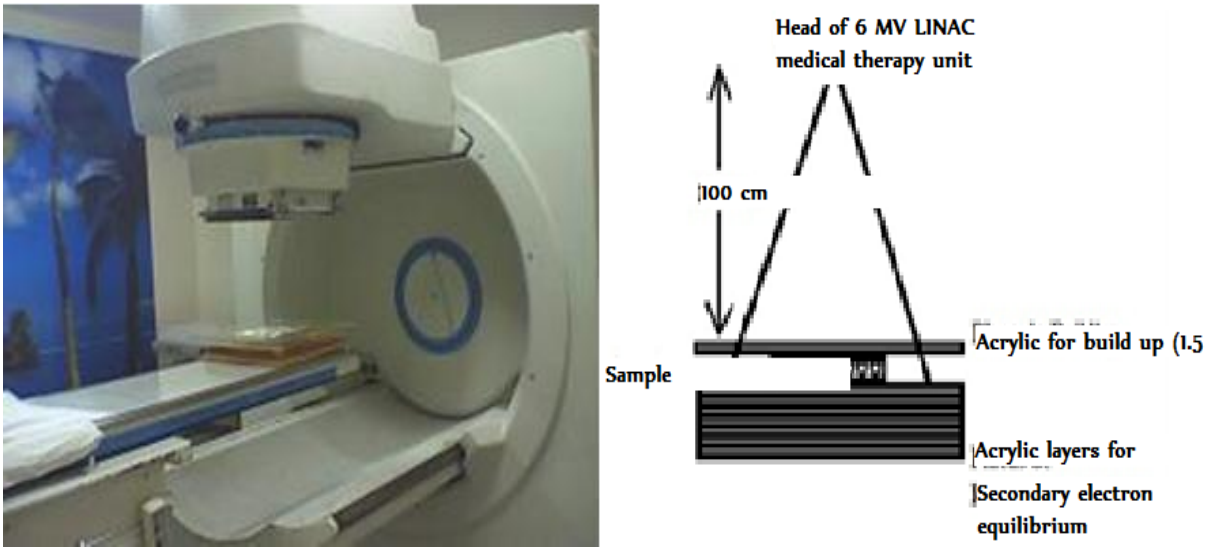

(a) (b)

Figure 18 (a) 6 MV Medical Linear Accelerator (b) a diagram showing the irradiation dimensions.

3.4.3. Co-60 Gamma cell 220 Excel

The Cy7-I/PVA and Cy7-I/PVA/TiO_2 gel films were placed in 4 mL vial and irradiated by the Co-60 Gamma cell 220 Excel (Indian) at the National Tse Tse Fly Eradication Institute (A.A, Ethiopia) with a dose rate of 0.87 Gy/Sec (Figure 19). The Cy7-PF_6 –ethanol-chloral hydrate and Cy7-I-acetone-chloral hydrate solutions as well as curcumin-ethanol-chloral hydrate solutions were irradiated in 4 mL vial. Calibration of the source was done using Fricke dosimeter. The dose rate after calibration with the Fricke dosimeter was calculated and found to be 0.81 Gy/sec (see Appendix 1).

Figure 19 Gamma Cell 220 Excel.

3.5. Methods for characterizing dosimetric solutions and films

3.5.1. UV-Vis absorption studies

The samples have been analyzed by UV-Vis absorption. Measurements of UV-Vis spectroscopy have been performed on a Shimadzu (UV mini 1240) for sections 4.2 to 4.6. UV-Vis spectroscopy measurements for films in section 4.7 and heptamethine dye/ethanol/acetone/chloral hydrate and curcumin/ethanol/chloral hydrate solutions have been performed on a Perkin Elmer 950 UV-Vis/NIR Spectrophotometer.

3.5.2. Photoluminescence studies

The fluorescence measurements have been performed using a Varian fluorimeter (Cary Eclipse). The samples of Cy7-PF_6 and Cy7-I solutions have been excited with a wavelength of 254 nm and

292 nm. The samples of curcumin solutions have been excited with a wavelength of 400 nm and 450 nm. The samples of P3HT solutions have been excited with a wavelength of 500 nm.

These wavelengths were chosen after analyzing the fluorescence excitation spectra of pristine and irradiated dye and polymer solutions.

3.5.3. FTIR studies

Fourier transform infrared (FTIR) spectra have been recorded as films deposited from ethanol solutions by using ZSM-5 cells, on a Bruker Vertex 70 Fourier transform spectrometer.

3.5.4. MS studies

Mass spectra of the un-irradiated and radiation-induced decomposition products were acquired on a quadruple-stage mass spectrometer (Quadruple coupled to Tandem Xevo^{TM} T-QS ; Acquitty H-Class, Waters Corporation) equipped with a positive electrospray ionization (+ESI) interface.

3.5.5. Optical Densitometry

Optical density measurements of the un-irradiated and irradiated gel films were carried out using a radiochromic reader instrument (Far West Technology Inc) of Tse Tse Fly Erradication Institute (AA, Ethiopia). Figure 20 shows a photograph of the radiochromic reader used. The optical density measurements are done by inserting the gel films in the sample holder.

Figure 20 A photograph of the radiochromic reader used for optical density measurement.

3.5.6. Stability studies

For studying the effects of light on the stability of response during pre and post-irradiation storage, the irradiated solutions were exposed to diffused sunlight inside the laboratory and the results were compared with the solutions stored in the dark. For checking the effects of different temperature on the pre and post-irradiation stability of response, the solutions before and after irradiation were stored at temperatures using a constant temperature oven (60 °C), room temperature (22 – 25 °C) or a refrigerator (2 °C).

4. Results and discussion

4.1. Introduction

Ionizing radiation causes chemical and structural changes in materials with which it interacts [170 - 172]. The search for a dosimeter material that is inexpensive, user friendly and responds to low gamma radiation is an active research for material scientists, physicists, chemists and engineers. The quest for developing dosimeters is still continuing in many research laboratories of the world from a wide range of materials such as conducting polymers, conventional polymers, inorganic semiconductors, organic dyes, etc. Many research works have been conducted on dye dosimeters [97, 103, 173 - 175]. Similarly various investigators studied conventional as well as conducting polymers for radiation dosimetry applications [156 - 159, 176].

Most of these researches focus on high dose radiation dosimetry [64, 177 - 178]. Low dose radiation dosimetry has important applications in medicine as well as environmental monitoring. Treatment of cancer by radiotherapy has increased and developed greatly, therefore quality control of dosimetric techniques in medical applications are needed for providing accurate evaluation of doses absorbed in tumor volume and adjacent tissues [179]. Among the radiation oncology equipment available, some of the most popular for the treatment of deep seated tumors is the Linear Accelerator (LINAC), in which the external beam radiation therapy is delivered by means of high energy X-rays (6 MV) [180]. LINAC is the standard method for producing photons and electrons delivered to the tumor with extreme accuracy such as beam quality,

direction, and intensity. It is programmed to send precise doses of radiation directly to cancer cells in a much targeted way through a state-of-the-art therapy called Intensity Modulated Radiation Therapy. The majority of tumors require doses in the range of 8 – 70 Gy, fractionated in doses of 1.8 – 2.0 Gy once a day, five times a week for 5 – 7 weeks [181].

Several treatment errors and incidents were reported by software flaws and faulty programming due to LINAC's complexity. Such treatment errors and incidents have fatal consequences on the safety of patients [183]. American Association of Physicists in Medicine and the American Society of Radiation Oncology support the view that "error reporting systems should be developed in radiation therapy" to "protect the safety of each and every patient" [182 – 184]. From this point of view, an easy-to-use, easy-to-read and low-cost dosimeter, that is also more accessible to people in places with limited resources, may ensure that every treatment will be as safe as possible. Hence it is an innovative proposal for the psychological comfort of cancer patients as it ensures proper functioning of LINACs. In this case, each patient will be able to personally monitor the response of the radiation detector shortly before being irradiated [182-184]. Schimitberger et al [181] developed MEH-PPV/Alq_3 based hybrid device capable of recording the total dose delivered to the oncology patient shortly before a LINAC-based treatment.

The monitoring of radiation in the environment that is mainly caused by escape of radioactive gases from nuclear facilities or illicit uses of radioactive materials by terrorists is of paramount importance in keeping the public safe. Therefore, continuous monitoring of the environment for

radiation requires sensitive dosimeters that are cheap, easy to use and give real time dose readings.

Dye dosimetry is based on the fact that ionizing radiations interact with matter and cause the color change of the dye. This property of color change of dye can be used for dosimetry as the decomposition of dye is linear with respect to the amount of dose absorbed [104, 185 - 186].

Organic dyes generally show strong visible absorption bands in solutions, therefore several studies have been carried out to investigate the effects of radiation on dye solutions with the objective of developing convenient dosimeters [101]. A number of organic dye solutions have been investigated as potential chemical dosimeter for a wide range of radiation doses that are useful for dosimetry in industrial radiation processing, health physics and radiation research [101].

Neto et al [174] investigated the gamma ray dosimetric properties of conjugated polymer dye solutions. Their results indicate that the presence of unsaturated bonds along the chain of the polymer sets a desirable feature for the design of sensitive dosimetric systems based on polymers in halogenated solvents.

Polymer based dosimeters have been the subject of study for many years. Many of the studies are focused on conducting polymers [70, 155 - 157]. Some investigators focus in developing polymer gels from conventional polymers such as polyvinyl chloride and conducting polymers such as polyaniline [187 - 188]. A promising result was reported by Zhao et al [189].

4.2. Study of heptamethine Iodide and heptamethine PF_6 solutions in different solvents for the measurement of low doses of X-ray and gamma radiation

4.2.1. Introduction

Recently, cyanines have received much attention since these compounds have wide applications such as photo-sensitizers, dye lasers, optical recordings and storage media [190].

Different from most small molecules, cyanines are easily processed from solution, which makes them attractive for technological applications [191]. These tailor made low-band gap dyes have emerged as promising low-cost material systems for the use in optoelectronic devices [192]. However, their use as dosimeters has not received much attention.

The aim of the present work was to study the heptamethine cyanine dyes for their potential applications as cheap low dose X-ray and gamma-ray dosimeters. Their low-cost and easily solution processeability in different solvents makes them good candidates for low dose dosimetry in medical applications for precise monitoring of doses.

The dyes used in this study are heptamethine iodide (Cy7-I) and heptamethine hexafluorophosphate (Cy7-PF_6). The main objective of this study was to evaluate these dye solutions in various solvents if they can be used as low dose X-ray and gamma-ray dosimeters. Spectrophotometric and spectrofluorimetric parameters were used to evaluate the dosimetric characteristics such as useful dose range, pre-irradiation and post-irradiation stability in different solvents, under light and dark as well as under different temperature conditions.

4.2.2. Results

Spectrophotometric and spectrofluorimetic studies were conducted for both un-irradiated and irradiated dye solutions. The parameters evaluated using these methods include, visual color changes, effects of concentration, effects of solvents, effects of dose rate, useful dose range and effects of light and temperature on pre-irradiation and post-irradiation stability of dosimetric solutions. The parameters for Cy7-PF_6 and Cy7-I dosimetric solutions are presented below.

4.2.2.1. Visual color changes

Both Cy7-I and Cy7-PF_6 dosimetric solutions at 0.008 mg/mL have pale green color before irradiation. The color of both dosimetric solutions show color change proportional to the amount of irradiation dose and changes from pale green color to pale yellow and finally to pale orange color (Figure 21).

a) b)

Figure 21 Visual color changes of Cy7-PF6 solution in chloroform irradiated at (a) 30 Gy and (b) color changes of dosimetric solutions as a function of dose.

The change in color indicates the formation of new chromophoric structures as a result of the irradiation. Further spectroscopic and structural studies were conducted (presented in section 4.3) to account for the structural and color changes. The sensitivity of our dosimeter solution can fulfill the requirements for the applications in radiotherapy where low dose radiation (< 50 Gy) is used [189].

4.2.2.2. Dosimetric response curves

Spectrophotometric response curves

The absorbance spectra of un-irradiated and irradiated 0.007 mg/mL for Cy7-PF_6 dosimetric solutions in chloroform were measured in the range from 300 - 1100 nm using the spectrophotometer at a dose range of 0 - 30 Gy (Fiure 22).

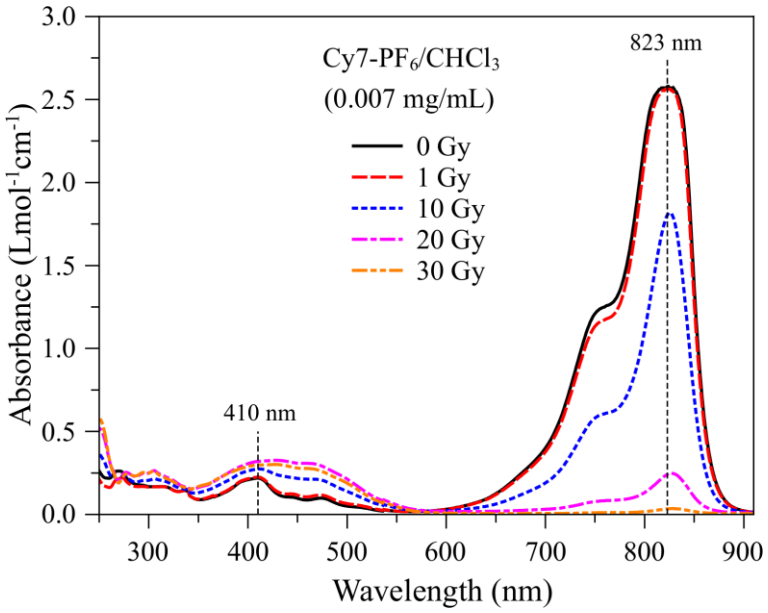

Figure 22 Absorbance spectra of un-irradiated and irradiated 0.007 mg/mL solution; top to bottom: un-irradiated, 1, 10, 20, and 30 Gy of the dosimetric solutions of Cy7- PF_6.

The absorbance spectra for Cy7-PF_6 showed absorption maxima of the main peak at 823 nm and two other small peaks at 410 nm and 475 nm. Similar absorbance spectra are observed for Cy7-I shown in Figure 23. The figures show a decrease in absorbance after irradiation i n the main peak in these dosimetric dyes as is observed in other dyes in the literature [69, 184, 192, 193 - 196] while increase in absorbance is observed after irradiation in both small peaks. A very slight red shift from 823 nm (un-irradiated) to 828 nm (after irradiaton) is observed for the main peak of these dosimetric solutions.

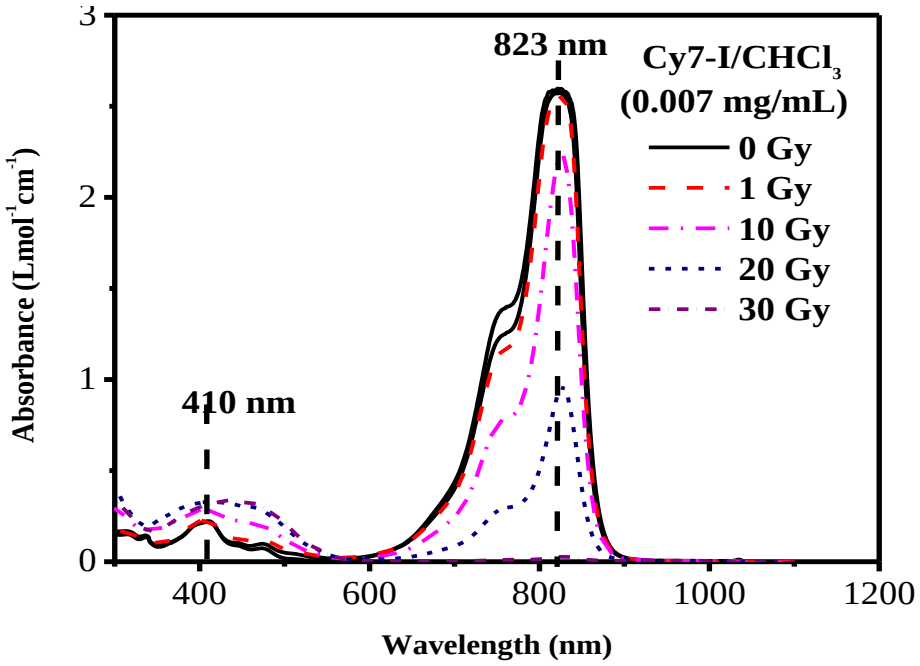

Figure 23 Absorbance spectra of un-irradiated and irradiated 0.007 mg/mL solution; top to bottom: un-irradiated, 1, 10, 20, and 30 Gy of the dosimetric solutions of Cy7- I.

On the other hand, the small peaks show greater shifts on irradiation. While the first small peak shows red shift from 410 nm to 432 (Cy7-I) or 429 nm (Cy7-PF_6), the second small peak shows a blue shift from 475 nm (Cy7-I or Cy7-PF_6) to 455 nm. The wavelength shifts for both dosimetric solutions are compiled in Table 5. These wavelength shifts could be ascribed to structural changes on these dosimetric dyes due to radiation induced degradation. Further structural spectroscopic studies are being carried out to account for the structural changes.

Table 5 Absorption maxima for the main peak and small peaks for irradiated dosimetric solutions of heptamethine iodide and heptamethine PF_6 solutions in $CHCl_3$.

Dose (Gy)	Main Peak Wavelength average 1 (nm)		Small Peak Wavelength average 2 (nm)		Small Peak Wavelength average 3 (nm)	
	Cy7-I	Cy7-PF_6	Cy7-I	Cy7-PF_6	Cy7-I	Cy7-PF_6
0	823	823	410	410	475	475
1	823	823	410	410	472	473
5	826	823	410	410	469	470
10	826	825	410	411	467	464
15	826	826	411	412	467	459
20	826	826	414	415	456	455
25	828	828	428	429	455	455
30	828	828	432	429	455	455

On the basis of the proportional decrease in absorbance of main peak at 823 nm (Cy7-PF_6) and increase in absorbance in the small peak at 410 nm (Cyc7-PF_6), the ratio of absorbance (A_{823}) of the main peak to the absorbance (A_{410}) of the small peak as a function of dose in the dose range of 0 to 20 Gy was used to draw the response plot. As can be seen from Figure 24, the response plot for the dosimetric dye solution shows linear response in the range of 0 to 20 Gy. Similar

responses are observed in both dosimetric dye solutions (Cy7-I and Cy7-PF_6) at different concentrations i.e. 0.007 mg/mL and 0.009 mg/mL.

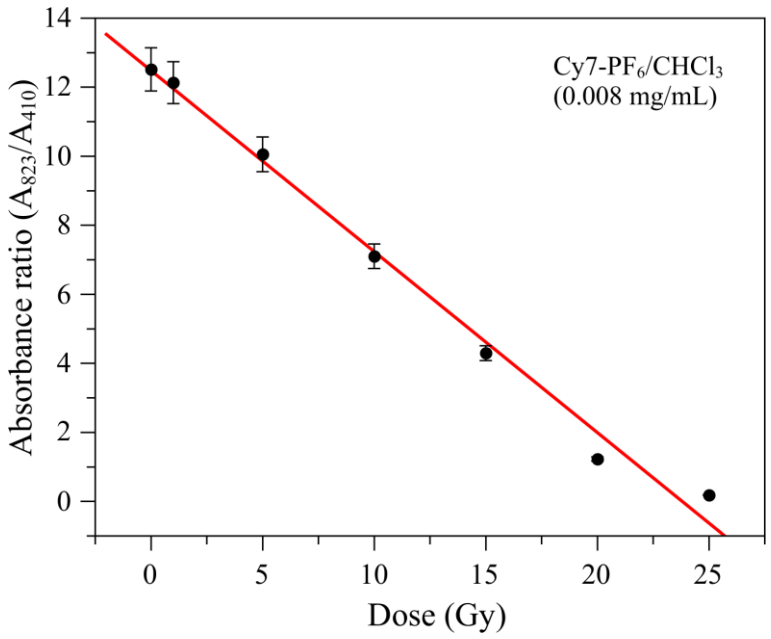

Figure 24 Response plot for Cy7- PF_6 (0.008 mg/mL) solution in $CHCl_3$ showing absorbance maximum ratio versus absorbed radiation.

The ratio of A_{823}/A_{410} was used to draw the response plots as these plots would help minimize variations that would arise due to concentration variations and sample positioning problems that induce increase or decrease in absorbance values not related to irradiation effects.

Other parameters were also calculated and plotted as used in the literature by other researchers to evaluate dosimetric responses of dyes [65, 193, 197 - 198]. Our results show linear behavior between 0 to 20 Gy for Cy7-I (Figure 25).

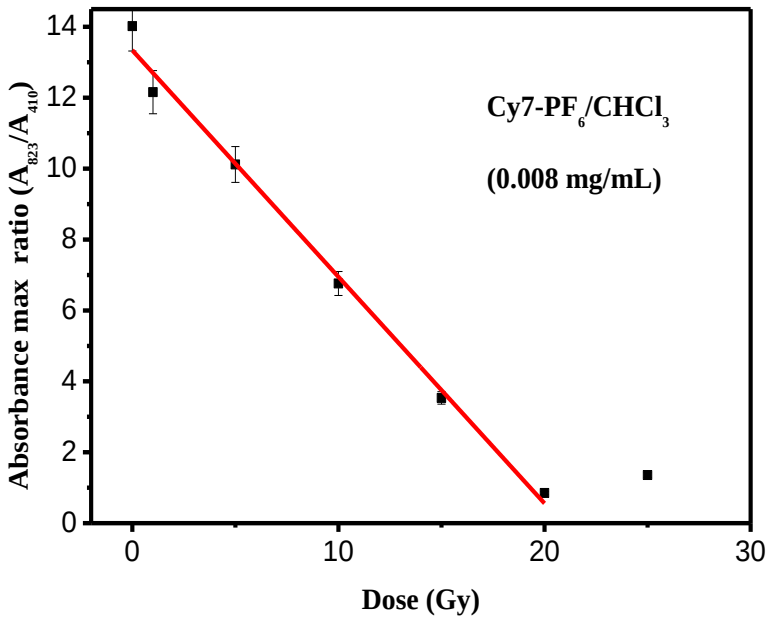

Figure 25 Response plot for Cy7- I (0.008 mg/mL) solution in $CHCl_3$ showing absorbance maximum ratio *versus* absorbed radiation.

Spectrofluorometric Response Curves

The photoluminescence spectra of un-irradiated and irradiated 0.009 mg/mL for Cy7-PF_6 solutions in chloroform were measured in the range from 300 - 1100 nm using the spectrofluorimeter at a dose range of 0- 30 Gy (Figure 26). The spectrofluorometric response plot obtained from emission spectra of the dosimetric dye solution of Cy7-PF_6 shows linear relation *versus* absorbed doses (Figure 27). One of the important parameters of dosimeters is having constant sensitivity across the dose range of interest [199]. Figure 33 shows linear response in the range from 0 to 30 Gy. The linear response can be written for Cy7-PF_6 as $E_{379}/E_{584} = (0.26 \pm 0.10) + (0.32 \pm 0.00)$ D with $R^2 = 0.999$. D stands for applied dose and R^2 the

square of linear correlation parameter. Using the angular equation of the proposed equation, a sensitivity of (0.32 ± 0.00) Gy^{-1} for Cy7-PF_6 was obtained.

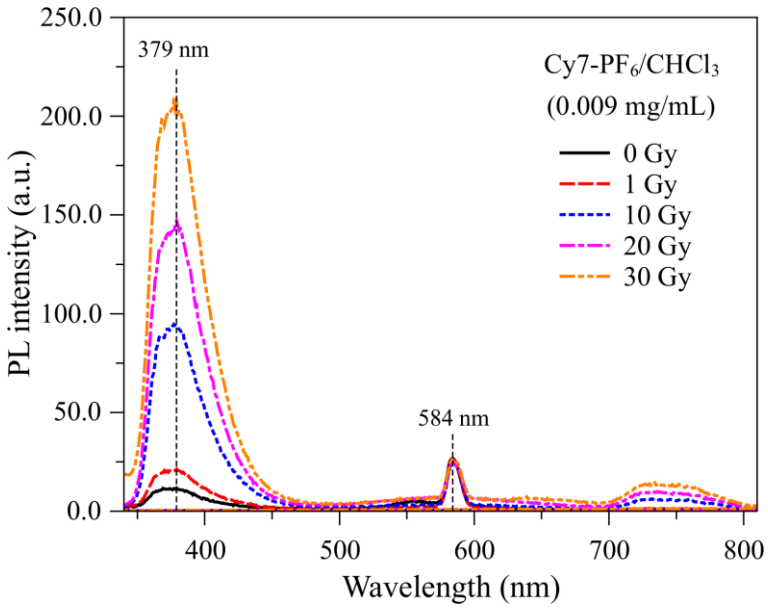

Figure 26 Photoluminescence spectra of un-irradiated and irradiated 0.009 mg/mL solution; top to bottom: unirradiated, 1, 10, 20 and 30 Gy of the dosimetric solutions Cy7- PF_6 at 292 nm excitation.

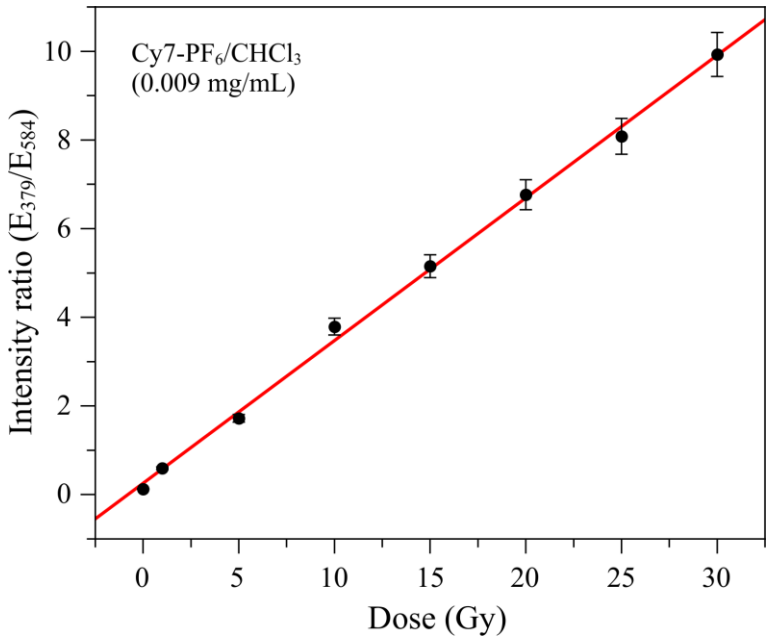

Figure 27 Response plot for Cy7- PF_6 (0.009 mg/mL) solution in $CHCl_3$ showing emission amplitude ratio of main peak to small peak (at 292 nm excitation) *versus* absorbed radiation dose.

4.2.2.3. Pre-irradiation and post-irradiation stability

Pre-irradiation stability

The pre-irradiation stability study shows Cy7-PF_6 solutions in $CHCl_3$ were found to be quite stable at room temperature (i.e. 22 - 25 °C) in the dark and when kept in a refrigerator at 2 °C up to 20 days. On the other hand the stability decreases with time when kept in an oven at 60 °C and in the laboratory diffused light. A temperature of 60 °C was used to evaluate the stability of the dye solution at very high temperature.

The amplitude ratio being higher for both samples kept at 60 °C and in laboratory diffused light even after three days storage. The samples kept in laboratory diffused light become more unstable as time progresses as is clearly seen from the emission spectral response curves (Figure 28) whereas the variation in responses for dosimetric solutions kept in the dark at room temperature and in the refrigerator at 2 °C for 20 days as can be seen from the dosimetric response curves (Figure 29) is very slight. Cy7-I solutions in $CHCl_3$ also show similar trend. Therefore, both dosimetric solutions can be used as dosimeters by keeping them in a dark at low or room temperatures.

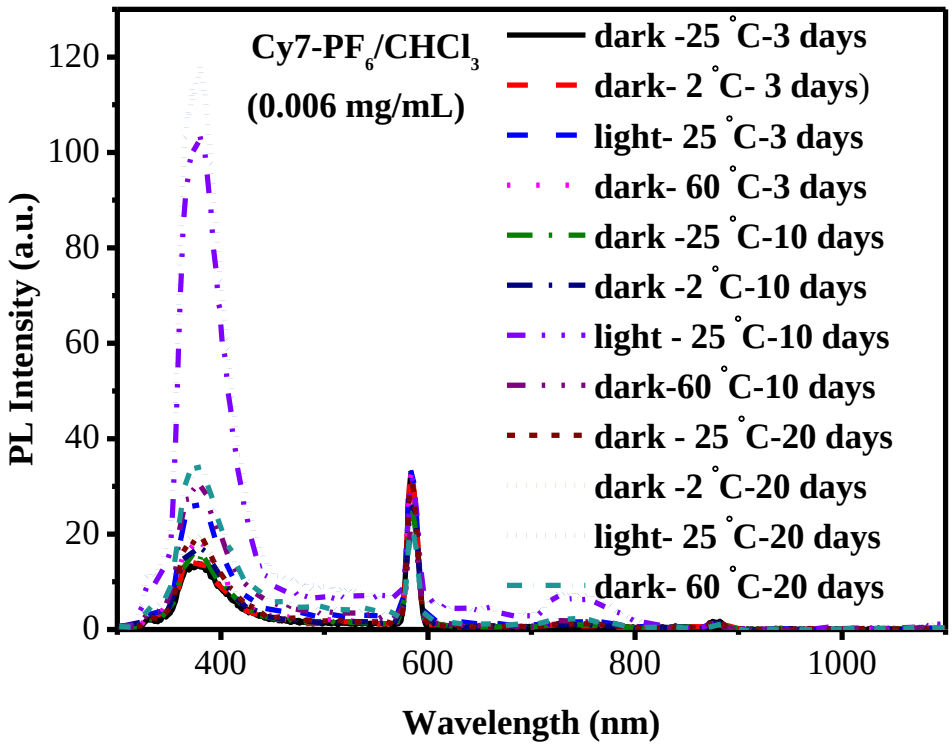

Figure 28 Emission spectra of Cy7-PF6 (0.006 mg/mL) in $CHCl_3$ solution pre-irradiation stability study (temperature and light effects) at 292 nm excitation.

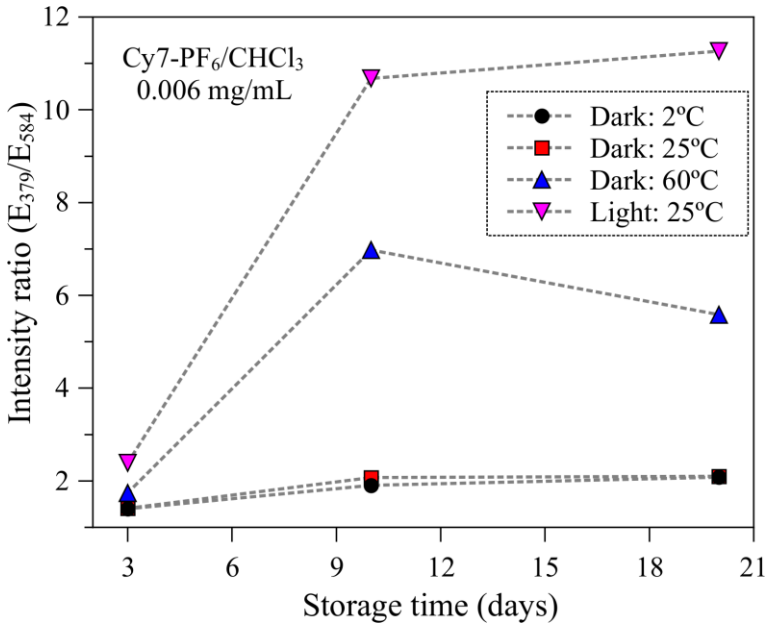

Figure 29 Response plot of amplitude ratio (E_{379}/E_{509}) of emission spectra (Excitation Wavelength: 254 nm) *versus* storage time of Cy7-PF_6 solution (0.006 mg/mL) in $CHCl_3$ for pre-irradiation stability study.

Post-irradiation stability study

We evaluated the post irradiation stability of the heptamethine dye dosimetric solutions (Cy7-PF_6) on one dosimetric solution irradiated at 10 Gy by evaporating the chloroform by N_2 bubbling 1 month after irradiation and re-dissolved in chloroform by adding the same volume of solvent to maintain the concentration the same. We observed similar stability even after one month (Table 6). Further work was conducted to study the post irradiation stability of the dosimetric solutions under different temperature and light conditions. The change in emission amplitude ratio at 15 and 30 Gys irradiation when the dosimetric solutions were kept at 2 °C is less than 4%. On the other hand, when the dosimetric solutions were kept on a laboratory

diffused light, the change in the emission amplitude ratio is 27% at 15 Gy, and 12% at 30 Gy, respectively. Here we observe pronounced change in the amplitude ratio at 15 Gy because of incomplete degradation of the dosimetric solutions at 15 Gy.

Table 6 Percent change of amplitude ratio of Cy7-PF_6 solution (0.006 mg/mL) in $CHCl_3$ one month after irradiation.

Dose (Gy)	% Change of amplitude ratio		
	2 °C	Light	60 °C
15	3.6	27	47
30	3	12	10

The dosimetric solutions kept at 2 °C show very small change in amplitude ratio as shown in Table 6. Therefore, these solutions can be used for tracking records one month after measurements have been done.

Spectrofluorometric studies show reasonable stability when kept at 2 °C in the refrigerator one month after irradiation. Therefore, the irradiated samples could be kept in the refrigerator or in the dark at room temperature for tracking of records of doses. Figure 30 shows the response curves of post-irradiation stability studies.

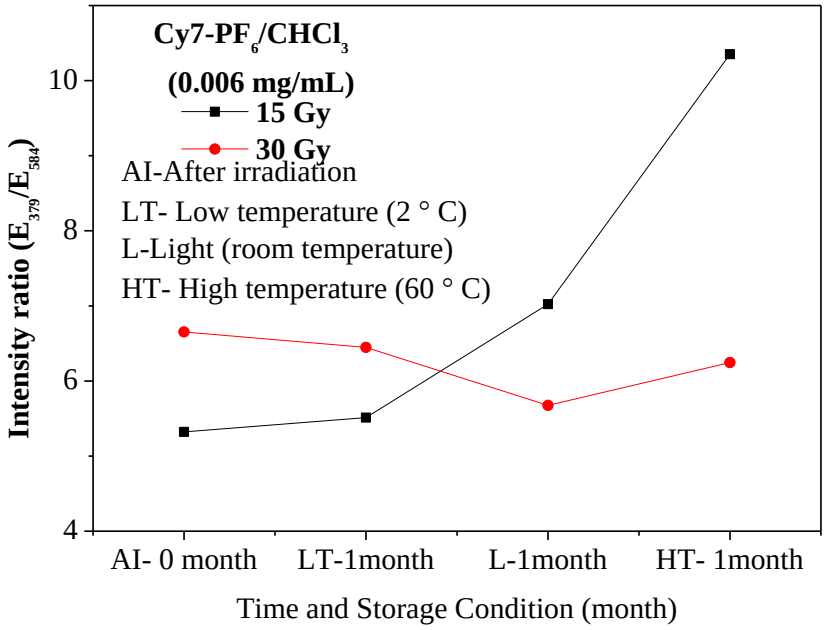

Figure 30 Response plot emission spectra Amplitude ratio (E_{379}/E_{584}) as a function of time for Cy7-PF_6 solutions (0.006 mg/mL in $CHCl_3$) at excitation wavelength 292 nm -post irradiation stability study.

4.2.2.4. Effect of solvents on dosimetric characteristics

Non-halogenated solvents (ethanol and toluene) were used to prepare dosmetric solutions of Cy7-PF_6 to evaluate their dosimetric characteristics. The results are presented below.

Non-halogenated solvents: ethanol and toluene

Dosimetric dye solutions of Cy7-PF_6 in ethanol and toluene were prepared in a similar way as of chloroform dye solutions at a concentration of 0.008 mg/mL. These solutions were tested for dosimetry in doses of 0, 1, 10 and 30 Grays. Absorption and emission spectra were taken for the control and irradiated samples in similar way as of chloroform dosimetric dye solutions. No dosimetric characteristics were observed. The reason for the absence of any change in the absorption and emission spectra peaks may be ascribed to absence of radical generating species in ethanol and toluene which is responsible for dosimetric characteristics observed in chloroform dosimetric dye solutions.

Dichloromethane

We evaluated the effect of dichloromethane dye solutions for their dosimetric characteristics following the work by Bronze-Uhle et al [200]. The spectrophotometric responses observed in $CHCl_3$ solutions show more pronounced wavelength shift on irradiation compared to the dichloromethane solutions of the same concentrations as was observed in a work of Bronze-Uhle et al [200]. Moreover, the % color bleaching in chloroform solutions of both dyes is higher than the dichloromethane solutions which show greater degree of attack on the conjugated bond of the dyes by the radicals generated from radiation induced dehydrochlorination of $CHCl_3$ than

CH_2Cl_2. The difference in responses may be ascribed to the higher average bond energy of CH_2Cl_2 compared to $CHCl_3$ [201] as is seen in Table 8 which makes the radical generation to be greater in $CHCl_3$ resulting in the attack of the conjugated bond of the dye molecules easier in $CHCl_3$ than in CH_2Cl_2. Table 7 depict these results.

Table 7 Absorption maxima and emission intensities of heptamethine dye solutions in $CHCl_3$ and CH_2Cl_2 as a function of radiation dose.

Cy7-I										
	CH_2Cl_2				$CHCl_3$				% color bleaching	
Dose	λ_1	A_1	λ_2	A_2	λ_1	A_1	λ_2	A_2	CH_2Cl_2	$CHCl_3$
0	825	2.592	410	0.1985	825	2.1255	410	0.127	0	0
15	825	2.4	411	0.2235	827	0.555	425.5	0.227	7	70
30	826	1.0715	411	0.2525	828	0.0515	436	0.2265	59	80
Cy7-PF_6										
0	825	2.165	410	0.0925	825	1.925	411	0.115	0	0
15	825	1.55	410	0.1045	826	0.585	414	0.22	28	70
30	826	0.225	410	0.12	830	0.029	428	0.185	90	98

Table 8. Bond dissociation energies of dichloromethane and chloroform [22]

Solvent	Chemical Bond	Bond Dissociation Energies, $kJmol^{-1}$ (at 298.15 K)
Dichloromethane	CH_2Cl-Cl	338.1
Chloroform	$CHCl_2$-Cl	320.5 ± 6.3

4.2.2.5. Effect of Dose Rate

The effect of dose rate on the dosimetric characteristics was evaluated following the work of Basfar et al [105]. The absorbance maximum ratio and amplitude ratio are used to evaluate the effect of dose rate on the dosimetric characteristics of both dosimetric dye solutions. Our results show dose rate to have little or no significant effect on the dosimetric characteristics of the dyes. Figures 31 and 32 depict the effect of dose rate on dosimetric characteristics.

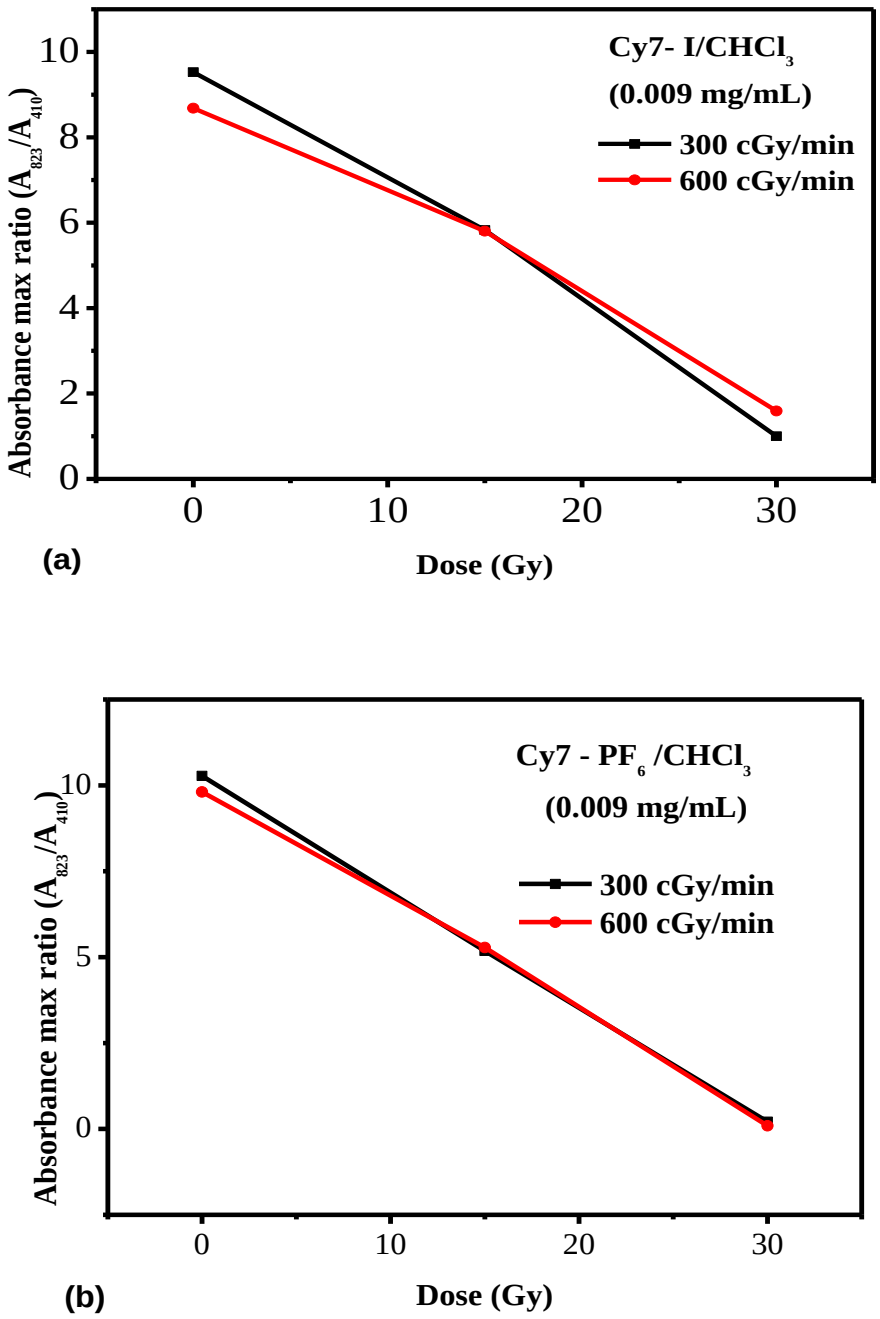

Figure 31 Absorbance max ratio (A_{823}/A_{410}) as a function of dose of a) Cy7-I and b) Cy7-PF_6 solutions (0.009 mg/mL in $CHCl_3$) at different dose rates.

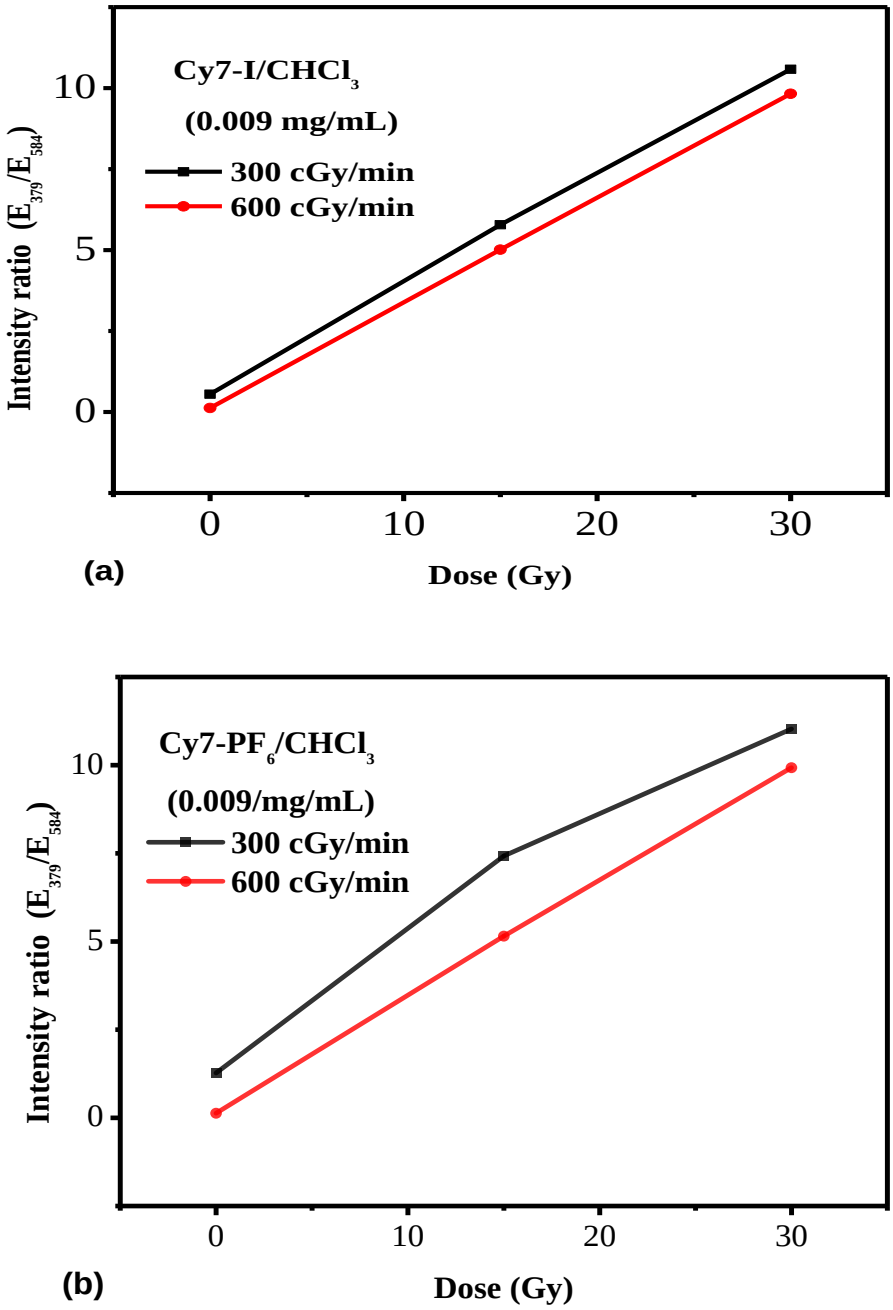

Figure 32 Emission amplitude ratio (E_{379}/E_{584}) at 292 nm excitation as a function of dose of a) Cy7-I and b) Cy7-PF_6 solutions (0.009 mg/mL in $CHCl_3$) at different dose rates.

4.2.2.6. Dosimetric responses below one gray

The best chemical dosimeters developed so far can measure doses down to 10 Gy [202 - 203]. More sensitive dosimeters are required for monitoring personal doses and for environmental monitoring. With this in mind we evaluated the dosimetric characteristics of Cy7-PF_6 solutions in $CHCl_3$ in the dose range of 0 to 1 Gy spectrophotometrically and spectrofluorometrically. The dyes showed linear response (Figure 33) with a reasonably good sensitivity and reproducibility. The sensitivity obtained from the linear fit of the spectrofluorometric response curves is E_{379}/E_{584} = (0.52163 ± 0.01381) + (0.59933 ± 0.02281) D with R^2 = 0.997.

The detection limit (LD) was calculated using methods in the literature [96, 204]. It was calculated by the formula shown in Equation 18, where F is a factor equal to 3.3, SD, Standard deviation of the blank, standard deviation of the ordinate intercept, or residual standard deviation of the linear regression and b slope the regression line.

$$LD = \frac{F \; x \; D}{b} \qquad (18)$$

Hence, the LD value for Cy7-PF_6 calculated from the linear regression slope (b), standard deviation of ordinate intercept is 0.08. Our value is an order of magnitude lower than recently reported in the literature [202 - 203].

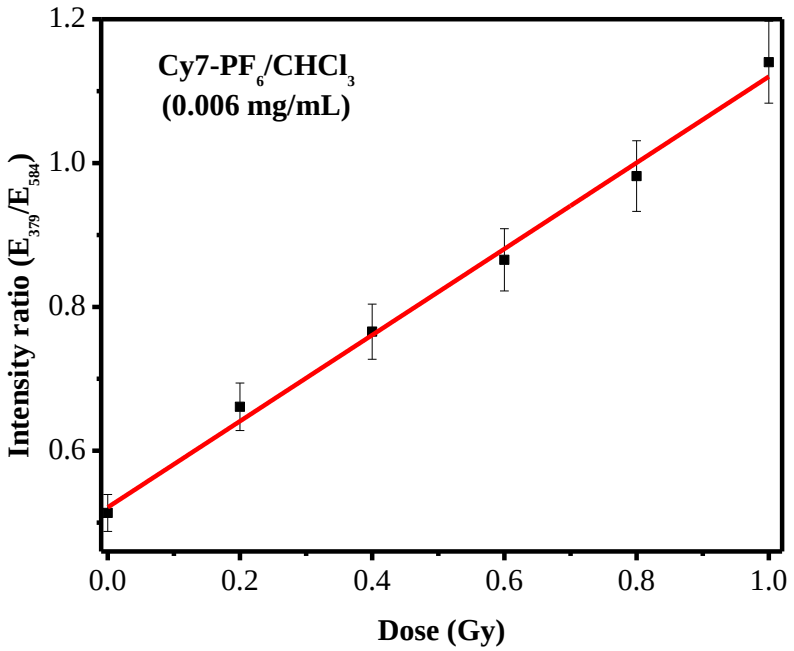

Figure 33 Response plot of emission amplitude ratio at 584 to the main peak at 379 (E_{379}/E_{584}) at excitation wavelength of 292 nm as a function of dose for Cy7-PF_6 solutions (0.006 mg/mL) in $CHCl_3$.

4.2.3. Discussion

Cy7-PF6 and Cy7-I solutions in $CHCl_3$ and other halogenated and non-halogenated solvents for dosimeteric characteristics were investigated at different doses. Pre-irradiation and post-irradiation stabilities under laboratory diffused light and different temperatures were also studied.

The most striking result of our study is the response of the dosimetric dye solutions in chloroform for doses below 1 Gy. As seen from Figure 33, the response plot of emission amplitude ratio (E_{379}/E_{584}) *versus* absorbed dose shows linear relation. Moreover, the limit of

detection (LD) obtained from the linear plot gave 0.08 which is roughly an order of magnitude lower than recently reported in the literature [202 - 203]. Therefore, the dosimeters can be used for low doses as low as below one gray and can be applicable for radiation safety and environmental monitoring. Work has been done to look into the possibility of lowering the limit of detection by introducing some additives and nanoparticles as was done by other investigators [108, 205] and using non-toxic solvents such as ethanol (as presented in section 4.4).

Another interesting finding of our result is the visual color changes these dosimetric solutions undergo in halogenated solvents. The changes are from pale green color for the unirradiated samples to pale yellow, and finally to pale orange for the irradiated samples, the intensity of color being proportional to the amount of dose. The dose response from the spectrophotometic curves show decrease in absorbance ratio from 0 to the 30 Gy studied while a dose enhancement in emission amplitude ratio was observed in the same dose range studied. On the other hand, an attempt was made to study the dosimetric characteristics of the dyes in non-halogenated solvents such as toluene and ethanol. Our results show no color changes as well as no absorption or luminescence changes observed for samples prepared in such non-halogenated solvents on irradiation. These color changes in halogenated solvents could find applications in precise monitoring of radiation doses in radiotherapy. The radiation induced color changes and dosimetric behaviors of these dyes in halogenated solvents are discussed below.

Under gamma or X-ray irradiation, halogenated solvents undergo decomposition to produce some free radicals that can interact with the conjugated bonds of dyes and polymers resulting in dose response. For instance, chloroform decomposes to free radicals such as H, Cl, and other

radicals which are unstable and undergo recombination reactions to generate compounds such as HCl and other radicals [206 - 207] as shown in Equations 19 & 20.

$$CHCl_3 + \gamma\text{-radiation} \rightarrow .H + .Cl + \text{radicals} \quad (19)$$

$$.H + .Cl + \text{radicals} \rightarrow HCl + \text{other stable products} \quad (20)$$

Bronze-Uhle et al [202] discussed how these radicals attack the vinyl double bonds of MEH-PPV breaking the electronic conjugation and the chain resulting in dosimetric characteristics.

Here we also propose that the dosimetric characteristics observed in heptamethine dyes would be due to attack of HCl, Cl. and other radicals on the conjugated bonds of these dyes resulting in breakdown of the conjugation with formation of new chromophoric groups with smaller conjugation as is evidenced by the enhancement of peaks at shorter wavelengths and disappearance of peaks at longer wavelengths seen in the absorption spectra (Figures 22 and 23). The π- expanded derivatives of imidazole have great affinity for acids [208]. We propose that these dyes could form adducts by reacting with HCl.

The proposed mechanism for HCl and radicals attack on the conjugated vinyl bonds are shown in Equation 21.

$$Cy7^+ + HCl + \text{radicals} \rightarrow CG_1\text{-}HCl\ (\text{adduct}) + CG_2\text{-}Cl + CG_3\text{-}CHCl_2 + \ldots \quad (21)$$

CG_1, CG_2, CG_3 … stand for chromophoric groups (CGi) which are expected to be formed by radical initiated fragmentation reactions. V′eron et al [209] showed that small effect of different counterions of a cyanine dye on its properties in solution but found that the counter ion influences the packing and arrangement of the dyes in the crystalline state substantially. This is

in agreement with our finding that no major effect was observed by varying the counter ion from iodide ($Cy7^{+}$-I^{-}) to hexafluorophosphate ($Cy7^{+}$- $PF6^{-}$) in our dosimetric solutions.

Further structural studies were carried out to elucidate the structures and type of these chromophoric molecules (CG_i) formed (presented in section 4.3).

Other findings of our work are their dose rate independence and their pre-and post- irradiation stability at low and room temperature in dark. The dose rate independence and stability at low and room temperature in the dark make them good candidates for low dosimetry applications.

4.2.4. Conclusion

The heptamethinde iodide and heptamethine hexafluorophosphate solutions in chloroform appear to be suitable low dose smart dosimeters in the range from 0 to 30 Gy. Moreover, these dosimetric solutions also show linear behavior below one gray. The response curves of emission amplitude ratio (E_1/E_2) or absorbance maximum ratio (A_1/A_2) *versus* absorbed doses are linear up to 30 Gy and even below one Gy.

Other response curves such as A_1/A_0, $(A_1-A_0)/A_0$, and $\Delta A_1/A_2$ *versus* absorbed dose and their logarithmic curves also show linear and smooth curves. These dose responses in the range of 0 to 1Gy have a constant sensitivity and an order of magnitude lower detection limit than recently reported in the literature and could be useful in personal and environmental radiation monitoring applications. Their linear responses in the dose range of 1 to 30 Gy can be useful for medical applications.

The dosimetric dye solutions also show visual color changes with intensity of color being proportional to absorbed doses which is very useful for precise monitoring of doses delivered to patients in radiotherapy applications. The shelf life of the pre-irradiated dye solutions also show good stability up to 20 days.

4.3. Radiation- induced decomposition of heptamethine cyanine dyes for dosimetry applications

4.3.1. Introduction

Cyanine dyes are a large family of dyes that, in general, contain an unsaturated carbon chain linked by heterocyclic rings such as, but not limited to indole, quinoline, isoquinoline, benzothiazole, and benzooxazole [210]. These dyes (also called as polymethine cyanine dyes) are small organic molecules with two aromatic nitrogen-containing heterocycles linked by a polymethine bridge. Some cyanine dyes (such as Cy5, Cy5.5, Cy7 and their derivatives) are among most common NIR fluorescent dyes with high molar absorption coefficient (often reaching 200,000 mol^{-1} cm^{-1} L) and fluorescence quantum yield. These dyes have been applied widely as active ingredients in semiconducting materials, laser materials, optical recording media, paints, and bio probes for nucleic acids and protein [211]. However, their application in dosimetry is not common.

Therefore, these dye molecules by virtue of their having unsaturated carbon chain, high molar absorption coefficient and their availability at low cost make them good candidates for the development of dosimeters for low dose applications.

In our previous work, we observed that heptamethine cyanine dye solutions in chloroform showed dosimetric characteristics that are similar to works of Neto et al [174] and Bronze- Uhle et al [200, 212].

In this report, we elucidated the mechanism of radiation induced decomposition of the heptamethine dyes (Cy7-I and Cy7-PF_6) in chloroform solutions using UV-Vis, FTIR, and MS spectrometric methods which will be useful in understanding the dosimetric characteristics. The proposed mechanism reinforces the mechanism proposed by [174, 200, 212] and our previous work.

4.3.2. Results

4.3.2.1. Radiation- induced decomposition of Cy7-PF_6

Figure 34 shows UV-Vis spectra of Cy7-PF_6 at 0.006 mg/mL, before and after irradiation at 30 Gy. The main peak for the un-irradiated sample appears at 826 nm and two small peaks appear at 411 nm and 476 nm, respectively. For the irradiated sample, the intensity of the main peak is dramatically decreased while the intensities of the other two small peaks are increased confirming radiation-induced decomposition of the heptamethine dye cation ($Cy7^+$). This result is in conformity with the FTIR and MS data which show decomposition of the dye into various fragments.

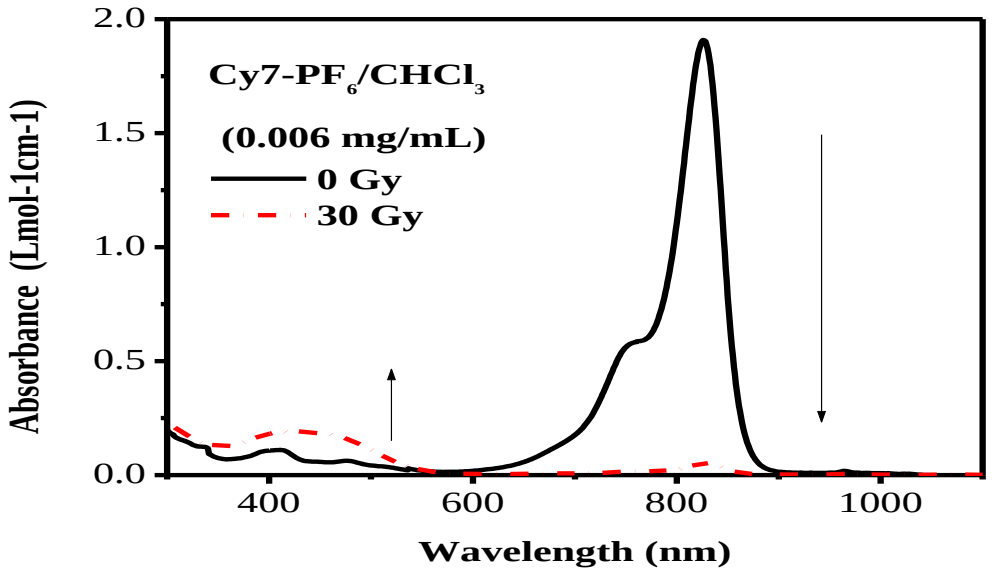

Figure 34 UV-Vis absorption spectra of 0.006 mg/mL Cy7-PF_6 solutions in chloroform, before (solid line) and after irradiation with 30 Gy (dashed line).

Mass spectra of Cy7-PF_6 (for un-irradiated and irradiated samples) seen in (Figure 35) resulted in mass to charge ratio (m/z) values shown in Table 9. The m/z values of Cy7-I (Figure 36) are similar to Cy7-PF_6 confirming the absence of counter ion effects in solutions compared to solid state films of these dyes as discussed by Véron et al [209].

Table 9 Mass to charge ratio of single peaks of Cy7-PF_6 for (a) un-irradiated (0 Gy) and (b) irradiated (30 Gy) of Cy7-PF_6 as determined by MS-ESI spectroscopy.

(a) Un-irradiated (0 Gy)

Peak	Mass to charge ratio (m/z)	Molecular Weight (MW)	Species	Structure
1	611.2	612	$Cy7^+$	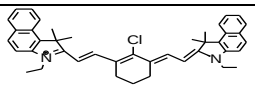

(b) Irradiated (30 Gy)

Peak	Mass to charge ratio (m/z)	Molecular Weight (MW)	Species	Structure
1	677	680.5	A	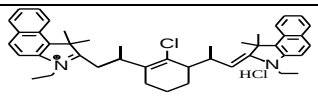
2	639	644	B	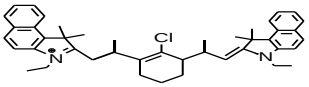
3	627.2	628	C	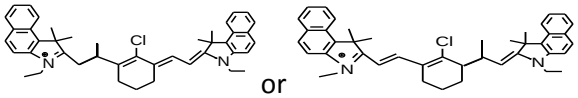
4	611.2	612	D	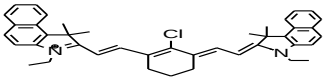
5	488	483	E	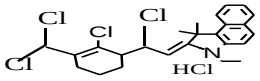
6	450	447.5	F	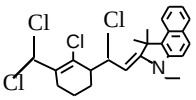
7	434	432.5	G	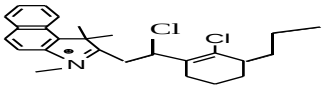

8	420	418.5	H	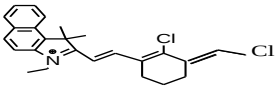
9	410	411	I	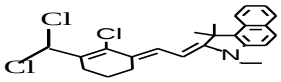
10	384	383	J	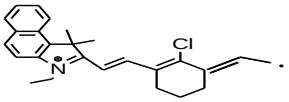
11	378	375.5	K	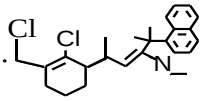
12	309	307.5	L	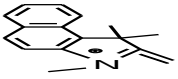

4.3.2.2. Postulated radiation-induced decomposition of Cy7-PF_6

The mass spectra for the un-irradiated Cy7-PF_6 show a mass to charge ratio (m/z) of 611.2 which stands for $Cy7^+$ with molecular weight of 612. The irradiated sample shows 12 major peaks (A - L). Broze-Uhle et al showed [200, 212] that halogenated solvents such as chloroform generate radicals which attack the conjugated bonds of MEH-PPV resulting in radical initiated degradation of the polymer in the presence of gamma radiation. Previously we observed similar behavior by Cy7-PF_6 in chloroform indicating the same mechanism. Our mass spectra results for the irradiated samples confirm these observations. Similar products were observed by mass spectrometry by Engel et al [213] on light-induced decomposition products of indocyanine

green, where the mechanism of decomposition involves singlet oxygen and formation of carbonyl compounds as decomposition products. In our results, it was not possible to explain as to the source of the CO-stretching band at 1707 cm^{-1} from the FTIR spectra.

For peak 'A' at m/z of 677, its corresponding molecular mass is 680.5 with a difference of 68.5 (from the un-irradiated molecular ion at 612) which could be due to reaction of $Cy7^+$ with successive addition of $.CHCl_2$ (attack on the double bond followed by dechlorination) and addition of HCl and 2H radicals. Peak 'B' appears at m/z of 639 with a corresponding molecular mass of 644. The difference for this species is 32 indicating a reaction of $Cy7^+$ with two CH_3 insertion (due to attack by $CHCl_2$ followed by declorination and addition of 2H radicals) and 2H radicals. Peak 'C' appears at m/z of 627.2 with a corresponding molecular mass of 628. The difference for this species is 16 indicating CH_3 insertion. Peak 'D' which appears at 611.2 with a corresponding molecular mass of 612 is due to $Cy7^+$. The proposed structures of the fragments 'A' to 'L' along their molecular formula and m/z values are listed in Table 9. As can be seen from the mass spectra (Figure 35(b)), the intensity of peak'D' is diminished greatly confirming the decomposition of $Cy7^+$ in to various fragments. This is in agreement with the reduced intensity of the absorption maximum at 826 nm as is shown in the UV-Vis spectra of the Cy7-PF_6 solution in chloroform (Figure 34).

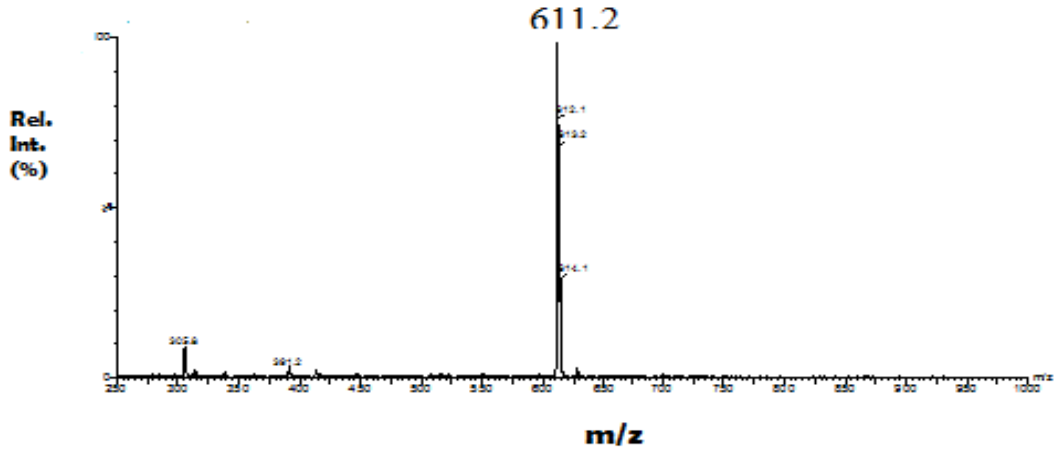

(a)

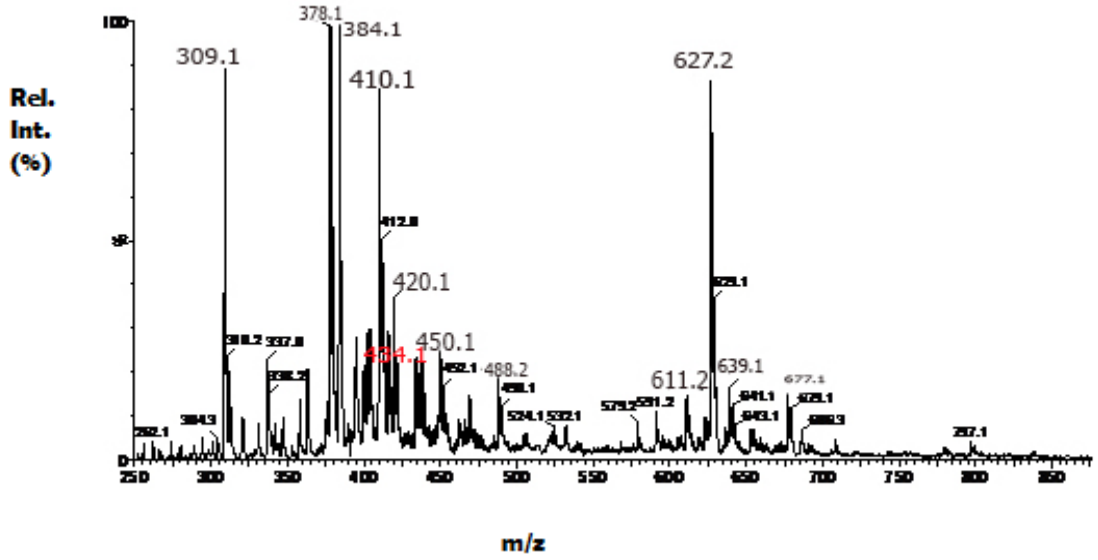

(b)

Figure 35 MS spectra of Cy7-PF_6 solution in chloroform (a) unirradiated and (b) irradiated at 30 Gy.

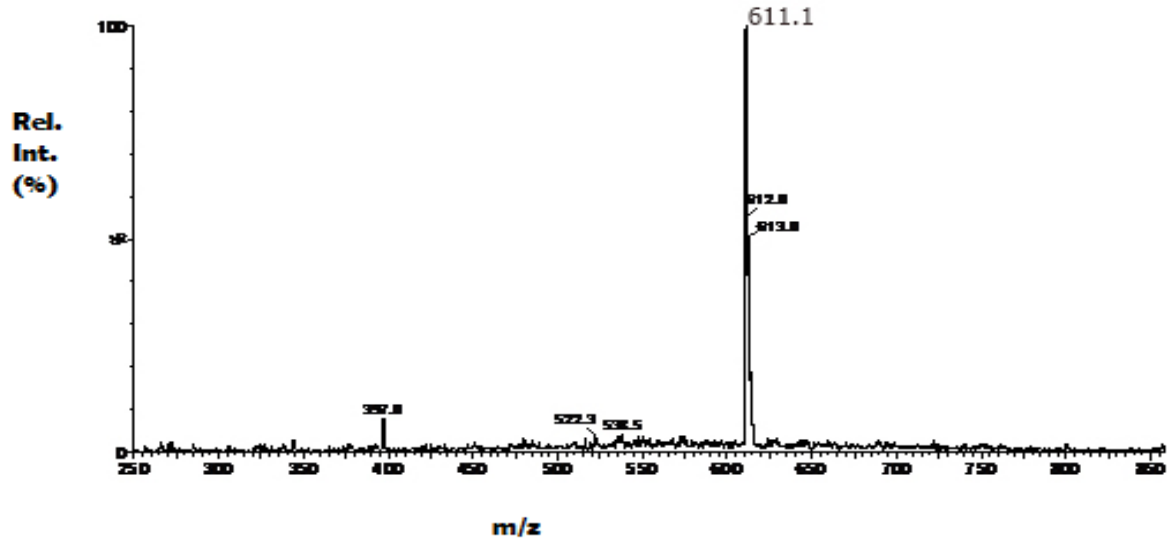

(a)

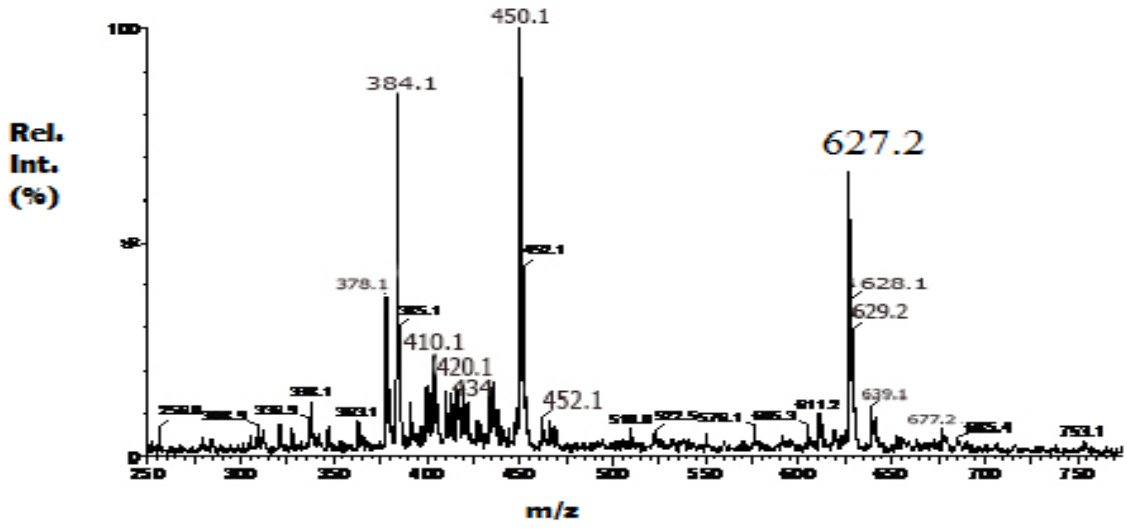

(b)

Figure 36 MS spectra of Cy7-I solution in chloroform (a) unirradiated and (b) irradiated at 25 Gy.

Peaks ‘E’ to ‘L’ are illustrated in the proposed reaction mechanism shown below (Figure 37, scheme).

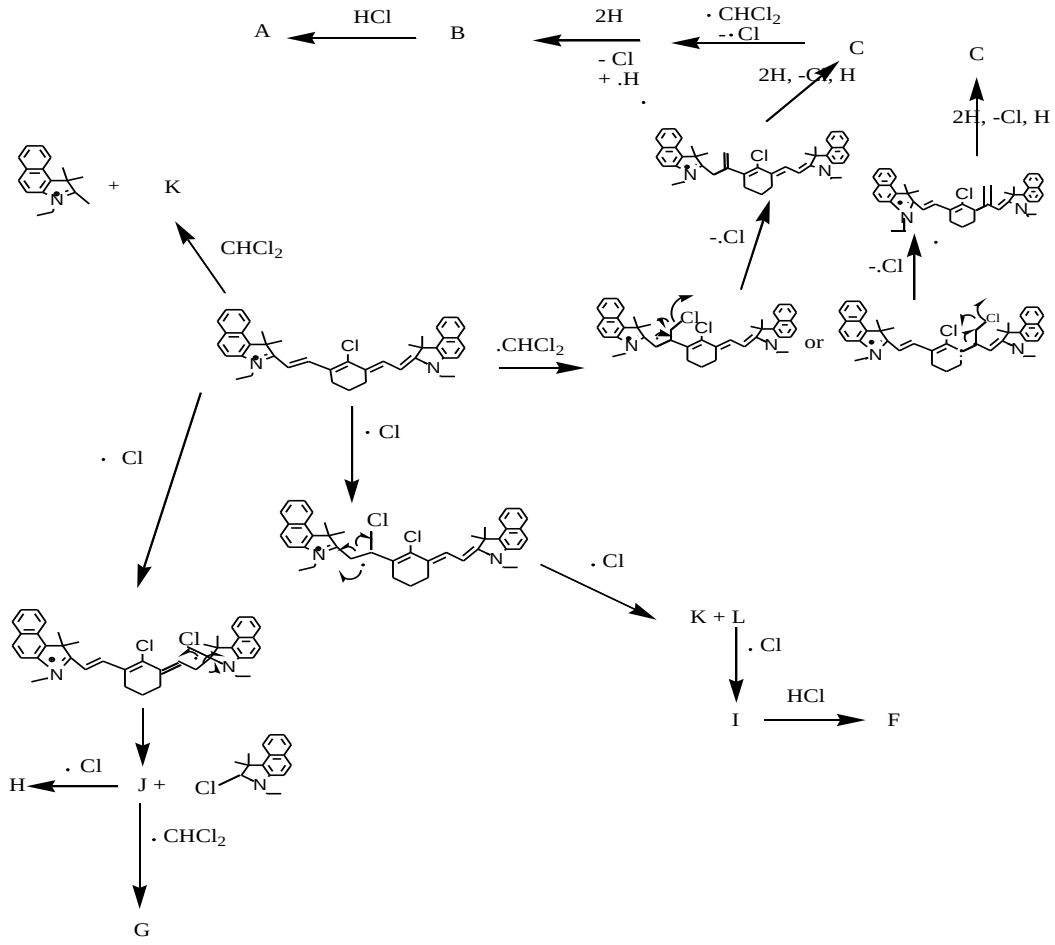

Figure 37 Scheme to illustrate the mechanism of the postulated radiation- induced decomposition of Cy7-PF_6.

The FT-IR spectra (Figure 38) show extensive degradation of conjugated bonds after irradiation (30 Gy) (1430 - 1016 cm^{-1}). Our FTIR result corroborates with the mass spectra data confirming the solvent assisted degradation of Cy7-PF_6 as observed by Bronze-Uhle et al [212] for MEH-PPV/$CHCl_3$ solutions. The main bands along their assignments for the un-irradiated (0 Gy) dye are listed in Table 10. New bands at 692, 745 and 809 indicate the insertion of chlorine atoms. New band at 1463 confirms H_2 addition reducing the degree of conjugation. A new band at 1707 confirms C=O-stretching of a ketone (its source not yet fully explained). Enhancement of the bands at 2925, 2952, and 2852 indicates increase in CH_3, CH, and CH_2-stretching of alkanes confirming decrease in degree of conjugation or increase in degree of saturation. The spectra are normalized to the aromatic stretching at 1548 cm^{-1} to remove small variations due to base line difference. This band was taken for normalization of the spectra because it does not change after irradiation.

The FTIR spectra of Cy7-I (Figure 39) shows similar behavior as of Cy7-PF_6 confirming absence of counter ion effects in solution as explained earlier.

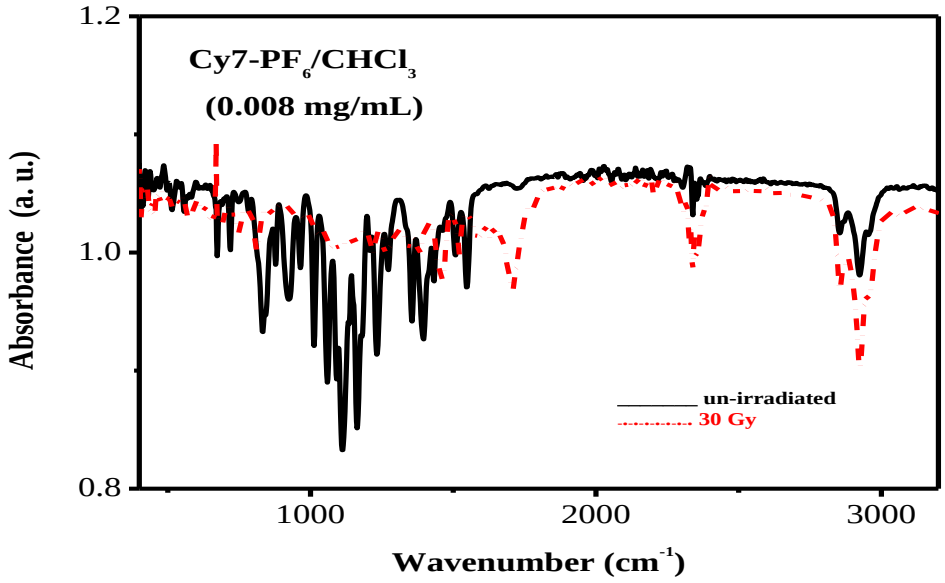

Figure 38 FTIR spectra of Cy7-PF_6 chloroform solution of un-irradiated (solid line) and irradiated solution with 30 Gy (dashed line).

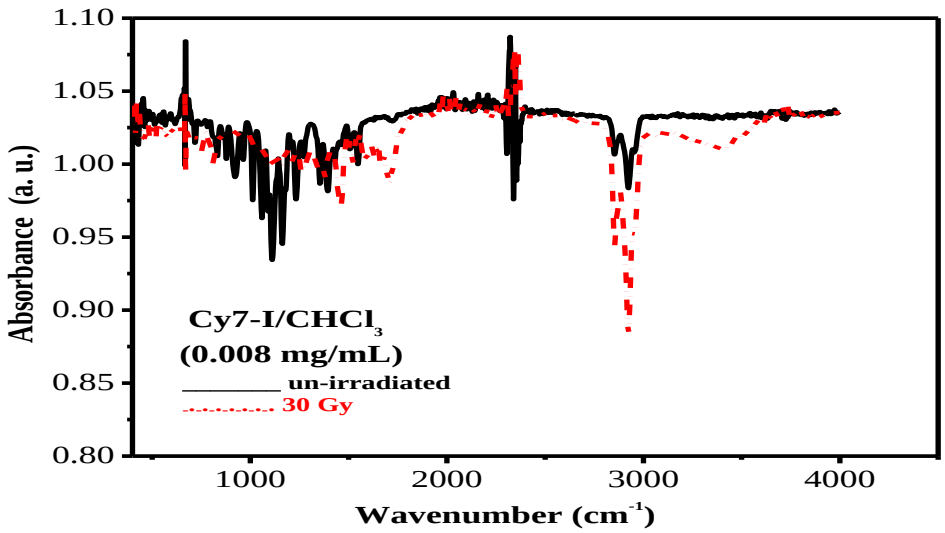

Figure 39 FTIR spectra of Cy7-I chloroform solution of un-irradiated (solid line) and irradiated solution with 30 Gy (dashed line).

Table 10 IR positions of un-irradiated Cy7-PF_6 [214].

Wavenumber (cm^{-1})	Assignment
3060	CH- stretching vinyl
2952	CH_3- asymmetric stretching
2925	CH- stretching
2852	CH_2 stretching
1548	C- C Stretching (aromatic ring stretching)
1505	C- C stretching (aromatic ring stretching)
1431	C-H in plane deformation ($R_1CH=CHR_2$-cis)-conjugation
1393	CH_3 bending (alkane)
1356	C-N vibration (aromatic tertiary amines)
1272	C-H in plane deformation ($R_1CH=CHR_2$-trans)
1240	C-H in plane deformation (tri-substituted alkenes)
1165	C-H in plane deformation(tri-substituted

	alkenes)
1112	C-H in plane deformation (tri-substituted alkenes)
1064	C-H in plane deformation (tri-substituted alkenes)
1011	C-H in plane deformation (tri-substituted alkenes)
963	C-H deformation (trans di-substituted alkenes)
930	C-H deformation ($C=CH_2$ –Vinyl)
840	C-H deformation (tri-substituted alkenes)
676 and 719	C-Cl (mono substituted)

4.3.3. Discussion

In our studies of section 4.2, we have shown that the heptamethine cyanine dyes Cy7-I and Cy7-PF_6 can be used as dosimeters for low dose gamma or X-ray radiation. Furthermore, an attempt was made to explain the dosimetric response of these dye solutions in halogenated solvents following the work of Broze-Uhle et al [212]. In our present work, we report the mechanism of radiation- induced decomposition of these dyes. Understanding the mechanism is one step-forward in the design of more sensitive, user friendly, cheap and tunable dosimeters for low dose

applications that can be done by synthesizing heptamethine cyanine dye derivatives with reasonable photo-stability or by blending these dyes with other polymers or by incorporating additives in the preparation of dosimetric solutions or films. Samanta et al [215] developed an NIR cyanine dye with excellent photostability by incorporating electron withdrawing acetyl group into NIR molecules such as indocyanine green (ICG).

It is with this aim that we investigated the mechanism of radiation- induced decomposition of Cy7-I or Cy7-PF_6 by applying UV-Vis, FTIR and MS spectrometric methods in order to be able develop dosimeters with reasonable stability, sensitivity and useful dose range from these dyes.
The mechanism of radiation-induced decomposition of Cy7-I/Cy7-PF_6 solution in chloroform is the new finding of our present work. As is shown in Figure 37, the proposed mechanism shows formation of various products as a result of attack on the conjugated bonds of these dyes by the radicals and stable molecules generated from the radiolysis of chloroform.

In summary radiolysis of chloroform produces different types of radicals and stable molecules [202]. We propose that the major radical species such as .Cl, .H, and .$CHCl_2$ and stable products such as HCl are responsible for the attack on the conjugated bonds of the heptamethine dyes. The general mechanism for the reaction involves two steps as discussed in [212]. The first step involves radiolysis of chloroform while the second step involves the attack by radicals like .Cl, $^{\cdot}$H or .$CHCl_2$ followed by degradation of the molecule into smaller radicals and molecules with subsequent attack by HCl and 2$^{\cdot}$H. The radical attack is mainly assumed to be by .Cl not by .$CHCl_2$ because of reactivity and steric consideration as shown by [216]. HCl forms adduct with

the nitrogen atom on the heterocycles of the heptamethine cyanine dye. This is consistent with works by Walba and Isensee [208].

4.3.4. Conclusion

Heptamethine cyanine dyes Cy7-PF_6 and Cy7-I in chloroform solutions show very promising characteristics as low-dose dosimeters by virtue of their availability at low cost, easily processablity and high molar extinction coefficient. In the current study the mechanism of radiation-induced decomposition in chloroform solutions which is responsible for their dosimetric character was elucidated using UV-Vis, MS and FTIR spectrometric methods. Our findings show that the mechanism responsible for the dosimetric character is the interactions of the radicals (.Cl or .$CHCl_2$) or stable molecule (HCl) with the conjugated polymethine bridge of the dye resulting in breaking of the π-bonds and breaking of the dye molecules in to various decomposition products. Understanding the mechanism is one step forward in developing more sensitive dosimeters for low dose dosimetry.

4.4. Investigation of heptamethine dyes in ethanol-trichloroacetic acid/chloral hydrate and acetone/chloral hydrate solutions for low dose dosimetry applications

4.4.1. Introduction

Organic dyes generally show strong visible absorption bands in solutions, therefore several studies have been carried out to investigate the effects of radiation on dye solutions with the objective of developing convenient dosimeters [217]. A number of organic dye solutions have been investigated as potential chemical dosimeter for a wide range of radiation doses that are useful for dosimetry in industrial radiation processing, health physics and radiation research [101].

Neto et al [174] investigated the gamma ray dosimetric properties of conjugated polymer dye solutions. Their results indicate that the presence of unsaturated bonds along the chain of the polymer sets a desirable feature for the design of sensitive dosimetric systems based on polymers in halogenated solvents.

In our studies in sections 4.2 and 4.3, the heptamethine dye solutions Cy7-PF_6 and Cy7-I in chloroform have shown dosimetric characteristics at low doses. In this work, the possibility of preparing a dosimetric solution in non-toxic solvents ethanol and acetone were done following the work done by Suslawati [218]. Trichloroacetic acid and chloral hydrate were added as radical generating species. The results of our studies is described and discussed.

4.4.2. Results and Discussion

4.4.2.1. Dosimetric characteristics of Cy7-PF_6/ethanol-trichloroacetic acid solution

The UV-Vis spectra (Fig.40) and PL emission spectra (Figure 41) show striking similarity with the dosimetric solution of heptamethine dyes in chloroform.

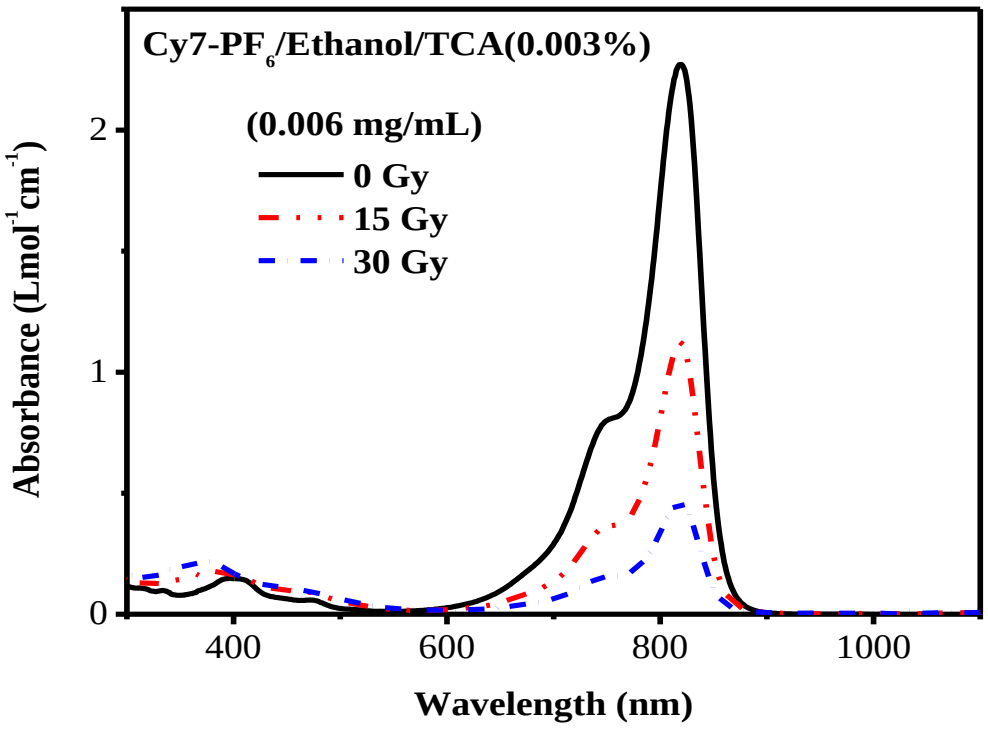

Figure 40 Absorbance spectra of un-irradiated and irradiated 0.006 mg/mL dye solution; top to bottom: un-irradiated, 15 and 30 Gy of the dosimetric solutions of Cy7- PF_6 in ethanol with 0.003 % trichloroacetic acid (TCA).

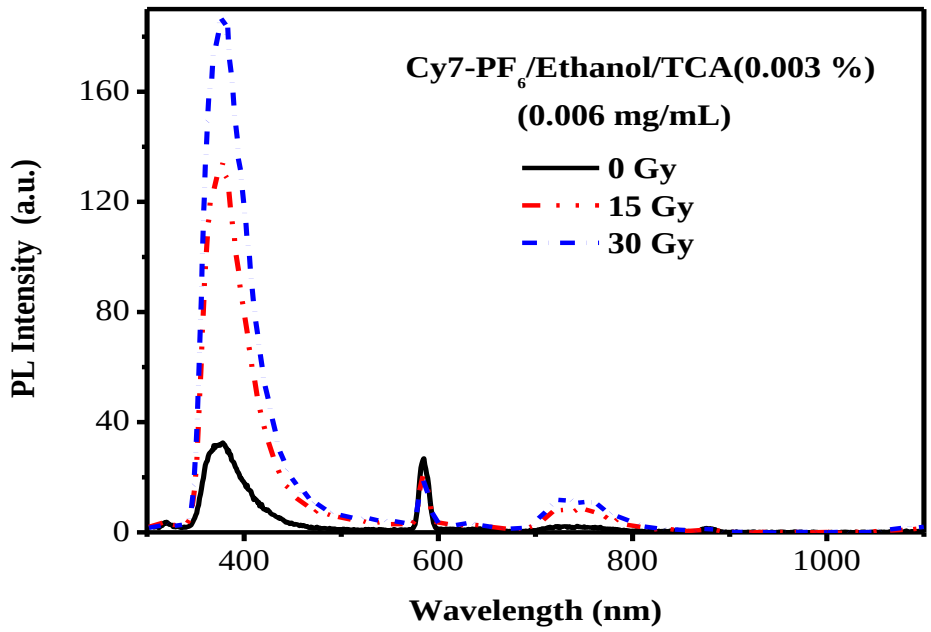

Figure 41 Photoluminescence spectra of un-irradiated and irradiated 0.006 mg/mL solution; top to bottom: unirradiated, 15 and 30 Gy of the dosimetric solutions Cy7- PF_6 in ethanol with 0.003 % trichloroacetic acid at 292 nm excitation.

This clearly shows the involvement of trichloroacetic acid as a radical generating species. The dosimetric response of the dye is a result of a two step reaction where in the first step radiation-induced decomposition of trichloroacetic acid happens resulting in the formation of radicals such as Cl and stable molecules such as HCl. In the second step, the radical Cl and stable molecule HCl attack the dye molecule resulting in a dosimetric response. The proposed mechanism is dicussed below.

To study the possibility of preparing dosimetric solutions using less toxic solvents, solutions of Cy7-PF_6 in ethanol with 0.003 % trichloroacetic acid was prepared and evaluated for dosimetric

characteristics. Trichloroacetic acid was used as radical generating molecule in place of chloroform as used by Susilawati et al [218]. Upon irradiation, trichloroacetic acid undergoes radiation- induced decomposition resulting in chlorine (Cl) and other radicals. Schumacher and Sundhoff [219] have shown that ethanol is an excellent scavenger of chlorine atoms (Equation 22).

$$CH_3\text{-}CH_2\text{-}OH + .Cl \rightarrow CH_3\text{-}^{\cdot}CH\text{-}OH + HCl \quad (22)$$

Furthermore, Gugumus [220] showed the formation of acetaldehyde from $CHCl_3$ in ethanol as shown in Equations 23 and 24.

$$CH_3\text{-}^{\cdot}CH\text{-}OH + CHCl_3 \rightarrow CH_3\text{-}CH(Cl)\text{-}OH + .CHCl_2 \quad (23)$$

$$CH_3\text{-}CH(Cl)\text{-}OH \rightarrow CH_3\text{-}CH{=}O + HCl \quad (24)$$

Trichloroacetic acid is expected to undergo similar reaction as shown in Equation 25 and hence enhanced HCl generation can happen following the decomposition of CH_3-CH(Cl)-OH.

$$CH_3\text{-}^{\cdot}CH\text{-}OH + Cl_3CCOOH \rightarrow CH_3\text{-}CH(Cl)\text{-}OH + .Cl_2CCOOH \quad (25)$$

We propose that the attack by Cl, HCl and other radicals to be responsible for the dosimetric response due to the interaction of the radicals or stable molecules with the conjugated bonds of the dye molecule. Spectrophotometric and spectrofluorometric curves of these dosimetric solutions show linear relations with the applied doses. The sensitivity obtained from the linear fit of the emission amplitude ratio (Figure 42) is (0.26 ± 0.02) with $R^2 = 0.998$ which makes it a very promising material for low dose dosimetry. The sensitivity is much lower than $CHCl_3$ based dosimetric dye solutions. This could be partly explained in terms of lower bond energy value for C-Cl bond in Cl_3CCOOH [221] compared to $CHCl_3$ as shown in Table 11 and also partly

explained due to enhanced HCl generation in the presence of ethanol as a solvent. Figures 42a and b depict the dosimetric responses for these solutions.

Table 11 Bond dissociation energies of dichloromethane and chloroform [221].

Solvent	Chemical Bond	Bond Dissociation Energies, $kJmol^{-1}$(at 298.15 K)
Dichloromethane	CH_2Cl-Cl	338.1
Chloroform	$CHCl_2$-Cl	320.5 ± 6.3
Trichloroacetic acid	Cl-Cl_2 COOH	277.4

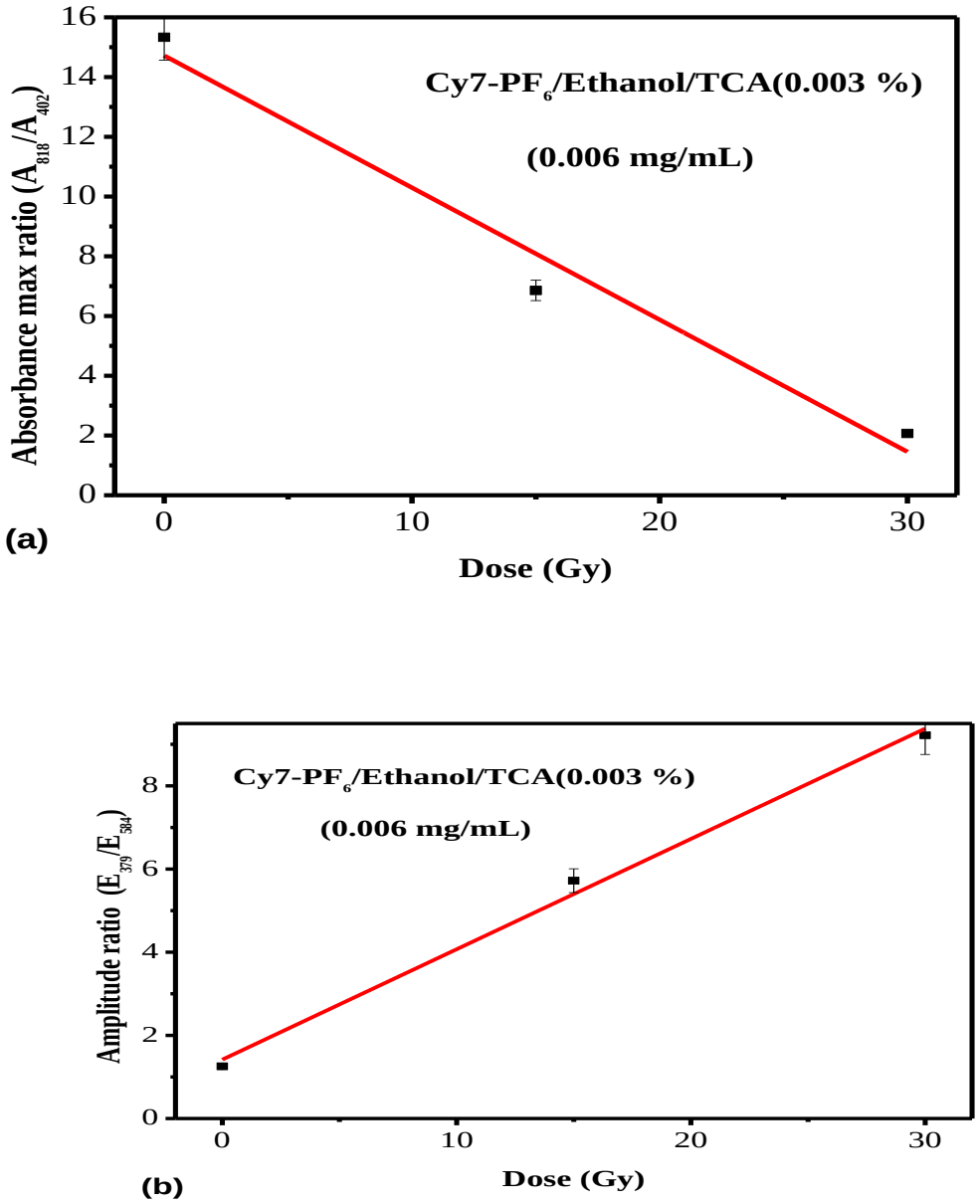

Figure 42 Response plot of a) absorbance max ratio (A_{818}/A_{402}) and b) emission amplitude ratio (E_{379}/E_{584}) at 292 nm excitation as a function of dose for Cyc7-PF_6 solution (0.006 mg/mL) solution in ethanol with 0.003 % Trichloroacetic acid (TCA)

The FTIR data (Figure 43) also confirms greater extent of loss of conjugation with increasing doses as is clearly seen at 30 Gy dose. There is a good agreement with the proposed mechanism which involves attack by chlorine radical, hydrogen chloride molecule and other radicals.

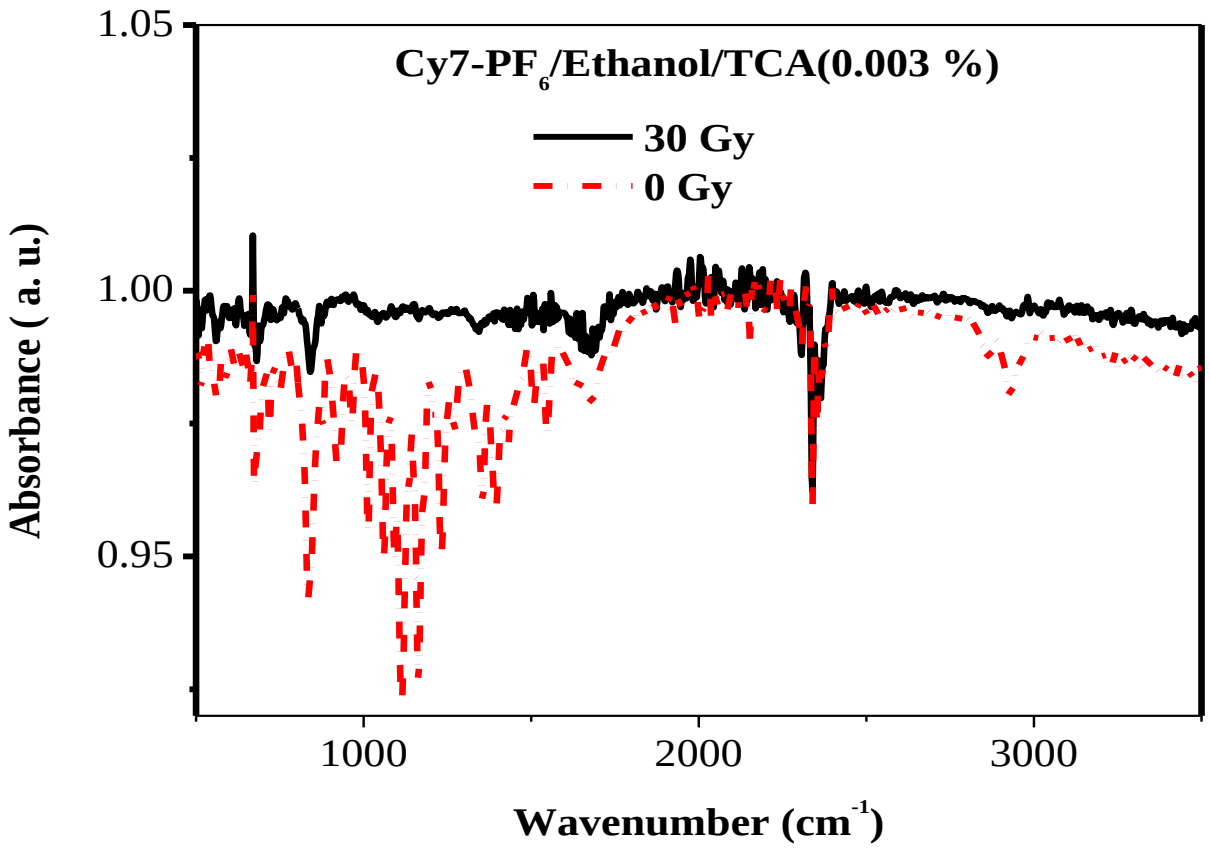

Figure 43 FTIR spectra of Cy7-PF_6 in ethanol with 0.003 % trichloroacetic acid solution of un-irradiated (solid line) and irradiated solution with 30 Gy (dashed line).

4.4.2.2. Dosimetric characteristics of Cy7-PF_6/Acetone-Chloral hydrate solution

In an effort to develop a dosimeter solution from non-hazardous solvents, Cy7-PF_6 in acetone with 80% chloral hydrate was prepared and evaluated for its dosimetric characteristics. Our result shows very similar dosimetric response as was demonstrated by Cy7-PF_6 in ethanol with 0.003 % trichloroacetic acid. As can be seen from the UV-Vis spectra in Figure 44, Cy7-PF_6 in acetone with 0.003% chloral hydrate can be used as a low dose dosimeter solution. Acetone undergoes acid catalyzed chlorination to produce chloroacetone and other chlorinated compounds as in [222].

$$CH_3\text{-}CO\text{-}CH_2\text{-}H + Cl_2 \rightarrow CH_3\text{-}CO\text{-}CH_2Cl + HCl \quad (26)$$

This reaction shown in Equation 26 results in generation of HCl which might be responsible for the dosimetric response observed.

The response plot based on A_{819}/A_{402} *versus* dose does not show linear relation while the response plot based on $(A\text{-}A_0)/A_0$ versus dose show linear relation as shown in Figure 45. The linear response from this curve is $(A\text{-}A_0)/A_0 = (0.024 \pm 0.026) + (0.007 \pm 0.001)$ D with $R^2 = 0.97$. Using the angular equation of the proposed equation a sensitivity of 0.007 ± 0.001 is obtained. Here also we find an enhanced sensitivity similar to the Cy7-PF_6/ethanol/TCA system partly due to low bond energy of C-Cl bond in chloral hydrate and partly due to enhanced HCl generation as shown in Equation 26.

Further work is needed to evaluate the similarities and differences in the structural changes that happen following irradiation and also the pre- and post irradiation stabilities of this dosimeteric solution with the Cy7-PF_6/$CHCl_3$ and Cy7-PF_6/ethanol/TCA systems.

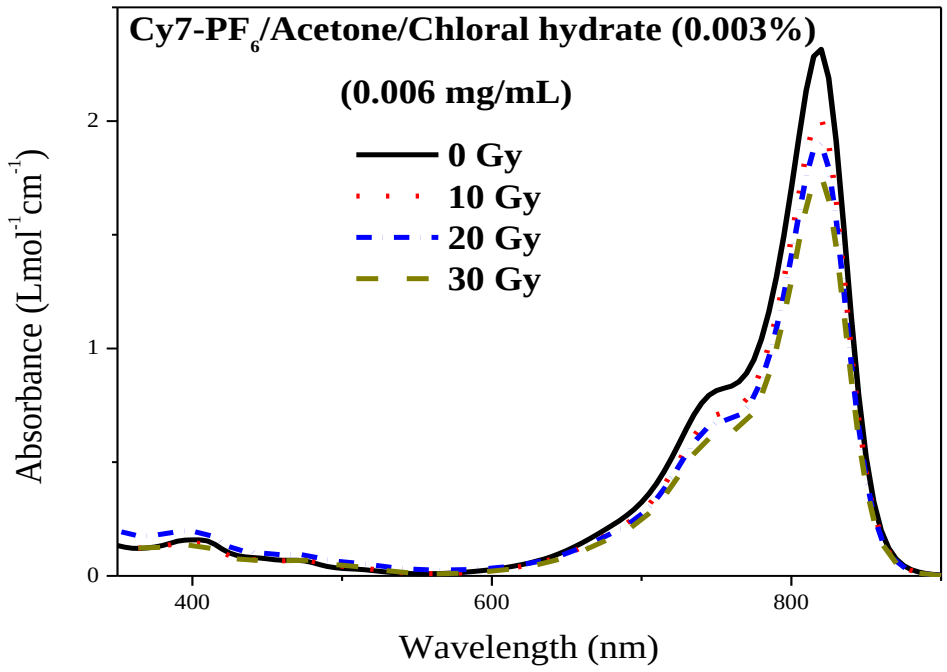

Figure 44 Absorbance spectra of un-irradiated and irradiated 0.006 mg/mL solution; top to bottom: un-irradiated, 10, 20 and 30 Gy of the dosimetric solutions of Cy7- PF_6 in acetone with 0.003% chloral hydrate (CH).

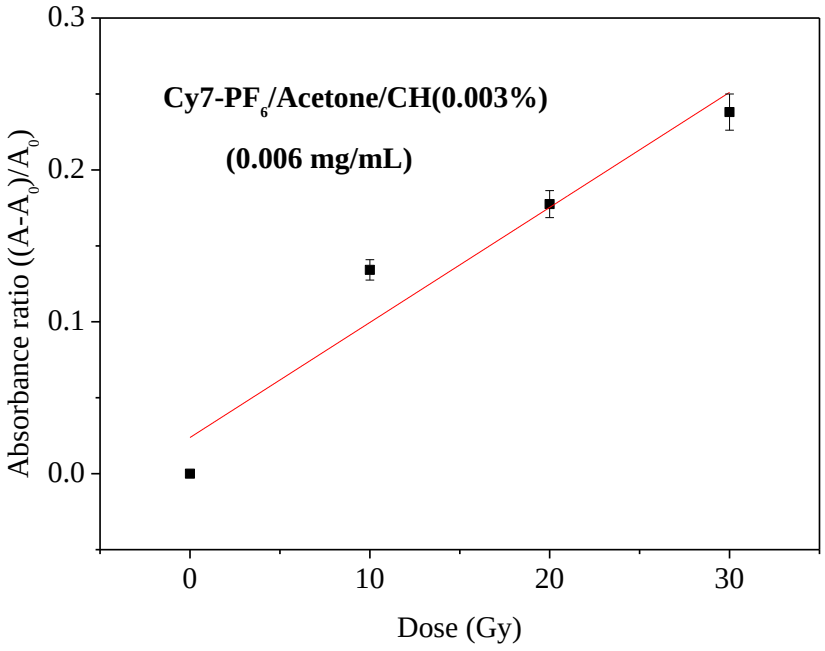

Figure 45 Response plot of absoption spectra of Cy7-PF_6 solution in acetone with 0.003% chloral hydrate.

4.4.2.3. Dosimetric characteristics of Cy7-I in ethanol with 0.003% chloral hydrate

The dosimetric characteristics of Cy7-I in ethanol with 0.003% chloral hydrate was also evaluated encouraged by the results obtained for the Cy7-PF_6/ethanol/trichloroacetic acid (0.003%) system. As was predicted, the Cy7-I/ethanol/chloral hydrate (0.003%) system showed decrease in intensity of the main peak on irradiation as can be clearly observed in the UV-Vis spectra in Figure 46.

Our result shows that the heptamethine dyes can be used as low dose dosimeters using a non-hazardous solvent ethanol in the presence of chloral hydrate as alternate radical generating

species. Further work is required to evaluate the optimum concentration of chloral hydrate and pre- and post-irradiation stability, dose range and other related dosimetric characteristics.

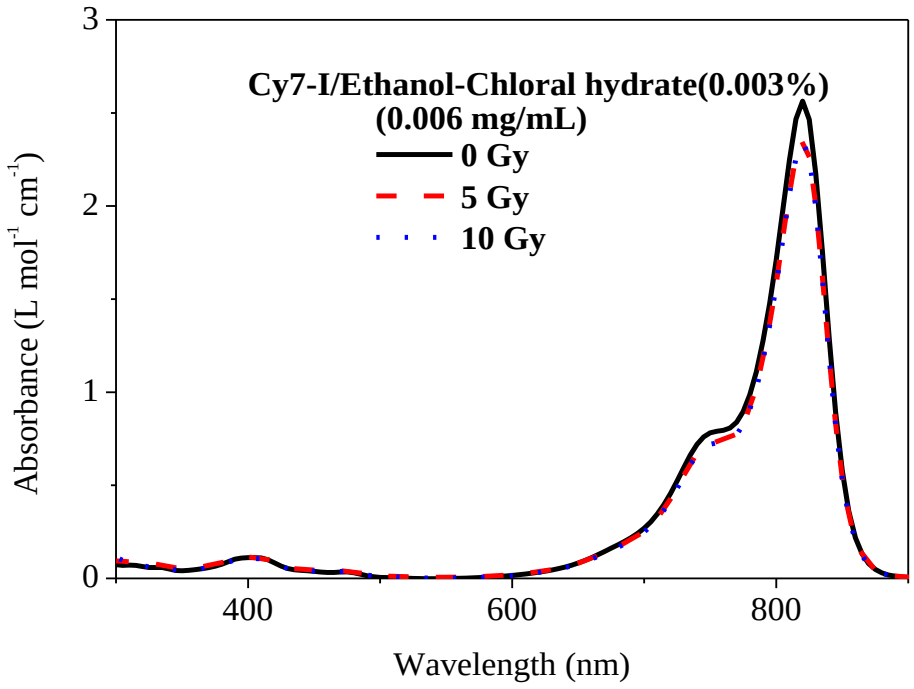

Figure 46 UV-Vis spectra of 0.006 mg/mL solution of Cy7-I in ethanol with 0.003% chloral hydrate. Top to bottom: unirradiated, irradiated at 5 Gy and 10 Gy.

4.4.3. Conclusion

The heptamethine dye Cy7-PF_6 solution in ethanol with 0.003% trichloroacetic acid was investigated using UV-Vis spectrophotometry, spectrofluorometry and FT-IR spectroscopy techniques for its dosimetric behavior. The study was conducted to evaluate the possibility of preparing a dosimeter solution using non-toxic solvent ethanol. The results of our studies show that Cy7-PF_6 solution in ethanol with 0.003% trichloroacetic acid is a promising dosimeter solution for low dose dosimetry.

The dosimetric characteristic is also similar to the heptamethine dye-chloroform solution which involves two steps. In the first step, radiation-induced decomposition of the trichloroacetic acid occurs resulting in the formation of Cl and other radicals as well as stable molecules such as HCl. In the second step, the Cl radical and HCl attack the π-bond at the middle of the heptamethine dye molecule resulting in decomposition of the dye molecule. This in turn, results in the dosimetric characteristics. The low bond-energy of C-Cl in trichloroacetic acid might be partly responsible for the enhanced sensitivity of this dosimetric solution. This is an advantage for the detection of low dose radiation.

The Cy7-PF_6/acetone/chloral hydrate and Cy7-I/ethanol/chloral hydrate solutions also showed dosimetic response at low doses. This confirms the involvement radical generating species chloral hydrate in non-halogenated solvents ethanol and acetone.

The non-toxic nature of ethanol and acetone used as solvents makes these dosimetric solutions as promising materials for dosimetric application in medicine and environment.

4.5. Study of curcumin solutions in chloroform and ethanol/chloral hydrate for low dose dosimetry applications

4.5.1. Introduction

Many dyestuffs have spectral properties that are quite γ-radiation dependent. Some of these molecules have been used as spectral probes i.e., dosimeter to monitor the environment of γ-radiation sources [223 - 225].

The use of natural dyes for developing radichromic dosimeters is advantageous because natural dyes are economical, eco-friendly, less toxic and less allergic [226 - 228]. Curcuma Longa is a small perennial herb native to India bearing many rhizomes on its root system which are the source of its culinary spice known as turmeric and its medicinal extract called Curcumin (Figure 22). In addition to its use as a spice, turmeric is used as a dye for cloth and coloring agent in food and cosmetics [226, 229- 230].

Shahid et al [226] investigated the possibility of using this tradiational turmeric dye (curcumin) as a radiochromic dosimeter film for high dose applications. They prepared polyvinyl alcohol (PVA) and curcumin dye films at three different concentrations and evaluated their dosimetric characteristics at high doses in acidic, neutral and basic conditions.

Curcimin dye solution in halogenated solvents such as chloroform and in non-hazardous solvent ethanol for low dose dosimetry has not been investigated. The structural similarity between heptamethine dyes and this turmeric dye molecule (i.e. both molecules have bridging π-bond)

prompted us to evaluate its dosimetric characteristics in chloroform and ethanol/chloral hydrate solution.

In this study the dosimetric characteristics of curcumin (a turmeric dye) as a dosimeter for low dose gamma and X-ray radiation was evaluated spectrophotometrically and spectrofluorometrically. The dosimetric characteristics, thus obtained, are described and discussed below.

4.5.2. Results and Discussion

4.5.2.1. Dosimetric characteristics of curcumin in chloroform

The UV-Vis spectra of curcumin dye solution in chloroform shows decrease in intensity of the main peak at 404 nm with increasing radiation dose to 15 Gy and 30 Gy showing blue shifts to 394 nm and 384 nm, respectively as was observed in the work of Batagin-Neto et al [173] for MEH-PPV solutions in chloroform. The blue shift in wavelength with increasing doses could be due to radiation induced loss of conjugation. This process involves two steps. In the first step, radiation-induced decomposition of chloroform occur which results in the formation of Cl, $CHCl_2$ radicals and other stable molecules such as HCl as was previously discussed. In the second step, Cl, $CHCl_2$ and other radicals as well as the stable molecules such as HCl attack the π-bond of the curcumin dye molecule resulting in loss of conjugation. Additional spectroscopic studies should be carried out to account the mechanism of the decomposition. At this point, it can be seen that curcumin in chloroform solution could be used for the detection of low dose radiation. Figure 47 shows the absorption spectra of curcumin solution in chloroform.

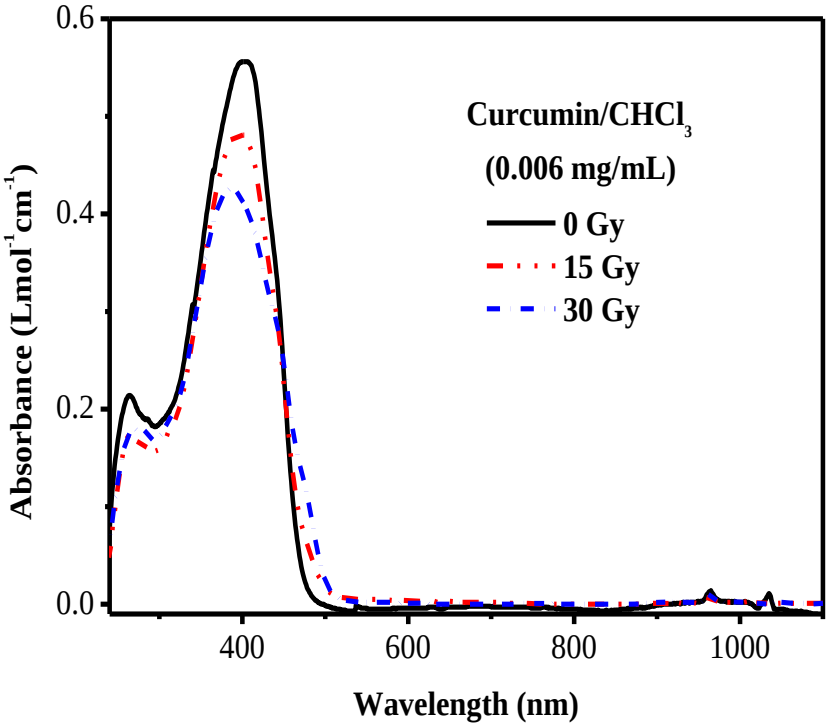

Figure 47 Absorbance spectra of un-irradiated and irradiated 0.006 mg/mL solution; top to bottom: un-irradiated, 15 and 30 Gy of the dosimetric solutions of curcumin.

The photoluminescence spectra of un-irradiated and irradiated 0.006 mg/mL of curcumin solutions in chloroform were measured in the range from 300 - 1100 nm using the spectrofluorometer at a dose range of 0 - 30 Gy (at 400 nm excitation) (Figure 48).

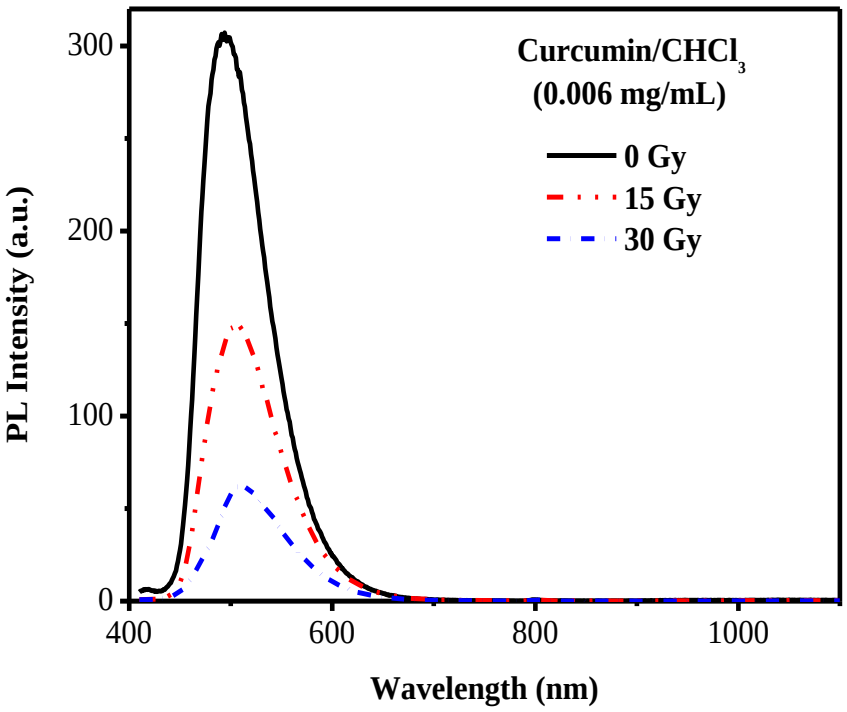

Figure 48 Photoluminescence spectra of un-irradiated and irradiated 0.006 mg/mL solution; top to bottom: unirradiated, 15 and 30 Gy of the dosimetric solutions curcumin at 400 nm excitation.

The emission spectral curves show decrease in intensity and also shifts in the main peak from 493 nm for the un-irradiated to 506 nm and 512 nm for the samples irradiated at 15 Gy and 30 Gy, respectively. The emission spectral curves obtained are completely different to those obtained for the heptamethine dye solution in chloroform. This might be due to differences in the products of the radiation-induced decomposition. A detailed spectroscopic study should be carried out to account for the mechanism.

The emission spectral response curve (Figure 49) plotted as intensity (emission amplitude) ratio of irradiated per un-irradiated sample (E/E_0) at 400 nm excitation as a function of radiation dose

shows linear relation. The linear response can be written for $E/E_{)0}$ = (0.96 ± 0.08) - (0.02 ± 0.00) D with R^2 = 0.98. D stands for applied dose and R^2 the square of linear correlation parameter. Using the angular equation of the proposed equation, a sensitivity of (0.02 ± 0.00) Gy^{-1} for curcumin was obtained which makes it a very promising material for low dose dosimetry. This shows the possibility of using curcumin solution in chloroform for low dose dosimetry.

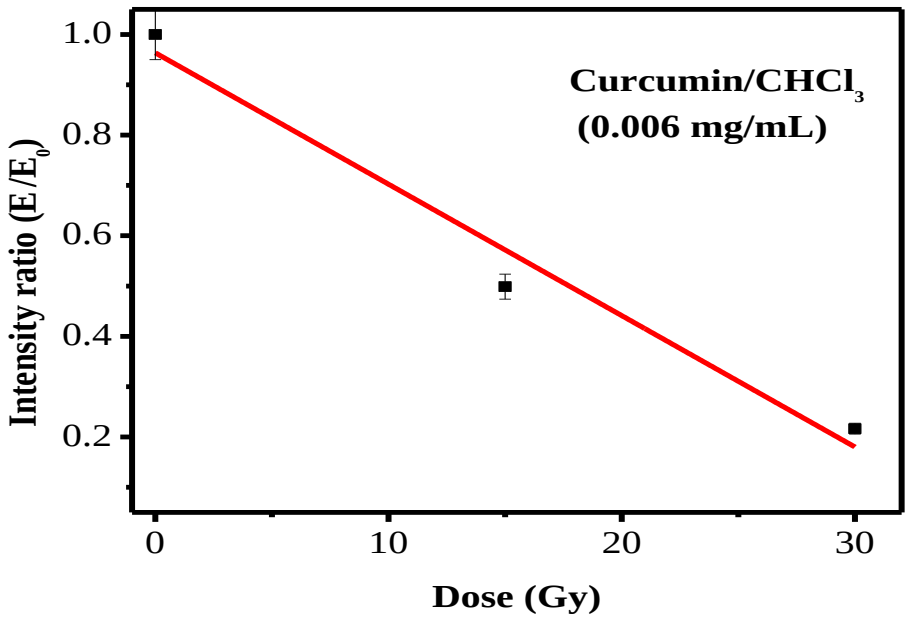

Figure 49 Response plot for curcumin (0.006 mg/mL) solution in $CHCl_3$ showing emission amplitude ratio (E/E_0) (at 400 nm excitation) *versus* absorbed radiation dose.

The pre-irradiation stability study of curcumin solution in chloroform in dark and light at room temperature was evaluated. Our results show that the solutions kept in the dark showed remarkable stability (with < 0.5 % decrease in absorbance change after 25 days). The solution kept in laboratory diffused light showed dramatic change in absorbance (~50%) which is similar

to properties of heptamethine dye chloroform solutions observed previously. Figure 50 depicts these results. Therefore, curcumin dye solution in chloroform could be kept in the dark to protect it from visible light in order to use it as a dosimeter solution.

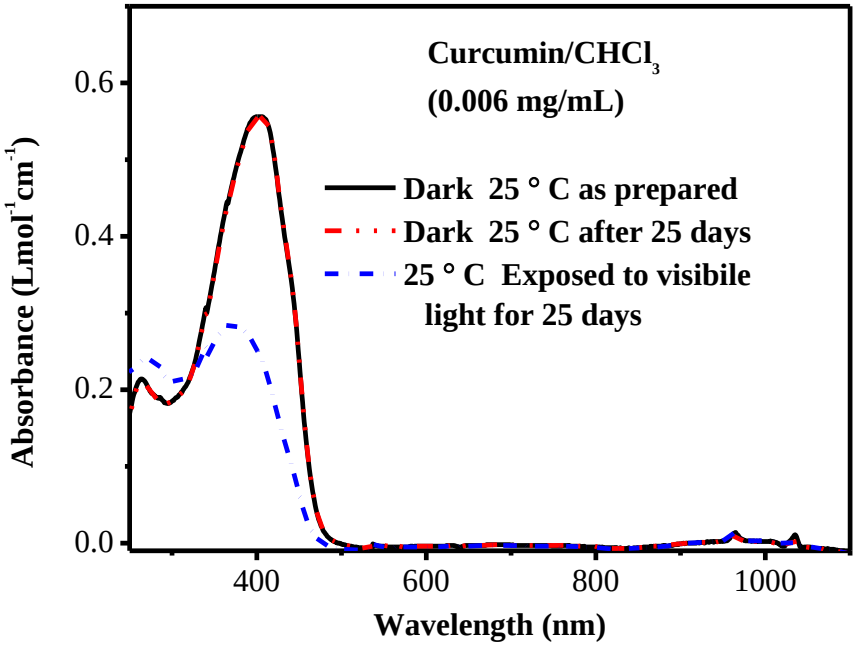

Figure 50 Absorption spectra of curcumin (0.006 mg/mL) in $CHCl_3$ solution pre-irradiation stability study (in dark and visible light).

4.5.2.2. Dosimetric characteristics of curcumin in ethanol with 0.003% chloral hydrate

The dosimetric characteristic of curcumin in ethanol was investigated using chloral hydrate as a radical generating species instead of chloroform. As was presented in section 4.4, the heptamethine dye Cy7-PF_6 in ethanol with 0.003% trichloroacetic acid showed dosimetric

characteristics. In this investigation, curcumin was evaluated if it shows dosimetric characteristics in a non-hazardous solvent ethanol with 0.003% chloral hydrate. Chloral hydrate was used following the work of Abdel-Fattah et al in [231]. As can be seen from the UV-Vis spectra in Figure 51, a slight decrease in intensity of the main peak was observed after irradiation (at 20 Gy) similar to the curcumin/chloroform solution dosimeter.

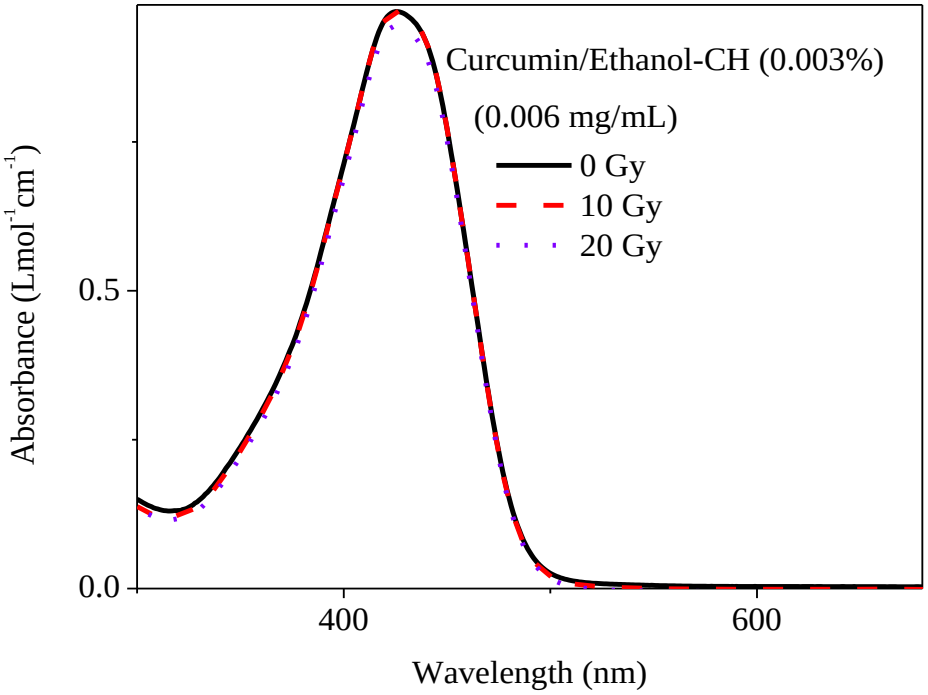

Figure 51 UV-Vis spectra of 0.006 mg/mL curcumin in ethanol with 0.003% chloral hydrate. Top to bottom: unirradiated, irradiated at 10 Gy and 20 Gy.

4.5.3. Conclusion

The turmeric dye curcumin solution in chloroform was investigated spectrophotometrically and spectrofluorometrically for its dosimetric characteristics for low dose dosimetry. The results of

our studies show curcumin dye solution in chloroform shows a promising response for low dose dosimetry in the range between 0 to 30 Gy. The absorption spectra show blue shifts with increasing dose as well as decrease in intensity of the absorption maximum. The blue shift could be caused by the loss of conjugation due to attack by Cl and other radicals as well as stable molecules such as HCl generated from the radiolysis of chloroform. The response curve of emission amplitude *versus* absorbed radiation dose shows linear relation. This shows that curcumin dye solution in chloroform is a promising material for low dose radiation dosimetry application in medicine as well as environment. We also found that curcumin could be a promising dosimeter in a non-hazardous solvent ethanol with chloral hydrate as a radical generating molecule.

4.6. Study of P3HT solutions in chloroform for low dose dosimetry applications

4.6.1. Introduction

There are several types of radiation sensors commercially available, including ionization chambers, Geiger counters, proportional counters, scintillators and solid state detectors. Each type has advantages, although many of these sensors require expensive electronics for signal amplification, are large and bulky, have limited battery life or require expensive materials for fabrication. A radiation sensor constructed of a polymeric material could be made flexible, light, and designed in various geometries to suit the application. Very simple and inexpensive electronics would be necessary to measure the change in conductivity with exposure to radiation. Essentially, an ‘‘alarm’’ is triggered when a set change in conductivity occurs in the sensor that corresponds to a predetermined radiation dose having been absorbed by the polymer [159]. Conducting polymers are getting the attention of researchers in the field of radiation detection because of their ability to respond to effects of radiation by changing their electrical as well as optical properties.

The first report on the use of conducting polymers for radiation detection was the work of Yoshino et al [92] who investigated the effects of electron irradiation on the electrical conductivity of polyacetylene in the early 1980s. In their experiment, they irradiated polyacetylene with an electron beam of 2 MeV in different dosages, and then doped with I_2 vapor. They found that increasing irradiation dosage resulted in a decrease in electrical

conductivity. From this they inferred that the conductivity was affected by the irradiation-induced imperfections, such as chain breaks and cross-linking.

There have been many reports by different authors on the study of conducting polymers for ionizing radiation dosimetry applications [178, 185 - 188, 232]. Raval et al [74] investigated the possibility of developing a radiation sensor based on poly 3-hexylthiophene, P3HT, for the measurement of high doses of radiation. They developed an organic field effect transistor (OFET) with the active component made of P3HT. The results of their study show the potential of using the sensor for detection of high dose radiation. Another study was done by Kingsley et al [233] on a MV X-ray detector consisting of a flexible phosphor layer in contact with an organic photovoltaic fabricated from P3HT:PCBM. X-rays incident on the phosphor generate luminescence that is then detected by the organic photovoltaic.

P3HT solutions in chloroform for low dose dosimetry have not been fully investigated. In the present work, we investigated the effect of low dose radiation on dosimetric characteristics of P3HT in chloroform solution in the presence and absence of 2, 2 - bis (4 - chlorophenyl) - l, 1, l – trichloroethane (DDT) as and additive spectrophotometrically and spectrofluorometrically. The results of our studies are described and discussed below.

4.6.2. Results and Discussion

DDT undergoes decomposition generating HCl under ionizing radiation as discussed in reference [234]. This shows the possibility of using P3HT/$CHCl_3$/DDT solution as a low dose dosimeter.

In this study, DDT was added with the objective of evaluating its ability as a radiosensitizer in the P3HT/DDT/$CHCl_3$ composite solution.

Our results show a slight shift in peak position of maximaum absorption as a function of dose in the UV-Vis spectra (Figure 52).

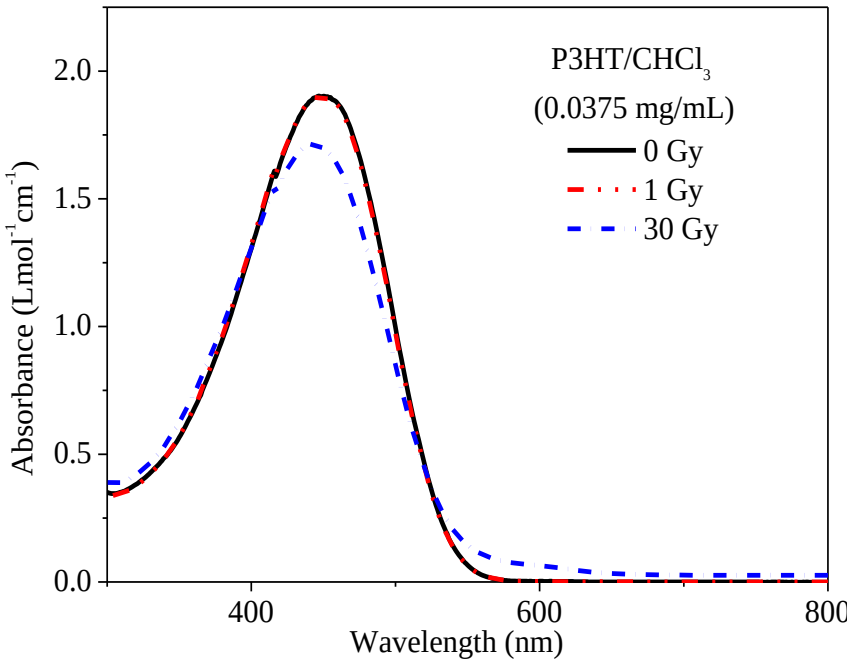

Figure 52 Absorbance spectra of un-irradiated and irradiated 0.0375 mg/mL solution; top to bottom: un-irradiated, 1 and 30 Gy of the dosimetric solutions of P3HT.

A decrease in intensity of luminescence spectra was observed in the P3HT/$CHCl_3$ solution with increasing dose (Figure 53).

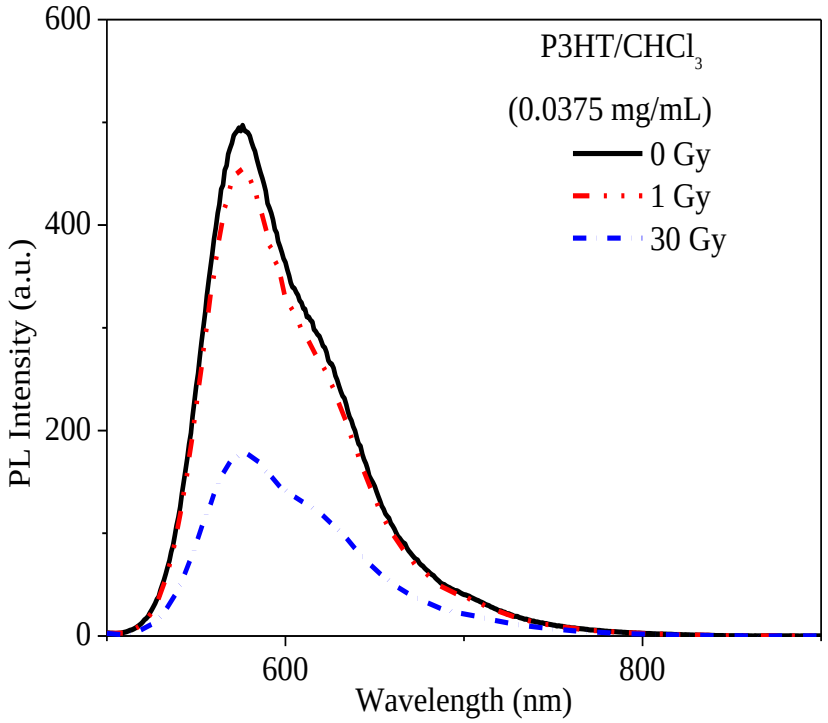

Figure 53 Photoluminescence spectra of un-irradiated and irradiated 0.0375 mg/mL solution; top to bottom: unirradiated, 1 and 30 Gy of the dosimetric solutions P3HT at 500 nm excitation.

On the other hand, the peak position in the UV-Vis spectra in the presence of DDT showed a dramatic shift after irradiation at 30 Gy (Figure 54).

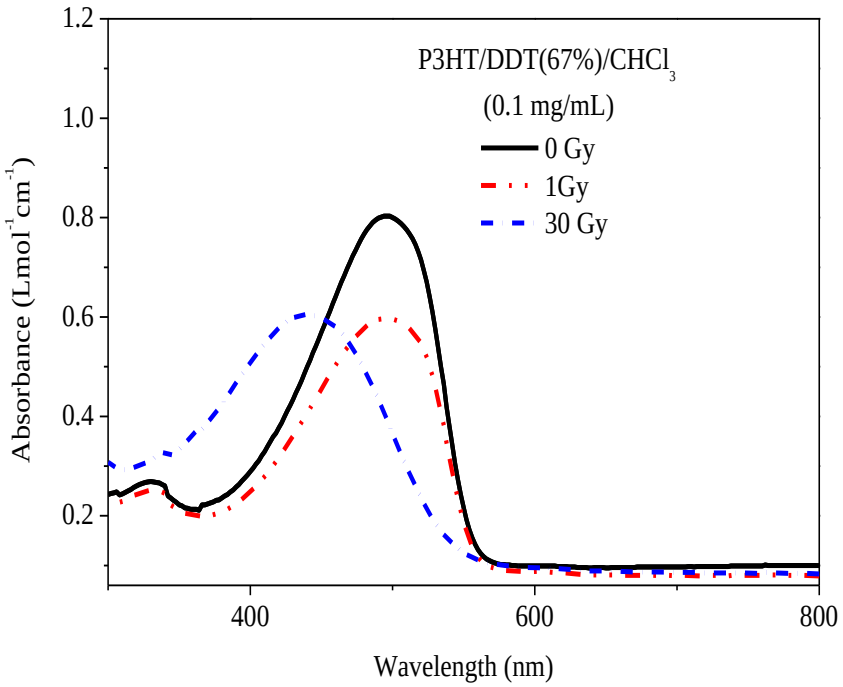

Figure 54 Absorbance spectra of un-irradiated and irradiated 0.1 mg/mL solution with 67% DDT; top to bottom: un-irradiated, 1 and 30 Gy of the dosimetric solutions of P3HT.

The addition of DDT resulted in enhancement of degradation effect on P3HT due to radiation induced decomposition of DDT. Irradiation of DDT, generates HCl together with the radiolysis products of chloroform enhances the degradation of P3HT resulting in better dosimetric response compared to the P3HT/chloroform solution. Here, HCl comes from two sources i.e. from the radiolysis of chloroform as explained earlier and radiation-induced degradation of DDT.

The peak shows blue shift from 495 nm to 440 nm which is more than a soloution of P3HT in chloroform.

This result opens the possibility to look into the use of other less hazardous radiosensitizers such as chloral hydrate and trichloroacetic acid along with less toxic non-halogenated solvents in developing P3HT based low dose dosimeters.

4.6.3. Conclusion

P3HT in chloroform solution shows slight change in peak position when irradiated at even 30 Gy doses. The addition of DDT was found to show enhancement in shift of peak position showing the enhanced degradation caused by the HCl generated from radiation induced decomposition of DDT. This finding is quite useful which will open the possibility of using other less hazardous chemicals such as chloral hydrate and trichloroacetic acid in other non-halogenated solvents to expolore the possibility of developing low dose dosimeter using P3HT as a reporter polymer and chloral hydrate or trichloroacetic acid as radiosensitizer molecules.

4.7. Investigation of the effects of titanium dioxide nanoparticles on PVA/heptamethine dye films for low dosimetric applications

4.7.1. Introduction

Radiochromic film dosimeters depend on permanent change in color due to radiation-induced chemical changes. This color change is proportional to absorbed dose [105]. Radiochromic film dosimeters have great potential because of their light weight, portability and low cost.

Such light weight and portable detectors, which can be easily put at any location, are very much needed. This would be of great help to detect nuclear sources or carrying the devices by terrorist groups [235].

Alqathami et al [205] investigated the dose enhancement capability of bismuth oxide nanoparticles on radiochromic dosimeter by embedding the naoparticles in the polymeric matrix. Their results suggest that bismuth-based nanomaterials are efficient dose enhancing agents and have great potential for application in clinical radiotherapy.

Inspired by this work, PVA/heptamethine dye/TiO_2 film was prepared and compared with PVA/heptamethine dye film to investigate the dose enhancement effect of TiO_2 nanoparticles on the radiochromic film for low dose dosimetric applications. UV-Vis absorption and optical densitometry studies were conducted on these radiochromic films. The result of our investigation is discussed below.

4.7.2. Results and discussion

4.7.2.1. Optical density studies

The optical densities for both the un-irradiated and irradiated films were measured using the radiochromic reader. The values for the films with and without TiO_2 nanoparticles are compiled in Table 12 below.

Table 12 The optical densities for the un-irradiated and irradiated Cy7-I/PVA/HCl and Cy7-I/PVA/HCl-TiO_2 films.

Dose (Gray)	Cy7-I/PVA/HCl	$[OD]_0/[OD]_{ir}$	Cy7-I/PVA/HCl-TiO_2 (25%)	$[OD]_0/[OD]_{ir}$
0	0.49	1.00	1.11	1.00
50	0.54	1.10	0.91	0.82
150	0.54	1.10	0.74	0.67
250	0.42	0.86	-	-

As can be seen from Table 12, the nanocomposite film with 25% TiO_2 shows enhanced sensitivity at lower doses. This is clearly seen at 50 Gy dose. On the other hand, the film with no TiO_2 nanoparticles does not show much change in optical density at low doses. The OD values remain almost constant upto 150 Gy. Slight change is observed at 250 Gy. This can be explained interms of the catalytic role of TiO_2 nanoparticles in the decomposition of Cy7-I as it interacts

with HCl produced from the radiation induced dehydrochlorination of PVC in the polymer matrix. The prepation of PVA film in HCl results in PVC as explained in [236].

4.7.2.2. UV-Vis absorption studies

Further studies were conducted on the TiO_2 nanoparticle doped and undoped films using UV-Vis absorption spectrometry. Our results show that the nanocomposite films at 25% TiO_2 doping (Figure 56) demonstrate dosimetric characteristics in conformity with the optical density changes shown in Table 12. The un-doped Cy7-I-PVA-HCl films (Figure 55) do not show dosimetric characteristics. This could be explained by the catalytic role TiO_2 nanoparticles play in the radiation induced decomposition of the heptamethine dye. Further structural studies are required to account for the observed dosimetric characteristics in the film.

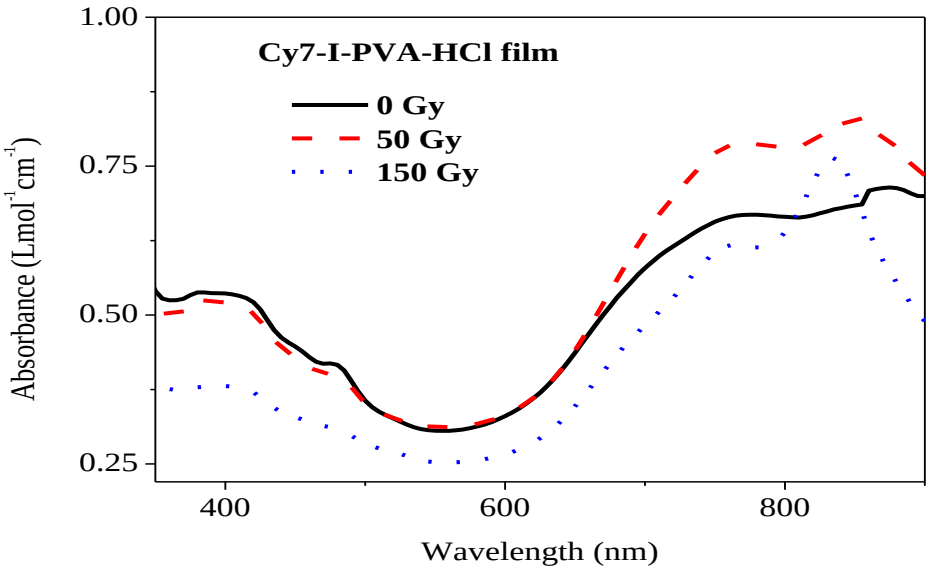

Figure 55 UV-Vis spectra of Cy7-I-PVA-HCl film top to bottom: unirradiated, irradiated at 50 Gy, and 150 Gy.

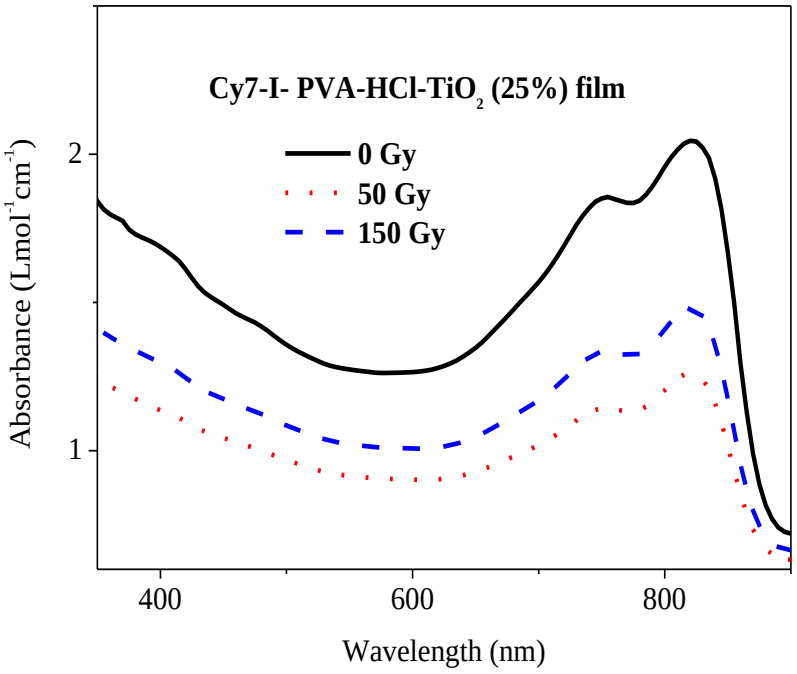

Figure 56 UV-Vis spectra of Cy7-I-PVA-HCl- TiO_2 (25%) film Top to bottom: unirradiated, irradiated at 50 Gy, and 150 Gy.

Radiation- Chemical Yield

The radiation chemical yield (G-value) of the Cy7-I-PVA-HCl-TiO_2 film is calculated using the general formula (Equation 14) as used by Abdel- Fattah et al [231]. Using the density of PVA (1.25 g/cm^3) [231], molar absorbitivity coefficient, ε, of 1450 $Lmol^{-1}cm^{-1}$ (calculated from concentration of Cy7-I, absorbance at 0 Gy and b value of 1 cm), and a dose of 50 Gy, the G-value was found to be 8.61 μmol/J. This shows that the doping of the film with TiO_2 nanoparticles might be responsible for the observed G-value. The G-value of the undoped Cy7-I-PVA-HCl film was not calculated as the UV-Vis spectra did not show change in absorbance on irradiation of the films. This nanocomposite film could be applied in environmental waste

treatment such as fluidized beds and streams. ISO/ASTM Guide 51261 provides information for the selection of dosimetry systems applicable to the diagnosis of irradiated fluid streams and fluidized beds over the dose rangeof interest; i.e. 10^1 to 10^5 Gy [237].

4.7.3. Conclusion

Heptamethine iodide/PVA/HCl film in the presence and absence of TiO_2 nanoparticles was investigated to look into the possibility of developing radiochromic films that could detect low dose gamma or X-ray radiation. The film Cy7-I/PVA/HCl/TiO_2 (25%) was found to show enhanced dosimetric response as we clearly observed in the optical density changes and UV-Vis spectral results. The TiO_2 nanoparticles are postulated to enhance the dosimetric characteristics (decrease in intensity of the main peak and enhanced radiation-chemical yield) *via* catalytic effect on the radiation induced decomposition of the heptamethine dye, Cy7-I. Futher work is needed to evaluate the mechanism of radiation-induced decomposition, shelf life of the film and the optimum concentration of the dye, HCl and the nanoparticles.

5. Conclusion

In this research undertaking heptamethine dye molecules (Cy7-I and Cy7-PF_6), curcumin dye, P3HT and polyvinyl alcohol (PVA) films were investigated to develop radiochromic dosimeters for low dose medical and environmental applications.

The heptamethinde iodide and heptamethine hexafluorophosphate solutions in chloroform can be used as low dose smart dosimeters in the range from 0 to 30 Gy. Moreover, these dosimetric solutions also show linear behavior below one gray. The dosimetric dye solutions also show visual color changes with intensity of color being proportional to absorbed doses which is very useful for precise monitoring of doses delivered to patients in radiotherapy applications. The shelf life of the pre-irradiated dye solutions also show good stability up to 20 days.

UV-Vis, FT-IR and MS spectroscopic studies were conducted to elucidate the mechanism of the dosimetric charactersics. Our results show that the mechanism responsible for the dosimetric character involves two steps. In the first step, radiolysis of chloroform results in formation of radicals such as Cl and $CHCl_2$ and stable molecule such as HCl. In the second step, the interactions of the radicals (Cl or $CHCl_2$) or stable molecule (HCl) with the conjugated polymethine bridge of the dye results in breaking of the π-bonds and breaking of the dye molecules in to various decomposition products. Understanding the mechanism is one step forward in developing more sensitive dosimeters for low dose dosimetry.

The dosimetric characteristics of heptamethine dye Cy7-PF_6 solution in ethanol with 0.003% trichloroacetic acid or chloral hydrate and in acetone with 0.003% chloral hydrate were

investigated. It showed similar dosimetric behavior as heptamethine dye solutions in chloroform. Enhanced sensitivity was observed in the heptamethine dye-ethanol-trichloroacetic acid, heptamethine dye-ethanol-chloral hydrate and hepatamethine dye- acetone/chloral hydrate due to partly the low bond energy of the C-Cl bond in trichloroacetic acid and chloral hydrate and partly due to enhanced generation of HCl via scavenging of chlorine by ethanol and acetone. The non-toxic nature of ethanol and acetone used as solvents makes these dosimetric solutions as promising materials for dosimetric application in medicine and environment.

The other dye dosimteric solution investigated was the curcumin solution in chloroform and ethanol. The curcumin dye solution in chloroform showed good dosimetric characteristics at low doses. Similar behavior was also observed by curcumin-ethanol/chloral hydrate solution which makes it a promising material for low dose applications in medicine and environment. An advantage of this dye is that it is eco-friendly and cost effective.

A conjugated polymer P3HT solution in chloroform in the presence and absence of DDT was investigated. Our results show an enhancement in dosimetric characteristics indicated by a dramatic blue shift in the absorption spectra. This opens a new dimension in developing P3HT based dosimetric solution by using radiosensitizer molecules such as DDT in place of the solvent chloroform. One possibility is to explore the dosimetric characteristics of P3HT using chloral hydrate and trichloroacetic acid in non-halogenated solvents.

The doped film Cy7-I/PVA/HCl/TiO_2 (25%) was found to show enhanced dosimetric response as opposed to the undoped Cy7-I/PVA/HCl film. The TiO_2 nanoparticles are postulated to enhance

the dosimetric characteristics *via* catalytic effect on the radiation induced decomposition of the heptamethine dye, Cy7-I. Futher work is needed to evaluate the mechanism of radiation-induced decomposition, shelf life of the film and the optimum concentration of the dye, HCl and the nanoparticles.

In this study, heptamethine dye solutions in chloroform and ethanol-trichloroacetic acid, ethanol-chloral hydrate, acetone-chloral hydrate, dichloromethane, toluene as well as curcumin dye solution in chloroform and ethanol-chloral hydrate, and P3HT in chloroform/DDT solution showed dosimetric behavior for low dose radiation dosimetry. The mechanism was proposed to be a two step process which involves radiolysis of the halogenated compounds chloroform, dichloromethane, trichloroacetic acid, chloral hydrate and attack on the π-bond of the dye molecules by the radicals and stable molecules. Further work on the effect of additives such as metal salts such as PbI_2, functionalized dye molecules, different solvents, concentration and proportion of various components would be of interest.

A fiber optic polymer-Dye Radiation Dosimeter (FPolyDRAD) or solid state probe could be fabricated with similar structure like a solar cell device with fiber optic cable connection for remote sensing. The dosimeter responses are electrical parameters which will make it more sensitive for low doses and could get technological applications.

Based on the UV-Vis, PL, FT-IR and MS data, a mechanism was proposed for the radiation induced decomposition of heptamethine dye solutions in chloroform. Additional studies using

HPLC, NMR, GC-MS would be of interest for the radiochromic dosimeters. AFM and SEM studies on the solid state films of these radiochromic dosimeters could also be an interest.

The work presented in this thesis establishes the mechanism of dosimetric characteristics of heptamethine dye and curcumin dye solutions of halogenated molecules such as chloroform, trichloroacetic acid and chloral hydrate as well as P3HT in chloroform/DDT solution. The dose enhancement effect of TiO_2 nanoparticles on the heptamethine dye/PVA/HCl film was also described which might open the possibility of developing a composite film for low dose medical and environmental applications.

This will give insight into development of radiochromic dosimeters in solid state and will be helpful in engineering design of radiochromic dosimeters.

6. References

1. B. Allen, L. Marcu, E. Lezak, *Biomedical Physics in Radiotherapy for Cancer*, CSIRO Publishing, **2012**.
2. K. Arshak, O. Korostynska, *Advanced Materials and Techniques for Radiation Dosimetry*, Artech House Inc., **2006**.
3. W. V. Elmpta, L. McDermottb, S. Nijstena, M. Wendlingb, P. Lambina, B. Mijnheera, , *Radiother. Oncol.*, **2008,** 88, 289.
4. S. P. Changlai, P. J. Chang, C. Y. Chen, *Cancer Biother. Radiopharm.*, **2008,** 23, 759.
5. S. Koyama, Y. Miyamato, A. Fujiwara, H. Kobayashi, K. Ajisawa, H. Komori, Y. Takei, H. Nanto, T. Kurobori, H. Kakimoto, M. Sakakura, Y. Shimotsuma, K. Miura, K.Hirao, T. Yamamoto, , *Sens. Mat.*, **2010,** 22, 377.
6. M. Hoshi, Y. O. Konstantinov, O. S. Moskalev, Y. Shibata. S. Yamashita, *Proceedings of the second Hiroshima International Symposium*, Hiroshima, Japan, **1997**.
7. M. A. Noriah, *Radiat. Prot. Dosim.*, **2007,** 125, 101.
8. D. Wehe, *Nucl. Eng. Technol.*, **2006**, 38, 311.
9. Controlling of degradation effects in radiation processing of polymers, IAEA-TECDOC-167, IAEA publications, **2009**.
10. J. Seco, B. Clasie, M. Partridge, *Phys. Med. Biol.*, **2014**, 59, R303.
11. A. Martin, S. Harbison, K. Beach, P. Cole, *An Introduction to Radiation Protection*, 6th ed., Hodder Arnold, **2012**.
12. G. F. Knoll, *Radiation Detection and Measurement*, 3rd ed., Wiley, **2000**.

13. A. N. Al-Kuraieef, A. H. Al-shawi, *IOSR-JESTF*, **2014,** 8, 36.

14. E. S. Josephson, *J. Food Safety*, **1983** 5, 161.

15. A. Parker, K. Metha, *Florida Entomologist*, **2007**, 90, 88.

16. D.M. Suckling, *New Zealand Plant Prot.*, **2003** 56, 21.

17. K. Makuuchi, S. Cheng, *Radiation Processing of Polymer Materials and its Industrial Applications*, John Wiley & Sons Inc., **2012**.

18. G. C. Lowenthal, P. L. Airey, *Practical Applications of Radioactivity and Nuclear Radiations*, Cambridge University press, **2001**.

19. R. L. Wahl, *J. Nucl. Med*, **1998**, 42, 1.

20. A. E. Waltar, *The Medical, Agricultural, and Industrial Applications of Nuclear Technology*, Global 2003, New Orleans, LA, **2003**.

21. J. R. Buscombe, J. B. Cwikla, D. S. Thakrar, A. J. Hilson, *Nucl. Med. Commun.*, **1997**, 18, 698.

22. A. Chiti, F. A. Schreiner, F. Crippa, E. K. Pauwles, E. Bombardieri, *Eur. J. Nucl. Med.*, **1999**, 26, 533.

23. S. M. Okarvi, *Nucl. Med. Commun.*, **1999**, 20, 1093.

24. H. W. Fischer, S. Ulbrich, D. Pittauerova, B. Hettwig, *J. Environ. Radioact.*, **2009**, 100, 1079.

25. *The Role of Nuclear Energy in Low –Carbon Energy Future*, Nuclear Energy Agency, OECD, **2012**.

26. *Technology Roadmap Nuclear Energy*, Nuclear Energy Agency/ International Atomic Energy Agency, OECD/IAEA, **2010**.

27. S. M. Alam, R. Ansari, M. A. Khan, *Online J. Biol. Sci.*, **2001,** 1, 82.

28. F. A.-Jarad, *Int. Symposium on the peaceful applications of Nuclear Technology in the GCC countries*, Jeddah, **2008**.

29. C. G. Orton, *Radiation Dosimetry physical and biological aspects*, Springer Science-Business Media New York, **1986**.

30. W. Huda, N. A. Gkanatsios, *Health Phys.*, **1998**, 75, 492.

31. S. U. Rahman, M. Rafique, A. Jabbar, A. Matiullah, *Rad. Prot. Dosim.*, **2012**, 1.

32. A. Antosik, M. Szejk, A. Gajek, H. M. Zbikowska, *Electronic International Interdisciplinary conference*, **2012**, 563.

33. F. A. Mettler, *J. Radiol. Prot.*, **2012**, 32, N9.

34. A. G. H.-Siedle, L. Adams, *Handbook of Radiation Effects*, 2nd ed., New York: Oxford University Press, **2002**.

35. C. Leroy, P.-G. Rancoita, *Principles of radiation interaction in matter and detection*, World Scientific Publishing, **2004**.

36. N. Tsoulfanidis, *Radiation Detection and Measurement*, 2nd Ed., Taylor & Francis, **1995**.

37. T. Tabata, R. Ito, S. Okabe, *Nucl. Instrum. Meth.* **1972**, 103, 85.

38. ICRU Report 16, *Linear Energy Transfer*, International Commission on Radiation Units and Measurements, **1970**.

39. S. N. Ahmed, *Physics and Engineering of radiation detection*, Acad. Press. Inc., **2007**.

40. A. Aridgides, R. N. Pinnock,D. F. Collins, *Am. J. Phys.*, **1976**, 44, 244.

41. L. P. Hunter, *Handbook of Semiconductor Electronics*, New York: McGraw-Hill, **1970**.

42. NCRP Report No. 82, *SI Units in Radiation Protection and Measurements*, National Council on Radiation Protection and Measurements, **1985**.

43. M. Nenoi, *Current topic in ionizing radiation research*, InTech, **2012**.

44. T. K. Gupta, Radiation, Ionization and Detection in Nuclear Medicine, Springer –Verlag Berlin, Heidelberg, **2013**.

45. *Nuclear Radiation and Health Effects*, World Nuclear Association, **2014**.

46. B. Dörschel, V. Schuricht, J. Steuer, *The Physics of Radiation Protection*, Ashford, Kent, U.K., Nuclear Technology, **1996**.

47. ICRP 91 and International basic safety for protection against ionizing radiation, **1991**.

48. S. M. Alam, R. Ansari, M. A. Khan, *Online J. Biol. Sci.*, **2001,** 1, 82.

49. Medical use of radioisotopes, American Nuclear Society, **2014**.

50. A. Waltar, Radiation and Modern Life: Fulfilling Marie Curie's Dream, Prometheus Books, **2005**.

51. G. A. Carlsson A. Bridier, J. J. Broerse, A. Dutreix, E. Holm, J. R. Johnson, A. M. Kellerer, K. Liden, J. T. Lyman, J. Zoetelief, *The dosimetry of ionizing radiation*, Vol.1, Academic Press Inc., **1985**.

52. K. Kalantar-Zadeh, B. Fry, Nanotechnology-Enabled Sensors, Springer Science, New York, **2008**.

53. S. Martínez-García, M .A. Carvajal, F. Simancas, J. Banqueri, A. M. Lallena, A. J. Palma, *Proceedings IWBBIO*, Granada, **2013**.

54. J. D. Jingle, *J. Chem. Educ.*, **1974**, 51, 101.

55. J. F. Pavoni, O. Baffa, Rad. Meas., **2012**, 47, 1074.

56. N. Purghel, N. Valcov, *Nucl Instrum Methods*, **1995**, B9, 7.

57. I. Kanno, R. Imamura, K. Mikami, A. Uesaka, M. Hashimoto, M. Ohtaka, K. Ara, S. Nomiya, H. Onabe, *J. Nucl. Sci. Technol*, **2008**, 11, 1165.

58. N. Souza, A.N. Farag, Int. J. Appl. Radiat. Isot., **1990**, 41, 739.

59. K.L. Chopra, *Thin Film Phenomena*, Malabar, FL: Robert E. Krieger, **1979**.

60. O. S. Heavens, *Optical Properties of Thin Solid Films*, New York: Dover, **1991**.

61. N. F. Mott, E. A. Davis, *Electronic Process in Non-Crystalline Materials*, Oxford, U.K.: Clarendon, **1979**.

62. C. G. Soares, *Rad. Prot. Dosim.*, **2006**, 120, 100.

63. K. Kinashi, Y. Miyashitab, K. Ishidab, Y. Ueda, *J. Phys. Org. Chem.*, **2012**, 25, 427.

64. K. A. Rabaeh, A. A. Moussa, A. A. Basfar, R. I. Msalam, *Physica Medica*, **2013**, 29, 374.

65. M.F. Barakat, K. El-Salamawy, M. El-Banna, M. Abdel-Hamid,A. Abdel-Rehim Taha, *Rad. Phys. Chem.*, **2001**, 61, 129.

66. O. Korostynska, K. Arshak, J. Harris, *Materials Science*, **2009**, 15, 16.

67. A. P. L. Pacheco, E. S. Araujo, W. M. de Azevedo, *Mat. Charact.*, **2003**, 50, 245.

68. E.A.B. Silva, J.F. Borin, P. Nicolucci, C.F.O. Graeff, T.G. Netto, R.F. Bianchi, *Appl. Phys. Lett.*, **2005**, 86, 131902.

69. H. M. Khan, M. Anwer, Z. S. Chaudhry, *Rad. Phys. Chem.*, **2002**, 63, 713.

70. F. A. Boroumand, M. Zhu, A. B. Dalton, J. L. Keddie, and P. J. Sellin, *Appl. Phys. Lett*., **2007**, 91, 033509.

71. T. K. Maity, S. L. Sharma, *Bull. Mat. Sci.*, **2008**, 31, 6, 841.

72. H. Bodugöz-Sentürkb, O. Güven, *Radiat. Phys. Chem.*, **2011**, 80, 153.

73. J. M. Lobez, T. M. Swager, *Angew. Chem. Int. Ed.*, **2010**, 49, 95.

74. H. N. Raval, S. P. Tiwari, R. R. Navan, and V. R. Rao, *Appl. Phys. Lett.*, **2009**, 94, 123 304.

75. I. Ercan, I. Günal, O. Güven, *Radiat. Phys. Chem.*, **1995**, 46, 813.

76. R. G. Sonkawade, V. Kumar, L. Kumar, S. Annapoorni, S. G. Vaijapurkar, A. S. Dhaliwal, Indian J. Pure Appl Phys., **2010**, 48, 453.

77. R. L. Murray, K. E. Holbert, *Nuclear Energy*, 6th Ed., Elsevier, USA, **2009.**

78. S. C. Curran, W. R. Baker, *Rev. Sci. Instrum.*, **1948**, 19, 116.

79. S. E. Derenzo, M. J. Weber, W. E. Bourret-Courchesne, M. K. Klintenberg, *Nucl. Instrum. Meth. A*, **2003,** 505, 111.

80. D. Natali, M. Sampietro, *Nucl. Instrum. Meth. A*, **2003**, 512, 419.

81. F. D. Brooks, *Nucl. Instrum. Meth.*, **1979**, 162, 477.

82. R. Hofstadter, *Phys. Rev.*, **1948**, 74, 100.

83. R. Hofstadter, M. H. Stein, *IEEE Transact.*, **1975**, 22, 13.

84. E. V. D. van Loef, P. Dorenbos, C. W. E. van Eijk, K. Kramer, H. U. Gudel, *Appl. Phys. Lett.*, **2001**, 79, 1573.

85. K. W. Kramer, P. Dorenbos, H. U. Gudel, C. W. E. van Eijk, *J. Mat. Chem.*, **2006**, 16, 2773.

86. A. Hallam, J. B. Birks, *J. Phys. B. Mol. Opt.*, **1978,** 11, 3273.

87. Q. Chen, T. Hajagos, Q. Pei, *Annu. Rep. Prog. Chem., Sect. C*, **2011,** 107, 298.

88. K. G. Mckay, *Phys. Rev.*, **1949**, 76, 1537.

89. J. Mayer, B. Gossick, *Rev. Sci. Instrum.*, **1956**, 27, 407.

90. E. Sakai, *Nucl. Instrum. Meth. Phys. Res.*, **1982**, 196, 121.

91. P. S. Rao, J. Anand, S. Palaniappan, D. N. Sathyanarayana, E*uro. Poly. J.*, **2000**, 36, 915.

92. K. Yoshino, S. Hayashi and Y. Inuishi, *Jpn. J. Appl. Phys. Part 2-Lett.*, **1982**, 21, L569.

93. K. Yoshino, S. Hayashi, G. Ishii and Y. Inuishi, *Sol. Stat. Commun.*, **1983**, 46, 405.

94. J. G. Drobny, *Ionizing radiation and polymers, principles, technology and applications*, William Andrew, **2012**.

95. L.A. Currie, *Anal. Chem.*., **1968**, 40, 586.

96. A. Shrivastava, V. B. Gupta, *Chronicles of Young Scientists*, **2011**, 2, 22.

97. S. Akhtar, T. Hussain, A. Shahzad, Q.-ul-Islam, *J. Basic appl. Sci.*, **2013**, 9, 420.

98. M. Kattan, Y. Daher, H. Alkassiri, *Rad. Phys. Chem.*, **2007**, 76, 1195.

99. J. Batool, S. A. Shahid, Ramiza, N. Akhtar, A. Naz, M. Yaseen, I. Ullah, M. Nadeem, I. Shakir, Bull. Korean Chem. Soc., **2012,** 33, 2265.

100. M. El Kelany, *Chem. Mat. Reas.*, **2012**, 2, 71.

101. H. M. Khan, A. A. Khan, *J. Radioanal. Nucl. Chem.*, **2010**, 284, 37.

102. H. Kassis, G. Valencia, *European J. Chem. Eng. Chem.*, **2013**, 10, 2668.

103. M. Kattan, H. Al Kassiri,Y. Daher, *Appl. Rad. Isotopes*, **2011**, 69, 377.

104. A. A. Al Zahrany, K. A. Rabaeh, A. A. Basfar, *Rad. Phys. Chem.*, **2011**, 80, 1263.

105. A. A. Basfar, K. A. Rabaeh, A. A. Moussa, R. I. Msalam, *Rad. Phys. Chem*., **2011**, 80, 763.

106. J. Vandecasteele, S. Ghysel, S. H. Baete, Y. De Deen, *Phys. Med. Biol.,* **2011**, 56, 627.

107. A. A. Abdel-Fattah, Y. S. Soliman, A. M. M. Bayomi, A. A. Abdel-Khalek, *Appl. Rad. Isotopes*, **2014**, 86, 21.

108. K. A. Rabaeh, A. A. Basfar, A. A. Moussa, *Rad. Phys. Chem.*, **2012**, 81, 479.

109. J. Mandel, *JTEVA*, **1997**, 25, 151.

110. D. Harvey, Modern Analytical Chemistry, McGraw-Hill, **2008**.

111. C. G. Soares, *Rad. Meas.*, **2007**, 41, S100.

112. A. S. Guerra, R. F. Laitano, M. Pimpinella, *Phys. Med. Biol.,* **1996**, 41**,** 657.

113. H. Palmans, R. Thomas, M. Simon, S. Duane, A. Kacperek, A. DuSautoy, F. Verhaegen, *Phys. Med. Biol.,* **2004**, 49, 3737.

114. J. Seuntjens, S. Duane, *Metrologia*, **2009**, 46, S39.

115. G. G. Jayson, B. J. Parsona, A. J. Swallow, *Int. J. Rad. Phys. Chem.,* **1975**, 7, 363.

116. R. H. Chapman, *Chemical Dosimetry I-The Fricke Dosemeter*, National Radiation Laboratory (NRL) Report 1980/7, **1980**.

117. E. G. Yukihara, S. W. S. McKeever, *Phys. Med. Biol.,* **2008**, 53**,** R351.

118. T. Kron, *Phys. Eng. Sci. Med.*, **1994**, 17, 175.

119. M. Moscovitch, T. J. St. John, J. R. Cassata, P. K. Blake, J. E. Rotunda, M. Ramlo, K. J. Velbeck, L. Z. Luo, *Radiat. Prot. Dosim.* **2006**, 119, 248.

120. J. Kosar, *Light-Sensitive Systems,* Wiley, New York, **1965**.

121. G. H. Dorion, A. F. Wiebe, *Photochromism,*The Focal Press, London, **1970**.

122. G. H. Brown, *Photochromism,* Wiley-Interscience, New York, **1971**.

123. N.W. Holm, R. J. Berry, *Manual on Radiation Dosimetry*, Dekker, New York, **1970.**

124. L. Bordier, *Arch. Roentgen Ray*, **1906**, 11, 6.

125. F. H. Attix, W. C. Roesh, E. Tochilin, *Radiation Dosimetry*, second Ed.. Academic Press, New York, **1966**.

126. M. C. Saylor, T. T., Tamargo, W. L., McLaughlin, H. M., Khan, D. F., Lewis, R. D.., Schenfele, *Radiat. Phys. Chem.,* **1988**, 31, 529.

127. S. G. Vajapurkar, A. Bera, *Indian J. Pure Appl. Phys.,* **2010**, 48, 830.

128. M. A. Ali, E.Saion, A. A. Al-Zahrany, Y. Noorhana, K. H. M. Dahlan, A. Kassim, K. A. Rabaeh, M. H. Hamzah, *J. Eng. Sci. Technol.*, **2010**, 5, 244.

129. S. Devic, *Physica Medica*, **2011**, 27, 122.

130. S.A. El-Fiki, M. S. Abdel-Wahab, M. El-Sherief, S. A. Nooh, M. A. El- Fiki, *Rad. Phys. Chem.*, **1996**, 47, 761.

131. N. M. Ali, C. E. Tucker, F. A. Smith, *Thin Solid Films,* **1996**, 289, 267.

132. J. M. G. Laranjeira, *Physica E: Low-Dimensional Systems and Nanostructures,* **2003**, 17, 666.

133. M. A. Parada, *Surface and Coatings Technology*, **2005**, 196, 378.

134. R. L. Clough, et al., *Rad. Phys. Chem.*, **1996,** 48, 583.

135. G. Wegner, *Chem.*, **1972**, 154, 35.

136. G. Cao, T. E. Mallouk, *J. Solid State Chem.*, **1991**, 94, 95.

137. G. N. Patel, *Rad. Phys. Chem.*, **1979**, 14, 729.

138. G. N. Patel, *Rad. Phys. Chem.*, **1981**, 18, 913.

139. M. C. Janzen, J. B. Ponder, D. P. Bailey, C. k. Ingison, k. S. Suslick, *Anal.Chem.*, **2006**, 78, 3591.

140. X. Hu, X. Li, *J. Polym. Sci. PartB Polym. Phys.*, **2002**, 40, 2354.

141. M. J. Butson, P. K. N. Yu, T. Cheung, P. Metcalfe, *Mat. Sci. Eng. R,* **2003**, 41, 61.

142. R. D. Evans, *The atomic nucleus*, McGraw Hill Pub, New York, **1955**.

143. A. Niroomand –Rad, C. R. Blackwell, B. M. Coursey, K. P. Gall, J. M. Galvin, W. L. McLaughlin, A. S. Meigooni, R. Nath, J. E. Rodgers, C. G. Soares, *Med. Phys.*, **1998**, 25, 2093.

144. M. A. Ebert, A. H. Asad, S. A. Siddiqui, *J. Appl. Med. Phys.*, **2009**, 10, 232.

145. A. Moussa, M. Baranyai, L. Wojnarovits, A. Kovacs, W. L. McLaughlin, *Rad. Phys. Chem.*, **2003**, 68, 1011.

146. M. Farahani, W. L. McLaughlin, *Rad. Phys. Chem.*, **1988**, 32, 683.

147. J. V. Vandacasteele, S. Ghysel, Y. D. Deene, *J. Phys. Conference Series*, **2010**, 250, 012009.

148. M. Alqathami, A. Blencowe, U. J. Yeo, S. J. Doran, G. Qiao, M. Geso, *Int. J. Rad. Oncology Biol. Phys.*, **2012**, 84, e549.

149. J. M. G. Laranjeira, H.J. Khoury, W.M. de Azevedo, E.A. de Vasconcelos, E.F. da Silva Jr., *Mat. Characterization*, **2003**, 50, 127.

150. D.A. Bradley, R. P. Hugtenburg, A. Nisbet, A. T. A. Rahman, F. Issa, N. M. Noor, A. Alalawi, *Appl. Rad. Isotopes*, **2012**, 71, 2.

151. D. S. Woodhead, *Environmental Dosimetry: The Current Position and the Implications for Developing a ramework for Environmental Protection*, Environmental Agency, Rio House, Bristol, **2000**.

152. W. L. McLaughlin, A. W. Boyd, K. H. Chadwich, J. C. McDonald and A. Miller, *Dosimetry Radiation Processing*, Taylor & Francis, London, **1990**.

153. S. J. Doran, *Appl. Radiation Isotopes*, **2009**, 67, 393.

154. D. Renker, E. Lorenz, J. Inst., **2009,** 4, 04004.

155. P. J. Sellin, J. Vaitkus, *Nucl. Instr. Methods Phys. Res. A*, **2006,** 557, 479.

156. J. C. Blakesley, P. E. Keivanidis, M. Campoy-Quiles, C. R. Newman, Y. Jin, R. Speller, H. Sirringhaus, N. C. Greenham, J. Nelson, P. Stavrinou, *Nucl. Instr. Methods Phys. Res. A*, **2007**, 580, 774.

157. C. A. Mills, A. Intaniwet, M. Shkunov, J. L. Keddie, P. J. Sellin, *Proc. of SPIE*, **2009**, 7449, 74491I.

158. D. L. M. Bazani, J. P. H. Lima, A. M. de Andrade, *IEEE Sensors J.*, **2009**, 9, 748.

159. M. C.Kane, R. J. Lascola, E. A. Clark, *Rad. Phys. Chem.*, **2010**, 79, 1189.

160. C. A. Mills, Y.-Fong Chan, A. Intaniwet, M. Shkunov, A. Nisbet, J. L. Keddie, P. J. Sellin, *Phys. Med. Biol.*, **2013**, 58, 4471.

161. J.-Min Han, M. Xu, B. Wang, N. Wu, X. Yang, H. Yang, B. J. Salter, L. Zang, *J. Am. Chem. Soc.*, **2014**,136, 5090.

162. M.J.M. Abadie, *Radiat. Phys. Chem.*, **1982**, 19, 63.

163. R. W. Hummel, A. B. Van Cleave, J. W. T. Spinks, *Can. J. Chem.*, **1954**, 32, 522.

164. F. P. Abramson, R. F. Fireston, *J. Phys. Chem.* **1966**, 70, 3596.

165. J. J. J. Mayron, G. R. Freeman, *Can. J. Chem.*, **1965**, 43, 381.

166. J. Kučera, *Collect. Czech. Chem. Commun.*, **1963**, 28, 1162.

167. V. S. Kosobutskii, *High Energy Chem.*, **2001**, 35, 202.

168. H. L. Andrews, P. A. Shore, *J. Chem. Phys.*, **1950**, **18,** 1165.

169. S. Ebraheem, M. El-Kelany, *Open J. Polym. Chem.*, **2013**, 3, 1.

170. M.Y. Hussain, N.A.Shad, A. Nasim, S. Ali, T. Hussain, I. ul-Haq, *J Agric Sci*, **2009**, 46, 78.

171. S. Mak, N. Kousar, N. Akhtar, *J Basic App Sci*, **2012**, 8, 508.

172. T. Hussain, M. A. K. Shahid, M. Shahbaz, I.ul-Haq, H. Farooq, *J. Basic Appl. Sci.*, **2012**, 8, 581.

173. A. Batagin- Neto, E. S. B. Uhle, M. V. G. Vismara, A. P. Assis, F. A. Castro, T. Geiger, F. C. Lavarda, C. F. O. Graeff, *Curr. Phys. Chem.*, **2013**, 3, 431.

174. M. Y. Hussain, T. Hussain, I. Toqeer, N. Akhtar, I.ul-Haq, H. Farooq, *J. Basic Appl. Sci.*, **2012**, 8, 482.

175. H. A. Hussain, A. H. M. Al-Hashimi, P. Pand, F.Y. Naza, J. Basrah Res. (Sci.), **2013**, 39, 112.

176. H. M. Khan, G. Ahmad, *J. Radioanal. Nucl. Chem. Art.*, **1988**, 125, 127.

177. H. H. Mai, D. N. Duong, T. Kojima, *Radiat. Phys. Chem.*, **2004**, 69, 439.

178. D. Greene, P.C. Williams, *Linear Accelerator for Radiation Therapy*, second ed., Taylor & Francis, **1997**.

179. T. Schimitberger, G.R. Ferreira, M.F. Saraiva, A.G.C. Bianchi, R.F. Bianchi, *Sensors & Actuators B,* **2012**, 168, 131.

180. W.R. Hendee, M.G. Herman, *Med. Phys. Lett.*, **2011**, 38, 78.

181. S.J. Goetch, *Int. J. Radiat. Oncol. Biol. Phys.*, **2008,** 71, 118.

182. R.V. Souza, *Braz. J. Phys*, **2009**, 39, 292.

183. D.V. Parwate, I.D. Sarma, R. J. Batra , *Rad. Meas.*, **2007**, 42, 1527.

184. Y. P. Chen, S.Y. Liu, H. Q. Yu, H.Yin, Q. R. Li, *Chemosphere,* **2008**, 72, 532.

185. W. L. McLaughlin, N. W. Holm, R. J. Berry, *Manual on radiation dosimetry*, Marcel Dekker, New York, 129, **1970**.

186. O. Güven, *Rad. Phys. Chem.*, **2007**, 76, 1302.

187. U.A. Sevil, O. Güven, Ö. Birer, Ş. Süzer, *Synth. Met.*, **2000**, 110, 175.

188. Y. S. Zhao, H. Zhong, Q. Pei, *Phys. Chem. Chem. Phys.*, **2008**, 10, 1848.

189. S. Kim, J. I. Shin, S.Y. Park, K. Jun, Y.A. Son, *J. Korean Soc. Dyers & Finishers,* **2009**, 21, 35.

190. F. A. Castro, H. Benmansour, J.-E. Moser, C. F. O. Graeff, F. Nüesch, R. Hany, *Phys. Chem. Chem. Phys.*, **2009**, 11, 8886.

191. S. Günes, H. Neugebauer, N. S. Sariciftci, *Chem. Rev.*, **2007**, 107, 1324.

192. N. B. El-Assy, C. Y. Dong, M. L. Walker, M. Al-Sheikhly, W. L. McLaughlin, *Radiat Phys Chem*, **1995**, 46, 1189.

193. A. Kovacs, L. Wojnarovits, C. Kurucs, M. Al-Sheikhly, W. L. McLaughlin, *Radiat Phys Chem*, **1998**, 52, 539.

194. Z. Ajji, *Radiat Meas.*, **2006**, 41, 438.

195. S. Ebraheem, A.A. Abdel-Fattah, W.B. Beshir, H. M. Hassan, A. Kovacs, L. Wojnarovits, *Radiat Phys Chem*, **2007**, 76, 1218.

196. H. M. Khan, M. Anwar, *J Radioanal Nucl Chem Lett*, **1993**, 175, 191.

197. N. B. El-Assy, C. Yun-Dong, M. L. Walker, M. Al-Sheikhly, W.L. McLaughlin, *Radiat Phys Chem*, **1995**, 46, 1189.

198. H. M. Khan, S. Tabassum, M. S. Wahid, *J Radioanal Nucl Chem*, **2009**, 280, 635.

199. E. S. Bronze-Uhle, A. Batagin-Neto, D. M. Fernandes, I. Fratoddi, M. V. Russo, C. F. O. Graeff, *Appl.Phys. Lett*, **2013**, 102, 241917.

200. E. S. Bronze-Uhle, J. F. Borin, A. Batagin.-Neto, M. C.O. Alves, C. F.O. Graeff, *Mat. Chem. Phys.*, **2012**, 132, 846.

201. R.F. Cossiello, L. Akcelrud, T.D.Z. Atvars, *J. Braz. Chem. Soc.*, **2005**, 16, 74.

202. E. S. Bronze-Uhle, A. Batagin-Neto, F. C. Lavarda, C. F. O. Graeff, *J. Appl. Phys.*, **2011**, 110, 073510.

203. A. Singh, K. Chen, S. J. Adelstein, A. I. Kassis, *Radiat. Res*., **2007**, 168, 233.

204. S. Chandran, R. S. Singh, *Pharmazie*, **2007**, 62, 4.

205. M. Alqathami, A. Blencowe, U. J. Yeo, R. Franich, S. Doran, G. Qiao, M. Geso, *J. Phys. Conference Series*, **2013**, 444, 012025

206. M. Ottolenghi, G. Stein, *Radiat. Res.*, **1961**, 14, 281.

207. H.R. Werner, R.F., Firestone, *J. Phys. Chem.*, **1965**, 69, 840

208. H. Walba, R. W. Isensee, *J. Org. Chem.*, **1961**, 26, 2789.

209. A. C. Véron, H. Zhang, A. Linden, F. Nüesch, J. Heier, R. Hany, T. Geiger, *Organic Letters*, **2014**, 16, 1044.

210. D. D. Nolting, J. C. Gore, W. Pham, *Curr. Org. Synth.*, **2011**, 8, 521.

211. U. B. Lade, P. K. Bhoyar, M. H. Hingankar**,** W. J. Pharm. Pharmaceut. Scie., **2014**, 3, 2193.

212. E. S. Bronze-Uhle, A. Batagin-Neto, F. C. Lavarda, C. F. O. Graeff, *J. Appl. Phys.*, **2011**, 110, 073510.

213. E. Engel, R. Schram, T. Maisch, K. Kobuch, B. Ko¨nig, R. -M. Szeimies, J. Hillenkamp, W. Ba¨umler,R. Vasold, *IOVS*, **2008**, 49, 1777.

214. B. D. Mistry, A hand book of Spectroscopic Data Chemistry, Oxford Book Company, **2009**.

215. A. Samanta, M. Vendrell, R. Das, Y.-T. Chang, *Chem. Commun.*, **2010**, 46, 7406.

216. F. M. Salih, A. E. Pillay, *J. Radioanal. Nucl. Chem.*, **2004**, 261, 665.

217. W. L. McLaughlin, N. W. Holm, R. J. Berry, *Manual on radiation dosimetry*, Marcel Dekker, New York, 129, **1970**.

218. Susilawati, A. Doyan, *Am. J. Appl. Sci.*, **2009**, 6, 2071.

219. Y. -R. Luo, *Handbook of Bond Dissociation Energies in Organic Compounds*, CRC Press LLC, **2003**.

220. F. Gugumus, Doctrate Thesis of science, Strasbourg, **1965**.

221. H. J. Schumacher, D. Sundhoff, *Z. Physik.Chern.*, **1936**, 834,300.

222. J. D. Roberts, M. C. Caserio, *Basic Principles of Organic Chemistry*, 2nd Ed., W. A. Benjamin Inc., USA, **1977**.

223. M. J. Day, G. Stein, *Radiat. Res.*, **1957**, 6, 666.

224. B. L. Gupta, E. J. Hart, *Radiat. Res.*, **1971**, 48, 8.

225. N. B. El-Assy, A. Allan, F. Abdel-Rahim, H. Roushdy, *Intern. J. Appl. Radiat. Isotopes*, **1982**, 33,433.

226. M. A. K. Shahid, B. Bashir, H. Bashir, A. Mubashir, *Peak J. Pub. Health Manag.* **2014**, 2, 1.

227. A. Baha, N. H. M. Hashini, N. H. A. Halim, N. A. Z. Abidin, R. Me, S. Hassan, *Degradation of Rhizophora apiculata dye solution under sunlight exposure, IEE Business, Engineering and Industrial Application Colloquim (BEIAC)*, **2012**.

228. M. D. Teli, A. N. Nayak, V. B. Nawathe, R. V. Adiivarekar, *Dyeing of cotton with turmeric*, Univ. Department of Chem. Technol. Bombay, **1994**.

229. K. Sachin, V. P. Kapoor, *Indian J. Tadit. Knowl.*, **2007**, 6, 270.

230. I. A. Bhatti, S. Adeel, M. A. Jamal, M. Safdar, M. Abbas, Radiat. Phys. Chem., **2010,** 79, 622.

231. A. A. Abdel-Fattah, M. El-Kelany, F. Abdel-Rehim, *Rad. Phys. Chem.*, **1996**, 48, 497.

232. P. Nanda, S. Maity, N. Pandey, R. Ray, A. K.Thakur, S. Tarafdar, *Rad. Phys. Chem.*, **2011**, 80, 22.

233. J. W. Kingsley, A. J. Pearson, L. Harris, S. J. Weston, D. G. Lidzey, *Org. Electronics*, **2009**, 10, 1170.

234. F. L**.** Lépine, F. Brochu, S. Milot, O. A**.** Mamer, Y. Pépin, *J. Agric. Food Chem.*, **1994**, 42, 2012.

235. N. V. B. Bhat, M. M. Nate, R. M. Bhat, B. C. Bhatt, *Indian J. Pure & Appl Phys.*, **2007**, 45, 545.

236. N. V. Bhat, M. M. Nate, A. V. Gore, R. M. Bhat, J. Appl. Polym. Sci., **2008**, 110, 2243.

237. *Standard Guide for Dosimetry In Radiation Processing of Fluidized Beds and Fluid Streams*, E-2381-04, ASTM International, 100 Barr Harbor Drive, PO Box C700, West Conshohocken, PA 19428-2959, United States, **2004**.

7. Appendix 1

Fricke dosimeter chemical yield determination for dose measurement standardization

Preparation of Fricke dosimeter solution

100 mL of the dosimeter solution was prepared by dissolving 39.2 mg Fe $(SO_4)_2(NH_4)_26H_2O$ and 5.84 mg of NaCl in 0.8 N H_2SO_4 as in reference [1].

Irradiation of the Fricke dosimeter solution

The Fricke dosimeter solution in 4 mL vials were irradiated with a Co-60 Gamma Cell Excel at 500 Gy dose.

UV-Vis absorption spectrometry

The UV-Vis absorption spectra of both the un-irradiated and irradiated solutions of the Fricke dosimeter solutions were measured using Perkin Elmer 950 UV-Vis/NIR spectrophotometer.

Calculation of radiation-chemical yield for standardization of the Co-60 Gamma cell source

The UV-Vis absorption spectra of the Fricke dosimeter solution obtained is depicted in Figure A1.

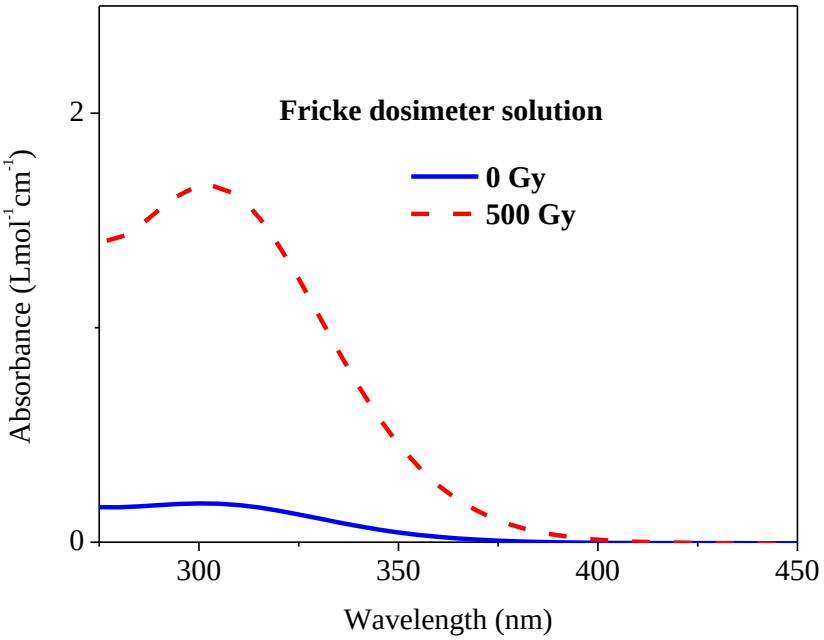

Figure A1 UV-Vis absorption spectra of Fricke dosimeter solution, top to bottom: irradiated at 500 Gy and un-irradiated solution.

From the absorption spectra, the radiation-chemical yield is calculated using Equation 14.

The values for G.ε, ρ and b are 312.5 $m^2.J^{-1}$, 1.024 kgm^{-3} and 10^{-2} m, respectively as used in [2]. The dose reading from the Co-60 Gamma cell is 500 Gy as read directly from the irradiation of the samples for 574.71 s at a dose rate of 0.87 Gy/s.

The dose calculated using the above equation at ΔA of 1.49 calculated from the absorption maxima at 303 nm of the UV-Vis spectra is equal to:

D = 1.49/312.5 x 1.024 x 10^{-2} = 465.25 Gy. This corresponds to a dose rate of 465.25 Gy/574.71 s = 0.81 Gy/s.

References:

1. 1. R. H. Chapman, *Chemical Dosimetry I-The Fricke Dosemeter*, National Radiation Laboratory (NRL) Report 1980/7, **1980**.
2. M. A. Bero, M. Zahili, *J. Phys. Conference Series*, **2009**, 164, 012011.